## ABSTRACT

MCCAIN, EMILY MASON. Understanding the Neuromechanics and Energetics of Clinical Gait using Joint Restrictions to Impose Asymmetric Stepping. (Under the direction of Dr. Katherine Saul).

This dissertation informs the design of assistive technology and rehabilitative techniques for improving walking function in clinical populations. Ankle-based exoskeletons have the potential to increase impaired limb function, reduce energetic requirements, and improve ambulation and quality of life. However, previously researched assistive ankle-based robotics have not impacted metabolic cost consistently, perhaps because walking speed was restricted below the speed where assistance was advantageous. We investigated impact of a novel speed-adaptive myoelectric exoskeleton applying assistance to the paretic ankle of six persons post-stroke walking at increasing walking speeds. Our exoskeleton controller successfully increased assistance with walking speed, and we observed increased paretic ankle joint power as well as total limb power. Interestingly, integrated paretic ground reaction forces decreased and there were no observable metabolic benefits. Reductions in paretic limb trailing limb angle were reduced with exoskeleton assistance suggesting that suboptimal limb poster may have limited joint level benefits from propagating to whole body walking improvements.

Secondly, we investigated the independent impacts of reducing lower limb joint motion on resulting gait deviations and metabolic consequences. Ankle and knee motion can be reduced by injury or disease-induced impairments and restrictions in motion at each joint are associated with metabolically expensive compensatory strategies. It is difficult to isolate the independent impacts of reducing ankle or knee motion because lower limb joint motion is neuromechanically coupled. Ankle and knee bracing were used to unilaterally reduce ankle motion (restricted-ank), knee motion (restricted-knee), and ankle and knee motion simultaneously (restricted-a+k) while 15

unimpaired participants walked on an instrumented treadmill. Restricting ankle motion resulted in decreased peak propulsion relative to the braced condition, and ipsilateral hip hiking when knee motion was restricted increased ipsilateral circumduction relative to the restricted-ank condition. Ankle restriction increased energy requirements compared to the braced condition, and simultaneous restriction of the ankle and knee was more expensive than restricting the knee. We reproduced gait deviations similar to clinical populations and results indicate that ankle-based rehabilitation has potential to improve metabolic outcomes.

Next, we investigated the interaction between walking asymmetry and metabolic cost by unilaterally (asymmetric) and bilaterally (symmetric) restricting the ankle, knee, and simultaneous ankle & knee joint motion in nine unimpaired participants. Asymmetry was not inherently metabolically expensive since metabolic cost increased with symmetric restrictions compared to asymmetric restrictions. The number of restricted joints or degrees of freedom correlated significantly with metabolic rate for 7 of the 9 participants, and this correlation accounted for between 63 and 96% of the variability in metabolic data. Thus, rehabilitation focusing on improving impaired limb function rather than symmetry metrics may have more promise to reduce energetic requirements.

Finally, we investigated impact of reduced joint motion and walking asymmetry on joint reaction forces associated with increased incidence of comorbidities including osteoarthritis and joint pain. Personalized musculoskeletal models were used with the computed muscle control algorithm to determine the joint reaction forces at the ankle, knee, and hip, with recorded EMG from six muscles used to constrained simulated muscle activities. Knee restriction resulted in increased limb loading quantified by ground reaction force peak and loading rate ipsilaterally but decreased peak ground reaction forces contralaterally in comparison to the braced condition.

Ground reaction force peak and loading rate increased with symmetric when compared to asymmetric restriction. We did not observe increases in joint reaction forces associated with increased limb loading; instead, a reduction in muscle forces during loading response counteracted changes in limb loading such that joint reaction forces were relatively unchanged. Our work demonstrates reduced muscle contributions can offset increased limb loading such that joint reaction forces are unaffected.

# Understanding the Neuromechanics and Energetics of Clinical Gait using Joint Restrictions to Impose Asymmetric Stepping

by
Emily Mason McCain

A dissertation submitted to the Graduate Faculty of
North Carolina State University
in partial fulfillment of the
requirements for the degree of
Doctor of Philosophy

Mechanical Engineering

Raleigh, North Carolina
2021

APPROVED BY:

| | |
|---|---|
| _____ | _____ |
| Dr. Katherine Saul<br>Committee Chair | Dr. Michael Lewek |
| _____ | _____ |
| Dr. Scott Ferguson | Dr. Matthew Bryant |

## DEDICATION

To my husband, Joshua Goughnour for his support while I pursued this degree and to my parents, Beth and Paul McCain for your love and guidance before and always.

## BIOGRAPHY

Emily Mason McCain was born and raised in Raleigh, North Carolina where she attended Needham Broughton High School. Upon graduation, she took a gap year before coming to North Carolina State University where she received a Bachelor's in Science in Mechanical Engineering in 2015. She began her graduate studies at North Carolina State University in the Department of Mechanical and Aerospace Engineering in 2016, and she will complete the requirements for her Ph.D. in Mechanical Engineering in June 2021.

## ACKNOWLEDGMENTS

It is with gratitude that I reflect on the past five years at NC State and the individuals who have made this day possible: the dedicated advisors and mentors who have provided professional insight and guidance and the friends and family who have supported me in ways tangible and intangible.

My primary advisor, Dr. Katherine Saul, is someone I have learned from both professionally and personally. Kate, the example you set as an engineer and professor made me interested in pursuing a PhD, and looking forward, it is an example worthy of emulation. For mentoring me through each research challenge, being the first to edit any manuscript or presentation, responding to every Google chat and text, guiding me toward beneficial career opportunities, providing unconditional encouragement, and so much more; Thank you! You made me a better scientist and a better engineer. I hope that the next 8 years will be at least half as fun as those we have shared together. I feel privileged to have had you as an advisor and to count you as a dear friend.

It is often said that good company makes the path seem shorter. In my case, Drs. Michael Lewek and Gregory Sawicki not only made the process of completing this dissertation possible but also more fun. They offered insightful expertise at all hours, feedback on every manuscript or presentation, and encouragement as research instruments and COVID-19 posed unexpected challenges. I extend additional thanks to Greg for his willingness to offer professional guidance throughout graduate school and beyond. Your curiosity for science is infectious, and I am grateful to have worked with you. Similarly, I thank Mike for his insight, welcoming me into his lab for my UNC-based research, and intentionally advocating for my success. Your dedication to your students and the clinical populations you serve is inspiring. Additionally, I offer thanks to Drs.

Scott Ferguson and Matthew Bryant for their willingness to support this dissertation as committee members and for their perspectives and insights. To Scott Ferguson, I am also grateful for your support in my professional explorations since instructing my sophomore dynamics class and for encouraging me to pursue graduate studies.

A special thank you must go to past and current lab mates who have been sounding boards for scientific challenges, walking buddies for mid-day breaks, and contributors to lunch time crossword puzzles. Thank you to Dr. Anthony Santago for providing guidance and advice as needed during my undergraduate and graduate studies. Thank you to Dr. Daniel McFarland, Dr. Nikhil Dixit, and Michael Poppo who helped make this lab such a friendly place to work my first year. Thank you to Matthew Berno and Theresa Libera for their help collecting the data presented and for their friendship. To my current lab mates, Matthew Berno, Morgan Dalman, Mikael Koeneke, Chris Jadelis, and Morgan Everly, thank you all for the Thursday Zoom meetings that helped keep me sane during quarantine. Thank you to Sandra Stangeland-Molo and Emily Fawcett for your encouragement and camaraderie both around campus and at conferences over the years.

Finally, I want to thank my family members who have been ever present throughout this process. To my parents, Beth and Paul McCain, thank you for your support through innumerable daily phone calls, meals offered, and for your unconditional love. To Elizabeth, John Wilson, and my beautiful niece, Blythe Alane Ray Irwin, thank you for the Facetime calls that lifted my spirits at the end of busy days. To my baby brother John, thank you for your “unshellfishness”, and for moving all my stuff into six different apartments throughout my years at NC State. Thank you to my grandmother, Betty McCain, who would have preferred that I attend a lighter blue university but believes strongly in the power of women to accomplish great things in the world and modeled this through example. To my extended Pleasants, Christie, and Peyton families, thank you for

shaping me into who I am; I continue to be grateful that all of you are in my life. To my uncle, Gary Pleasants, whose excitement and support were palpable, and whose curious spirit and dry wit benefited all those that were fortunate enough to know him, I must offer a special acknowledgement. Amy, David, and Jacob Goughnour, thank you for lovingly accepting me into your family and being a source of support and joy though much needed weekend fun and distractions over the past five years. To our dog Doolin, you are the best boy. Lastly, to my husband, Joshua Scott Goughnour, your love and support has been pivotal from the start, and I would not be here without you.

## TABLE OF CONTENTS

## LIST OF TABLES

## LIST OF FIGURES

# CHAPTER 1: Introduction

## Background

Walking supports physical and emotional health. It enables mobility (Graham et al., 2010) and higher walking ability correlates to better overall health (Fritz and Lusardi, 2009). Walking speed has even been deemed the "6$^{th}$ vital sign" (Fritz and Lusardi, 2009; Middleton et al., 2015) because it correlates with functional walking ability (Perry et al., 1995), and can predict the likelihood of future health issues (Studenski et al., 2003), functional decline (Brach et al., 2002), hospitalization (Montero-Odasso et al., 2005), and fall risk (Geerse et al., 2019). Walking performance can be reduced by acute or chronic injuries (Rambaud et al., 2017) or diseases (Amtmann et al., 2015; Perry et al., 1995). For individuals with limited walking ability, restoring mobility and regaining independence is a top priority (Combs et al., 2013; Pollock et al., 2014; Reiber et al., 2010), and when mobility is improved, it can result in increased community participation (Kim et al., 2014) and reported enhancement in quality of life (Shafrin et al., 2017).

When walking ability decreases after injury to a muscle/joint/limb or due to disease-induced physiological/neurological changes, clinical walking characteristics including increased asymmetry, metabolic cost, and joint loading may be affected. Asymmetric walking is common after acute or chronic injuries or diseases, including lower extremity amputations (Adamczyk and Kuo, 2015; Houdijk et al., 2009), knee or hip osteoarthritis (Creaby et al., 2012; Mills et al., 2013; Shakoor et al., 2003), hip arthroplasty (Lugade et al., 2010), and stroke (Brouwer et al., 2009; Chen et al., 2005b; Patterson et al., 2010; Wonsetler and Bowden, 2017). As clinicians rarely know pre-injury or disease walking performance, impaired limb performance is frequently compared to the unimpaired limb as a reference. This comparison of involved to uninvolved limb performance creates a measure of gait asymmetry. Gait asymmetry ratios of unimpaired vs impaired limb

contributions to joint power, limb propulsion, and step-length/time are used to quantify joint-level, limb-level, and whole-body level impacts of impairment. For example, impairments affecting ankle function often result in propulsive asymmetry (Awad et al., 2015a), which may correlate with decreased long-term walking function (Awad et al., 2015a; Chen et al., 2005c). Persons with lower limb amputation walking with a prosthesis have highly asymmetric step times and step lengths, ground reaction forces, joint mechanics, and muscle activity patterns (Fey et al., 2010; Isakov et al., 1997; Isakov et al., 2000; Sadeghi et al., 2001; Silverman et al., 2008; Silverman and Neptune, 2012; Winter and Sienko, 1988; Zmitrewicz et al., 2007; Zmitrewicz et al., 2006). Asymmetric walking is accompanied by increased energy requirements (Detrembleur et al., 2003; Mattes et al., 2000; Stoquart et al., 2012b) often attributed to asymmetric, poorly coordinated step-to-step transitions (Houdijk et al., 2009; Mahon et al., 2015) that require compensations including increased mechanical work to redirect the body's center of mass (Donelan and Kram, 2001; Donelan et al., 2002; Soo and Donelan, 2010). The metabolic energy cost of walking can increase by 10-70% in clinical populations when compared to unimpaired walking (Mattes et al., 2000; Nolan and Lees, 2000; Schmalz et al., 2002; Stoquart et al., 2012a); these substantial increases in metabolic cost can contribute to rapid exhaustion and reduced mobility. Mobility can be further limited by the increased incidence of secondary diseases including osteoarthritis and joint pain (Hampton et al., 2011) that are often attributed to altered joint loading (Mattes et al., 2000; Nolan and Lees, 2000; Schmalz et al., 2002) following musculoskeletal injury, amputation, or stroke. Eliminating the detrimental impacts of increased asymmetry, metabolic cost, and joint loading might be necessary to promote a full recovery of walking function following injury or disease induced impairments.

Assistive joint-level devices have the potential to improve impaired limb function in clinical populations and mitigate the harmful consequences clinical gait. Devices that apply assistance to the impaired limb can increase the impaired ankle moment (Takahashi et al., 2015b), and in some cases reduce metabolic cost (Awad et al., 2017a) in clinical populations. These designs are often rooted in literature suggesting that for those who cannot 'push-off' at all, even small improvements from powered assistance can make a big difference in step-to-step transition work and metabolic cost (Soo and Donelan, 2010, 2012), perhaps allowing patients to walk further and faster. While some devices providing assistance to the impaired limb have contributed to reductions in gait asymmetry and engendered metabolic benefits (Awad et al., 2017a), other devices improved joint metrics but did not reduce asymmetry or energetic requirements (Takahashi et al., 2015b). A better understanding of how an asymmetric intervention that targets individual joints can impact limb and whole-body walking outcomes is crucial for informed rehabilitative designs for those with asymmetric walking patterns.

Understanding interactions among altered joint function, gait compensations, and whole-body walking outcomes is especially challenging in clinical populations where neurological or anatomical changes make isolating any specific gait deviation difficult. While weakness at both ankle (Allen et al., 2014; Olney et al., 1991), and knee joints (Waters and Mulroy, 1999) in many clinical conditions are associated with limb-level compensations and increased energy requirements, independent roles of ankle and knee dysfunction are difficult to discern because ankle and knee motion are interrelated (Kerrigan et al., 2001; Little et al., 2014; Stanhope et al., 2014). Further, while many assume limb-level asymmetric gait deviations drive increased energy requirements, the metabolic impacts of interventions targeting improved walking symmetry in clinical populations is inconsistent in the literature (Awad et al., 2014a; Nguyen et al., 2020;

Padmanabhan et al., 2020; Sánchez and Finley, 2018), suggesting other factors may have a more direct metabolic impact. Although changes in joint loading are associated with increased incidence of osteoarthritis and joint pain (Imani Nejad et al., 2020), the relationship between walking asymmetry and altered joint loading is not well known; this is because investigations into the impact of walking asymmetry on joint loading are limited because joint loading cannot be experimentally measured without expensive (and invasive) implants, and because determining the impact of asymmetry would require the difficult, if not impossible, task of coaching clinical populations into symmetric walking.

The purpose of this dissertation is to enhance the design of joint-based assistive devices for improving walking function in clinical population. In specific aim 1 we evaluated the impact of ankle assistance applied to the paretic ankle of persons post stroke by a novel speed-adaptive myoelectric exoskeleton controller on walking performance outcomes. Our results elucidated limb level gait characteristics which may impede joint-level assistance from propagating to whole body energetic benefits. As a result, I developed a research plan to provide a better understanding of the impacts of reduced joint function and walking asymmetry on metabolic consequences and joint loading. This plan included investigations into the impact of (**Specific Aim 2**) reduced joint function on limb-level gait characteristics and metabolic cost, (**Specific Aim 3**) joint restriction induced asymmetry on metabolic cost, and (**Specific Aim 4**) joint restriction and asymmetry on joint loading. We hope that the results included here will guide the design of assistive technology and extend the ability of individuals with injury or disease induced asymmetric impairments to participate more fully in their community for decades.

## Specific Aims

**Specific Aim 1: Determine the impact of exoskeleton assistance across a range of walking speeds in persons post-stroke using a novel, speed-adaptive myoelectric exoskeleton controller to modulate the magnitude of torque with changes in walking speed and soleus EMG.** Understanding of the interaction between walking speed and the metabolic benefit of exoskeleton assistance would inform assistive device design. **Methods** We analyzed data from six stroke survivors walking with assistance applied to the paretic ankle by a speed-adaptive myoelectric exoskeleton controller. Participants started walking at 60% of their comfortable overground speed and then walking speed was increased by 0.1 $ms^{-1}$ each minute until reaching a stopping criterion. **Hypothesis 1:** Our novel speed-adaptive controller will scale exoskeleton assistance with increases in walking speed as intended. **Hypothesis 2:** Exoskeleton assistance will lead to increases in total average net paretic ankle power and limb power at all walking speeds. **Hypothesis 3:** Exoskeleton assistance will lead to metabolic benefits associated with improved paretic average net ankle and limb powers.

**Specific Aim 2: Determine how reduced range of motion at the ankle and knee joints impacts limb level gait characteristics and whole-body metabolic consequences.** Chronic injury or disease-induced weakness in ankle or knee function are associated with metabolically expensive gait compensations including reduced propulsion and "stiff-knee" gait. Ankle and knee motion are neuromechanically coupled, making the relative metabolic impacts of reduced function and range of motion at each joint unclear. Improved understanding of the metabolic increases resulting from reduced function and motion at each joint would provide guidance into the potential of interventions to be metabolically beneficial. **Methods.** We recorded data on healthy controls walking with bracing applied to restrict ankle and knee motion unilaterally. Data were recorded to

determine the presence of compensatory strategies and measure the metabolic cost of imposed kinematic changes. **Hypothesis 1:** Limiting ankle ROM would attenuate peak ankle power at pushoff, reduce peak limb propulsion, and require bilateral increases in sagittal hip power to compensate. **Hypothesis 2:** Limiting knee ROM would decrease knee flexion velocity at toe off, impair swing limb advancement and require increased circumduction via ipsilateral increases in frontal plane hip power. **Hypothesis 3:** The metabolic cost of compensatory mechanics resulting from restricting ankle ROM would be larger than the cost of compensations from restricting knee ROM.

**Specific Aim 3: Investigate interactions and relative metabolic impacts of gait asymmetry and joint restriction by unilaterally (asymmetric) and bilaterally (symmetric) restricting ankle, knee, and combined ankle+knee ROM in unimpaired individuals.** The relationship between impaired joint and limb function, walking asymmetry, and metabolic cost in clinical populations is inconsistently characterized (Awad et al., 2015b; Mahon et al., 2019; Roemmich et al., 2019). A better understanding of the relative metabolic impacts of impaired joint function and gait asymmetry would improve design of rehabilitative strategies and assistive technology. **Methods.** We will collect and process data from healthy controls walking with unilateral and bilateral braces restricting their ankle and knee range of motion. **Hypothesis 1:** (a) Induced asymmetry will be more metabolically expensive than induced symmetry (bilaterally restricted joints) (b) due to energetically expensive step-to-step transitions. **Hypothesis 2:** As a proxy for available DOFs, the number of joints restricted will correlate with a metabolic increase in asymmetric and symmetric conditions.

**Specific Aim 4: Determine the impact of joint restriction and walking asymmetry on joint reaction forces calculated using EMG-informed musculoskeletal simulations.** Illness or

injury-induced walking asymmetry is prevalent in clinical populations that have an increased incidence of comorbidities including osteoarthritis and joint pain thought to derive from changes in joint loading. Improving the understanding of the impact of walking asymmetry and joint motion restriction on joint loading is a pivotal first step toward understanding the etiology of comorbidities. **Methods.** We employed EMG-constrained musculoskeletal simulations of the healthy controls walking with unilateral and bilateral braces restricting their ankle and knee range of motion to compute joint loading. **Hypothesis 1**: Unilateral joint restrictions will result in increased knee and hip joint reaction force loading rate and first peak value on the (a) ipsilateral limb (due to reduced knee compliance) and (b) contralateral limb (due to asymmetric propulsion) when compared to unrestricted walking. **Hypothesis 2:** Unilateral restriction of the ankle and knee simultaneously will result in larger ipsilateral joint reaction force peak and loading rate when compared to unilateral restriction of the ankle or knee because reduced limb compliance. **Hypothesis 3** Bilateral joint restrictions will eliminate asymmetric propulsion thereby reducing JRF peaks and loading rates when compared to the unrestricted limb with unilateral restrictions.

## Structure of Dissertation

This dissertation consists of four chapters (Chapters 2-5) with the structure of independent journal articles. Chapter 2 (published in the Journal of NeuroEngineering and Rehabilitation) describes the impact of a novel speed-adaptive myoelectric exoskeleton applying assistance to the paretic ankle on post-stroke walking performance. Chapter 3 (published in the Journal of NeuroEngineering and Rehabilitation) presents an investigation of the relative metabolic impact of restricting ankle and knee joint range of motion unilaterally. Chapter 4 (accepted with minor revisions at the Journal of Biomechanics) describes an investigation into the relative metabolic impacts of restricting joint function and walking asymmetry. Chapter 5 (in preparation for the

Journal of Biomechanics) presents an investigation into the impacts of joint restriction and walking asymmetry on joint loading. In Chapter 6, I summarize significant findings and suggest future research of relevance and substantial potential impact.

# CHAPTER 2

## Mechanics and Energetics of Post-Stroke Walking Aided by a Powerful Ankle Exoskeleton with Speed-Adaptive Myoelectric Control (Published in Journal of NeuroEngineering and Rehabilitation, 2019)

Emily M. McCain, Taylor J.M. Dick, Tracy N. Giest, Richard W. Nuckols, Michael D. Lewek, Katherine R. Saul, Gregory S. Sawicki.

## Abstract

Background: Ankle exoskeletons offer a promising opportunity to offset mechanical deficits after stroke by applying the needed torque at the paretic ankle. Because joint torque is related to gait speed, it is important to consider the user's gait speed when determining the magnitude of assistive joint torque. We developed and tested a novel exoskeleton controller for delivering propulsive assistance which modulates exoskeleton torque magnitude based on both soleus muscle activity and walking speed. The purpose of this research is to assess the impact of the resulting exoskeleton assistance on post-stroke walking performance across a range of walking speeds.

Methods: Six participants with stroke walked with and without assistance applied to a powered ankle exoskeleton on the paretic limb. Walking speed started at 60% of their comfortable overground speed and was increased each minute (n00, n01, n02, etc.). We measured lower limb joint and limb powers, metabolic cost of transport, paretic and non-paretic limb propulsion, and trailing limb angle.

Results: Exoskeleton assistance increased with walking speed, verifying the speed-adaptive nature of the controller. Both paretic ankle joint power and total limb power increased significantly with exoskeleton assistance at six walking speeds (n00, n01, n02, n03, n04, n05).

Despite these joint- and limb-level benefits associated with exoskeleton assistance, no subject averaged metabolic benefits were evident when compared to the unassisted condition. Both paretic trailing limb angle and integrated anterior paretic ground reaction forces were reduced with assistance applied as compared to no assistance at four speeds (n00, n01, n02, n03).

Conclusions: Our results suggest that despite appropriate scaling of ankle assistance by the exoskeleton controller, suboptimal limb posture limited the conversion of exoskeleton assistance into forward propulsion. Future studies could include biofeedback or verbal cues to guide users into limb configurations that encourage the conversion of mechanical power at the ankle to forward propulsion.

## Introduction

Walking after a stroke is more metabolically expensive, leading to rapid exhaustion, limited mobility, and reduced physical activity (Michael et al., 2005). Hemiparetic walking is slow and asymmetric compared to unimpaired gait. Preferred walking speeds following stroke range between < 0.2 m s-1 and ~0.8 m s-1 (Perry et al., 1995) compared to ~1.4 m s-1 in unimpaired adults, and large interlimb asymmetry has been documented in ankle joint power output (Chen et al., 2005c; Jonkers et al., 2008). The ankle plantarflexors are responsible for up to 50% of the total positive work needed to maintain forward gait (Eng and Winter, 1995; Farris and Sawicki, 2012); therefore, weakness of the paretic plantarflexors is especially debilitating, and as a result, the paretic ankle is often a specific target of stroke rehabilitation (Awad et al., 2017b; Forrester et al., 2016; Forrester et al., 2010; Takahashi et al., 2015b). In recent years, ankle exoskeletons have emerged as a technology capable of improving ankle power output by applying torque at the ankle joint during walking in clinical populations (Awad et al., 2017b; Takahashi et al., 2015b) and healthy controls (Collins et al., 2015; Galle et al., 2017; Sawicki and Ferris, 2008; Wiggin, 2011).

Myoelectric exoskeletons offer a user-controlled approach to stroke rehabilitation by measuring and adapting to changes in the user's soleus electromyography (EMG) when generating torque profiles applied at the ankle (Koller et al., 2015). For example, a proportional myoelectric ankle exoskeleton was shown to increase the paretic plantarflexion moment for persons post-stroke walking at 75% of their comfortable overground (OVG) speed (Takahashi et al., 2015b); despite these improvements, assistance did not reduce the metabolic cost of walking or improve percent paretic propulsion. The authors suggested exoskeleton performance could be limited because the walking speed was restricted to a pace at which exoskeleton assistance was not needed.

Exoskeleton design for improved function following a stroke would benefit from understanding the interaction among exoskeleton assistance, changes in walking speed, and measured walking performance. Increases in walking speed post-stroke are associated with improvements in forward propulsion and propulsion symmetry (Awad et al., 2016), trailing limb posture (Hsiao et al., 2015; Tyrell et al., 2011), step length symmetries (Awad et al., 2015b; Tyrell et al., 2011), and greater walking economies (Awad et al., 2015b; Tyrell et al., 2011). This suggests that assistive technologies need to account for variability in walking speeds to further improve post-stroke walking outcomes. However, research to date has evaluated exoskeleton performance at only one walking speed, typically set to either the participant's comfortable OVG speed or a speed below this value (Awad et al., 2017b; Takahashi et al., 2015b). At constant speeds, ankle exoskeletons have been shown to improve total ankle power in both healthy controls (Collins et al., 2015) and persons post-stroke (Takahashi et al., 2015b), suggesting the joint powers and joint power symmetries could be improved by exoskeleton technology. Additionally, an exosuit applying assistance to the ankle was able to improve paretic propulsion and metabolic cost in persons post-stroke walking at their comfortable OVG speed (Awad et al., 2017b). Assessing the

impact of exoskeleton assistance on walking performance across a range of speeds is the next logical step toward developing exoskeleton intervention strategies targeted at improving walking performance and quality of life for millions of persons post-stroke.

In order to assess the impact of exoskeleton assistance across a range of walking speeds in persons post-stroke, we developed a novel, speed-adaptive exoskeleton controller that automatically modulates the magnitude of ankle torque with changes in walking speed and soleus EMG. We hypothesized that: 1) Our novel speed-adaptive controller will scale exoskeleton assistance with increases in walking speed as intended. 2) Exoskeleton assistance will lead to increases in total average net paretic ankle power and limb power at all walking speeds. 3) Exoskeleton assistance will lead to metabolic benefits associated with improved paretic average net ankle and limb powers.

## Methods

### Exoskeleton Hardware

We implemented an exoskeleton emulator comprised of a powerful off-board actuation and control system, a flexible Bowden cable transmission, and a lightweight exoskeleton end effector (Nuckols et al., 2015). The exoskeleton end effector includes shank and foot carbon fiber components custom fitted to participants and hinged at the ankle. The desired exoskeleton torque profile was applied by a benchtop motor (Baldor Electric Co, USA) to the carbon-fiber ankle exoskeleton through a Bowden-cable transmission system. An inline tensile load cell (DCE-2500N, LCM Systems, Newport, UK) was used to confirm the force transmitted by the exoskeleton emulator during exoskeleton assistance.

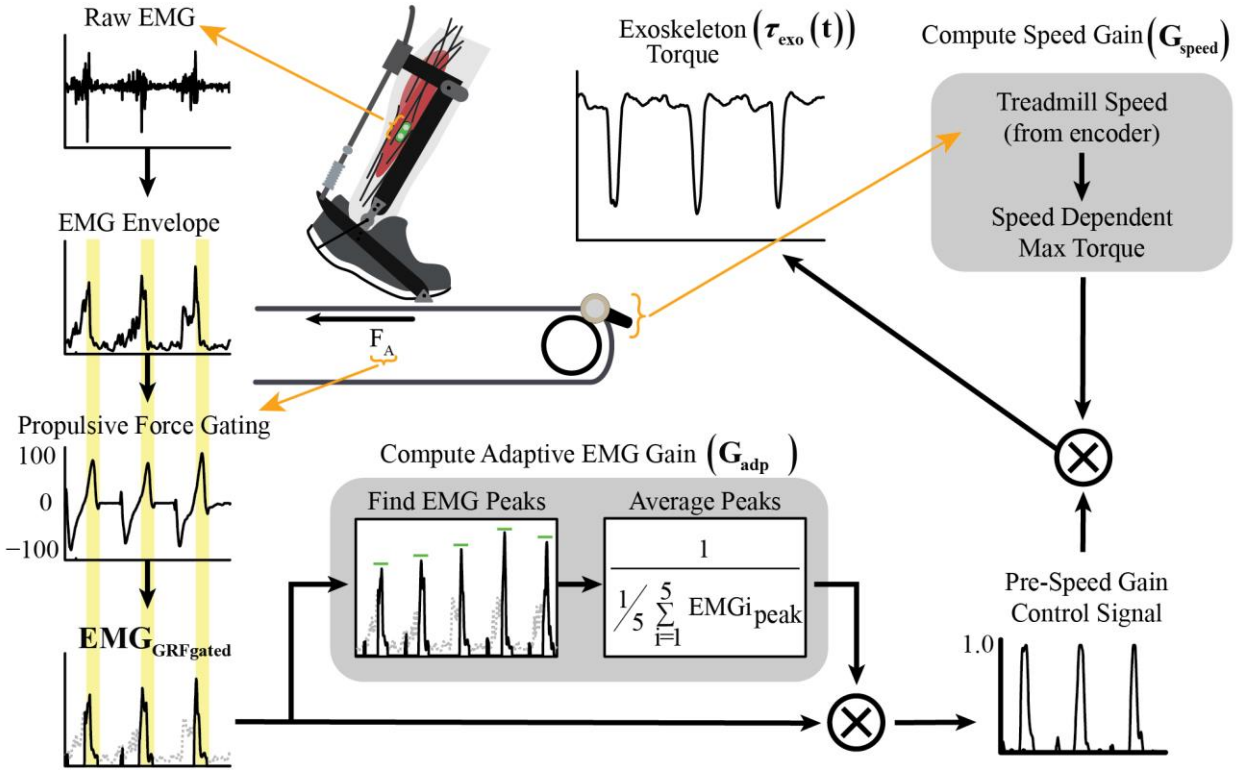


**Figure 2.1:** Novel speed-adaptive myoelectric exoskeleton controller.

The exoskeleton controller measures and adapts to users' soleus EMG signal as well as their walking speed in order to generate the exoskeleton torque profile. Raw soleus EMG signal is filtered and rectified to create an EMG envelope, and the created EMG envelope was then gated by anterior GRFs to ensure assistance was only applied during forward propulsion. The adaptive EMG gain is calculated as a moving average of peak force-gated EMG from the last five paretic gait cycles. The pre-speed gain control signal is product of the force-gated EMG and the adaptive EMG gain. The speed gain is determined using real-time walking speed and computed as 25% of the maximum biological plantarflexion torque at that given walking speed. Exoskeleton torque is the result of multiplying the speed gain with the pre-speed gain control signal.

**Speed-Adaptive Proportional Myoelectric Exoskeleton Controller**

Our exoskeleton controller alters the timing and magnitude of assistance with the user's soleus EMG signal and walking speed (Figure 2.1). The exoskeleton torque is determined from Equation 1, in which participant mass (mparticipant)is constant across speeds, treadmill speed (V) is measured in real-time, the speed gain (Gspeed) is constant for all subjects and across speeds, the adaptive gain (Gadp) is constant for a gait cycle and calculated anew for each gait cycle, and the force-gated and normalized EMG (EMGGRFgated) is a continuously changing variable.

$$\tau_{exo}(t) = m_{participant} \times V \times G_{speed} \times G_{adp} \times EMG_{GRFgated} \quad (1)$$

Surface EMG was collected for the paretic soleus at 960 Hz (SX230, Biometrics, Newport, UK), high pass filtered with a 2nd order dual-pass Butterworth filter (50 Hz), full-wave rectified, low pass filtered with 2nd order dual pass Butterworth filter (10 Hz) and normalized to one by the adaptive gain (Koller et al., 2015). In persons post-stroke, spasticity, altered coordination, and weakness (Lamontagne et al., 2002) can affect soleus activation timing and magnitude. In order to maintain volitional control while ensuring exoskeleton torque was only applied during forward propulsion, the EMG envelope was gated by anterior ground reaction forces (GRFs) (Takahashi et al., 2015b). Our adaptive EMG gain (Gadp) was calculated as the inverse of the moving average of the peak of the force-gated EMG envelope from the previous five gait cycles. Vertical GRFs were used to determine heel strikes. The EMG adaptive gain multiplied by the force-gated EMG signal produces the pre-speed control signal allowing the shape of the EMG envelope to be maintained, with the peak normalized to one. The speed-adaptive gain (Gspeed) was determined empirically from pilot data to scale the pre-speed control signal to ~25% of the maximum normal biological ankle plantarflexion moment as predicted from normative data relating peak plantarflexion given body mass and treadmill velocity; the speed gain has units of (N m (m s-1)-

1) kg-1. The participant's real-time walking speed and mass are multiplied by the speed gain and the pre-speed control signal to determine an exoskeleton torque in Newton-meters. Applying ~25% of normal biological ankle plantarflexion moment ensures the torque applied by our controller is comparable to that applied by previous ankle exoskeletons (Collins et al., 2015; Takahashi et al., 2015b). Instantaneous treadmill velocity was recorded by a speed encoder (1024cpr, Encoder Products Company, USA) secured to the split belt treadmill roller (Bertec, USA).

**Inclusion Criteria**

Participants were required to be at least six months post-stroke and to demonstrate persistent lower extremity hemiparesis with a comfortable OVG walking speed of at least 0.6 m s-1 and the ability to walk on a treadmill for at least five minutes at a time.

**Data Collection**

Data collection procedures were approved by the University of North Carolina at Chapel Hill institutional review board (IRB), and all participants signed an IRB approved consent form before data collections. Experimental data were collected from six persons post-stroke (Table 1) walking on an instrumented split belt treadmill (Bertec, USA): (1) wearing the exoskeleton on the paretic ankle, but without powered assistance (Unassisted) and (2) wearing the exoskeleton as it provided powered assistance (Assisted). Each session was performed on a separate day, and conditions were counter-balanced. Participants started by walking at 60% of their preferred speed (n00). At each consecutive minute, the treadmill speed was increased by 0.1 m s-1 (n01, n02, etc) until the subject reached one of several stopping criteria (heart rate reached 60% of their heart rate reserve; rate of perceived exertion exceeds 7 (on a Borg 1-10 scale); or the subject asked to stop). Preferred OVG walking speed was assessed over a 10 meter overground walkway. No body weight

support was provided; however, all participants wore a harness for fall prevention. Use of handrails mounted bilaterally was discouraged.

**Table 2.1:** Subject Characteristics

| Participant | Gender | Affected Side | Age (yrs) | Mass (Kg) | Height (m) | Months Since Stroke | OVG Speed ($ms^{-1}$) |
|---|---|---|---|---|---|---|---|
| 1 | F | L | 47 | 80.8 | 1.7 | 151.0 | 0.83 |
| 2 | M | R | 50 | 71.3 | 1.7 | 41.0 | 1.02 |
| 3 | M | R | 56 | 90.2 | 1.9 | 19.0 | 0.82 |
| 4 | F | R | 43 | 98.3 | 1.6 | 23.0 | 0.84 |
| 5 | F | L | 40 | 70.9 | 1.6 | 33.0 | 0.60 |
| 6 | M | R | 62 | 91.5 | 1.9 | 180.0 | 1.00 |
| **Average** | | **-** | **49.7** | **83.8** | **1.7** | **74.5** | **0.85** |
| **Std Dev** | | **-** | **8.2** | **11.3** | **0.1** | **71.5** | **0.15** |

An eight-camera motion analysis system (Vicon, Oxford, UK) recorded positions of 37 reflective markers attached to the pelvis and legs (modified Cleveland Clinic marker set, similar to (Farris et al., 2015)) at 120 Hz. The modified marker set consisted of 26 anatomical markers placed over: the greater trochanter, illiac crest, lateral femoral epicondyle, medial femoral epicondyle, lateral malleolus, medial malleolus, calcaneus and second metatarsophalangeal joint of both limbs. The remaining markers were placed in clusters of three or four on the pelvis, feet, thigh and shank segments. The foot clusters were attached to each participant's shoes. Raw marker positions were filtered using a second order low-pass Butterworth filter (cut-off frequency of 10 Hz). Anatomical markers from a static standing collection were used to scale and calibrate segments (pelvis, thighs, shanks and feet) for each participant; inertial properties were applied to scaled and calibrated segments, and default geometries used to create subject specific models (Visual 3D, C-Motion, USA). A second order low-pass Butterworth filter with a cutoff frequency of 40 Hz was applied to raw analog force platform signals. Rates of oxygen consumption and carbon dioxide production were recorded on a breath-by-breath basis using a portable metabolic

system (OxyCon Mobile, Carefusion, USA). To obtain baseline metabolic energy consumption during standing, measurements were made during five minutes of quiet standing prior to speed ramp sessions.

**Data Processing**

Detailed descriptions of the analyses used in this investigation have been provided previously (Farris et al., 2015; Takahashi et al., 2015b). Briefly, an inverse kinematics algorithm (Thelen and Anderson, 2006) was used to obtain ankle, knee, and hip joint angles processed in Visual3D (CMotion, USA) and MATLAB (Mathworks, USA) from filtered marker data and individual models. An inverse dynamics algorithm was used to determine joint moments and powers. To evaluate walking performance with and without the exoskeleton at different speeds, we obtained measures of exoskeleton assistance from a load cell within the device.

Exoskeleton assistance, joint and limb powers, integrated anterior GRFs, and trailing limb angle (TLA) were calculated as an average over paretic and non-paretic gait cycles in the five analyzed strides. Analyzed strides occurred during the latter half of each minute to allow for adjustment before and after changes in treadmill speed. Crossover steps were excluded from analysis. If a subject did not complete five strides at a speed before reaching the stopping criteria, the speed was not included in this study. At higher speeds, the sample size decreased as some participants reached the stopping criteria. Metabolic cost of transport was calculated for each subject as the total cost for the entire session over all recorded speeds.

**Exoskeleton assistance:** For *Assisted* conditions we determined exoskeleton torque about the ankle by multiplying the measured exoskeleton force from the in-series load cell by the moment arm, determined as the measured linear distance between the ankle joint center and the exoskeleton cable in a neutral position. Biological torque at the ankle was calculated as the difference between

the total ankle torque calculated from inverse dynamics and the applied exoskeleton torque. Multiplying torque and ankle joint angular velocity yielded the exoskeleton mechanical power contribution in watts (W) (Thelen and Anderson, 2006).

**Average Joint Power:** We calculated average positive, average negative and average net mechanical power for the ankle, knee, and hip joints and the exoskeleton. Calculations of average joint powers have been described previously (Farris et al., 2015). Briefly, positive and negative intervals of time series joint powers were separately integrated with time to determine total positive and negative work done. Positive and negative work were divided by the sum of the associated intervals of time to determine average positive and negative powers for a gait cycle. Average net power was determined from the integral of time series joint powers divided by the duration of the five integrated strides.

**Average Limb Power:** Calculations for average positive, average negative, and average net limb powers have been described previously (Farris et al., 2015). In brief, time series joint power curves were summed for each of the paretic and non-paretic limbs to yield limb power with time. Time series limb power was integrated to determine net work done. Net work was divided by the sum of the associated stride times to determine net power. Total positive and negative work done by the limb was determined by separately integrating positive and negative integrals of time series limb power. Limb powers were determined by dividing work by the associated time integrals from the five strides.

**Net Metabolic Power and Metabolic Cost of Transport:** We used a portable metabolic system was used to collect rates of oxygen consumption and carbon dioxide production during all data sessions as input into the Brockway equation to calculate metabolic power (W) (Brockway, 1987). Prior to walking, data from the last two minutes of five minute quiet standing were averaged

and used to determine metabolic power during standing. Net metabolic power was calculated by subtracting metabolic power during standing (W) from metabolic power during walking (W) and then normalized to individual body mass (kg). For both the *Assisted* and *Unassisted* data collection sessions, we integrated net metabolic power (W $kg^{-1}$) to determine energy consumed (J $kg^{-1}$) during each session. We then divided energy by the total distance traveled (m) during the walking session to calculate net metabolic cost of transport for the session (J $m^{-1}$ $kg^{-1}$).

**Paretic and Non-Paretic Propulsion:** Intervals of anteriorly directed GRFs were trapezoidally integrated with time over five gait cycles for the paretic and non-paretic limbs. Subject average paretic and non-paretic propulsion were calculated for each speed as well as the comfortable OVG speed (Peterson et al., 2010b).

**Peak Vertical Ground Reaction Force during Propulsion**: Peak GRFs occuring during periods of forward propulsion were identified as the second peak in vertical GRFS for five gait cycles on the paretic limb and normalized by body weight for each subject and at each speed (Hsiao et al., 2017; Kim and Kim, 2017). Peak values were averaged across gait cycles and across speeds.

**TLA:** TLA was defined in the sagittal plane as the maximum angle between the vertical axis and a line connecting the greater trochanter with the second metatarsophalangeal joint during double stance. Paretic and non-paretic double stances were defined between non-paretic heel strike and paretic toe off and between paretic heel strike and non-paretic toe off, respectively. Raw data were used to find paretic TLA at each time frame, and the maximum TLA was averaged across all paretic gait cycles and across speeds.

**Statistical Analyses**

Differences between *Assisted* and *Unassisted* conditions for each subject for peak average ankle power, joint powers, limb powers, integrated anterior GRFs, and TLA were evaluated using

paired t-tests (α=0.0), and effect sizes (Cohen's d) at each speed. Additionally, analysis of metabolic cost of transport included a paired t-test (α=0.05) to determine differences between the *Assisted* and *Unassisted* conditions measured across all speeds. Effect sizes (d) were calculated by dividing the mean difference by the pooled standard deviation (Raja et al., 2012).

## Results

**Exoskeleton Technology:** The speed-adaptive proportional myoelectric exoskeleton controller increased peak assistance with speed, verifying the effectiveness of the speed-adaptive gain (Figure 2.2.c). Peak exoskeleton assistance ranged between 0.216 ± 0.097 N $m^{-1}$ $kg^{-1}$ and 0.354 ± 0.018 N $m^{-1}$ $kg^{-1}$, and peak assistance occurred with timing ranging from 43.7% ± 2.1% of stride to 49.3% ± 3.0% of stride (Table 2.2, Figure S2.3). Peak total (biological + exoskeleton) paretic ankle power increased with exoskeleton assistance (Figure 2.2.b) when compared to the *Unassisted* condition (Figure 2.2.a) at all speeds with significance at three of the 8 speeds (*n01*: p=0.002, d=2.46; *n02*: p=0.047, d=1.71; *n04*: p=.015, d=1.19). There was no significant change detected for peak ankle power in the non-paretic limb between the *Assisted* and *Unassisted* conditions (Figure S2.4).

**Table 2.2:** Exoskeleton Peak Torque Timing and Magnitude with Walking Speed Sample Size

| Speed | Peak Torque ($Nm^{-1} kg^{-1}$) | | Timing of Peak Torque (% stride) | | Sample Size | |
|---|---|---|---|---|---|---|
| | **Average** | **Std Dev** | **Average** | **Std Dev** | ***Unassisted*** | ***Assisted*** |
| n00 | 0.216 | 0.097 | 49.3% | 3.0% | 6 | 6 |
| n01 | 0.267 | 0.044 | 46.6% | 1.4% | 6 | 5* |
| n02 | 0.247 | 0.095 | 44.9% | 1.8% | 6 | 6 |
| n03 | 0.276 | 0.048 | 45.8% | 1.6% | 6 | 6 |
| n04 | 0.29 | 0.051 | 44.1% | 2.5% | 5 | 6 |
| n05 | 0.352 | 0.014 | 43.7% | 2.1% | 3 | 3 |
| n06 | 0.338 | 0.011 | 44.1% | 0.6% | 3 | 2 |
| n07 | 0.354 | 0.018 | 43.6% | 0.1% | 2 | 2 |
| OVG | n/a | n/a | n/a | n/a | 6 | 6 |

**Joint Mechanics**: Paretic Limb: Average net total paretic ankle power increased with assistance when compared to the Unassisted condition at six speeds (n00: p=0.021, d=1.40; n01: p=0.008, d=1.23; n02: p=0.004, d=1.29; n03: p=0.003, d=1.35; n04: p=0.001, d=1.56; n05: p=0.013, d=1.60) (Figure 2.3.a) and at each users' preferred OVG speed (p=0.003, d= 1.26). Average net paretic knee power decreased significantly in the Assisted condition at one speed (n05: p=0.020, d=0.51) and increased significantly at each users' preferred OVG speed (p=0.007, d=0.20). No significant change was found in average net paretic hip power. Average positive and negative paretic joint powers were also calculated (Figures S2.5 and S2.6). Non-Paretic Limb: No significant change was found in non-paretic average net ankle or hip power at any speed (Figure S2.7). However, a significant decrease in average net knee power with exoskeleton assistance was seen at three speeds (n00: p=0.045, d=0.50; n04: p=0.030, d=0.60; OVG: p=0.014, d=0.60) (Figure S2.7). Non-paretic average positive and negative joint powers were also calculated (Figures S2.5 and S2.6).

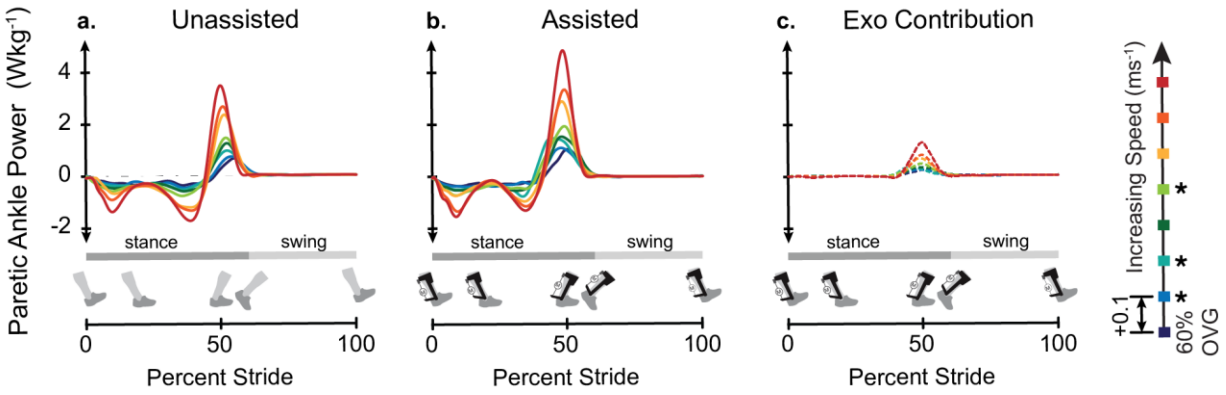


**Figure 2.2.** Ankle power analysis.

Peak paretic ankle power increased with walking speed and with exoskeleton assistance**.** Group average time-varying paretic ankle power in the *Unassisted* condition (A) and the *Assisted* condition (B), with the exoskeleton contribution isolated (C). Walking speed was increased from 60% of the users' comfortable OVG speed (OVG) by 0.1ms$^{-1}$ each minute.

**Limb Mechanics:** Average net paretic limb power increased with exoskeleton assistance at all speeds and with significance at seven speeds (*n00:* p=0.010, d=0.91; *n01:* p=0.026, d=0.60; *n02:* p=0.0003, d=0.80; *n03:* p=0.002, d=0.92; *n04:* p=0.006, d=0.65; *n05:* p=0.035, d=0.75; *OVG:* p=0.007, d=0.70). Average net non-paretic limb power was not significantly altered at any speed with exoskeleton assistance (Figure 2.3.d).

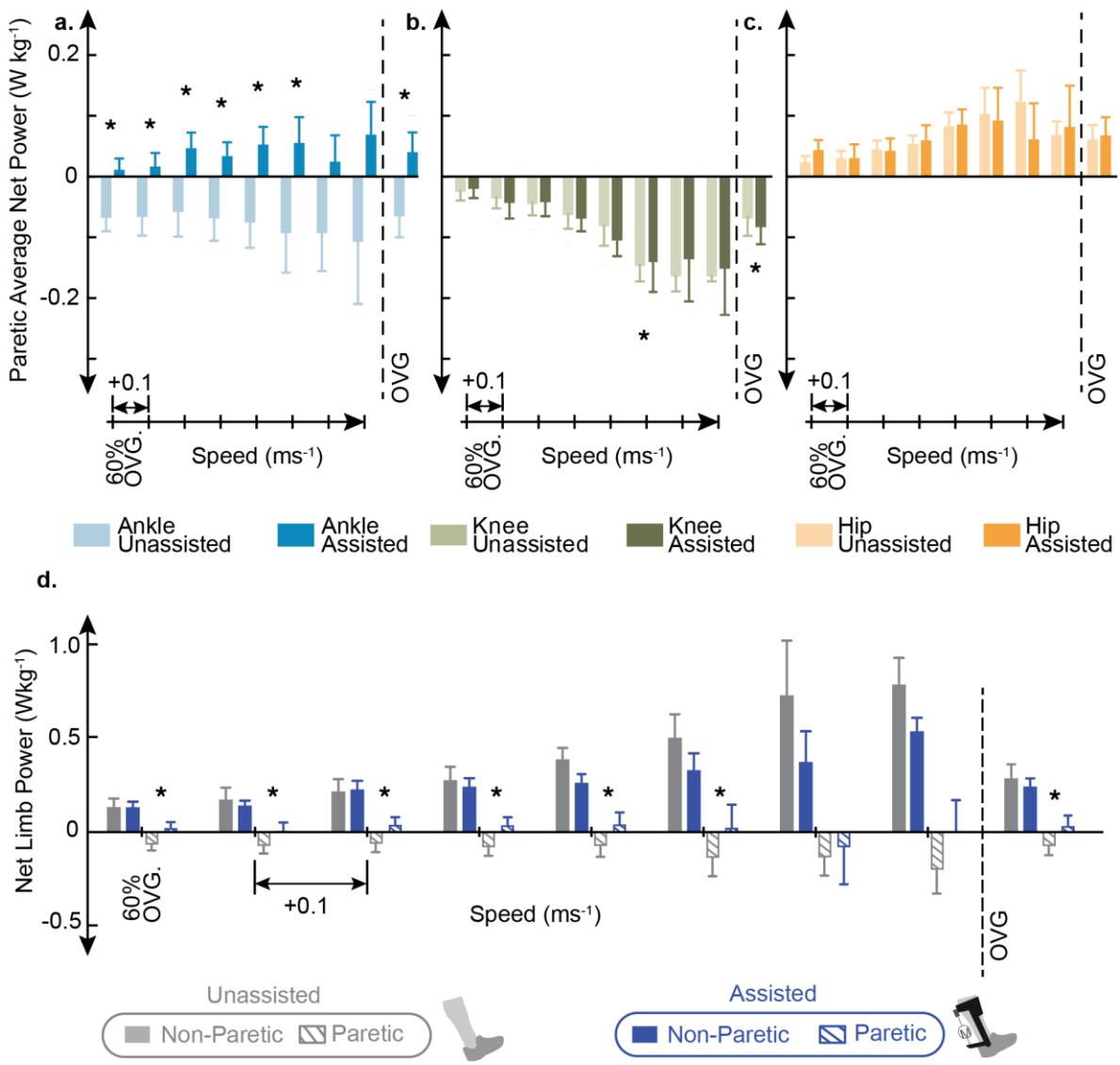


**Figure 2.3.** Joint and limb power analysis.

Average net paretic ankle and limb powers increased with exoskeleton assistance at all speeds. Average net paretic ankle (A), knee (B), and hip (C) power (± standard error) for the *Unassisted* (light colors) and *Assisted* (dark colors) conditions. Average net limb power (± standard error) for the paretic (hatch fill) and non-paretic (solid fill) limb with exoskeleton (blue) and without exoskeleton (grey) assistance (D). All values are calculated from subject averages over five gait cycles. To the right of the dashed line average net powers averaged at each user's comfortable OVG speed are shown.

**Metabolics:** Despite improvements in average net joint and limb powers on the paretic limb, we observed no significant change in the whole-body metabolic cost of transport with exoskeleton assistance (Table 3). Further, the impact of exoskeleton assistance on metabolic cost of transport was not consistent across individuals; with only two out of six participants experiencing a metabolic benefit with exoskeleton assistance (Table 3: Participant 4, Participant 6) (Figure S2.8), and the remaining four participants displaying an increased cost of transport. Breath-by-breath data informing these calculations are included in supplemental materials (Figure S2.8).

**Table 2.3:** Whole Body Metabolic Cost of Transport and Total Distance Traveled

| **Participants** | **Metabolic Cost of Transport** $\int W kg^{-1} / \text{Total Distance}$ | | **Total Distance Walked (m)** | |
|---|---|---|---|---|
| | **Unassisted** | **Assisted** | **Unassisted** | **Assisted** |
| 1 | 3.2 | 3.6 | 188.1 | 172.8 |
| 2 | 3.4 | 3.6 | 435.2 | 452.5 |
| 3 | 3.8 | 4.2 | 417.2 | 493.4 |
| 4 | 3.0 | 2.9 | 163.9 | 135.7 |
| 5 | 2.8 | 3.7 | 127.6 | 160.5 |
| 6 | 4.2 | 3.7 | 331.7 | 324.8 |
| **Average** | **3.4** | **3.6** | **277.3** | **290.0** |
| **Std Dev** | **0.5** | **0.4** | **134.7** | **157.0** |

**Paretic and Non-Paretic Propulsion:** Integrated anteriorly directed GRFs for the paretic limb were significantly lower with exoskeleton assistance when compared to the *Unassisted* condition at five speeds (*n00:* p=0.043, d=0.87; *n01:* p=0.033, d=0.87; *n02:* p=0.007, d=0.58; *n03:* p=0.008, d=0.45; *OVG:* p=0.025, d=0.38) (Figure 2.4). There were no significant changes in non-paretic propulsion (Figure 2.4).

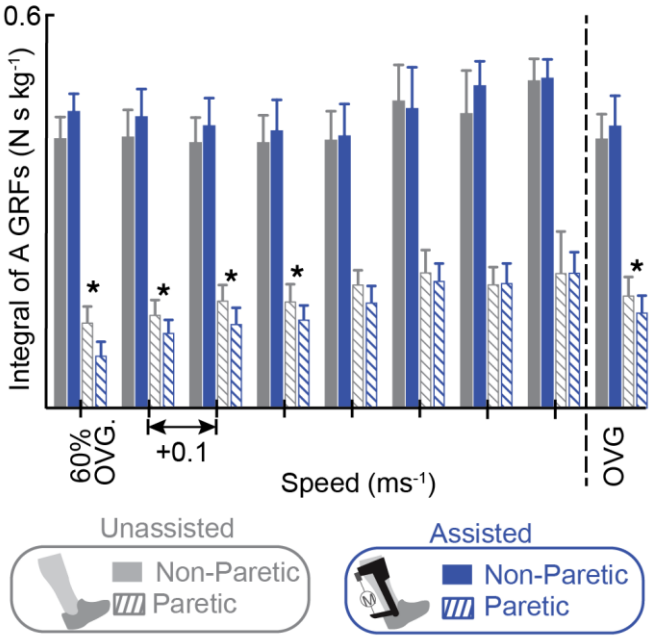


**Figure 2.4.** Cumulative Anterior GRFs.

Anterior Integrated anteriorly directed GRFs on the paretic limb decreased with exoskeleton assistance at the majority of speeds. The paretic (hatch fill) and non-paretic (solid fill) integrated anterior GRFs (± standard error) are plotted with (blue) and without (grey) exoskeleton assistance applied as walking speed increases. To the right of the dashed line integrated GRFs are averaged at users' comfortable OVG walking speed.

**Peak Vertical GRF during Propulsion:** During *Assisted* walking, subject averaged peak vertical GRF was increased when compared to the *Unassisted* condition at six speeds (Figure 2.6), (*n00:* p=0.026, d=0.73; *n01:* p=0.008, d=1.11; *n02:* p=0.002, d=1.01; n03*:* p=0.001, d=1.075; *n04:* p=0.001, d=1.08; *n06:* p=0.012, d=0.98; *OVG:* p<0.001, d=0.89).

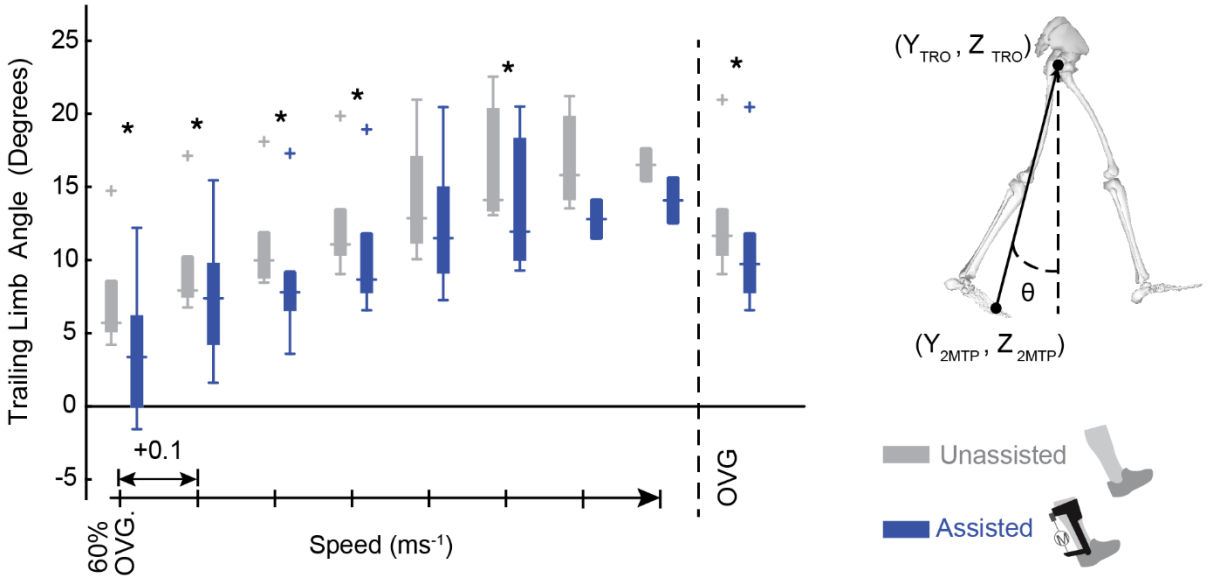


**Figure 2.5**. Trailing Limb Angle.

Reductions in TLA in the *Assisted* condition indicate suboptimal limb configuration during exoskeleton assistance. The paretic TLA is defined between the vertical plane and a line connecting the second Metatarsophalangeal (2MTP) joint and Greater Trochanter (TRO) during double stance. With exoskeleton assistance (blue) TLA is shown to decrease when compared to the *Unassisted* condition (grey) at all speeds. To the right of the dashed line TLA are averaged at each user's comfortable OVG speed.

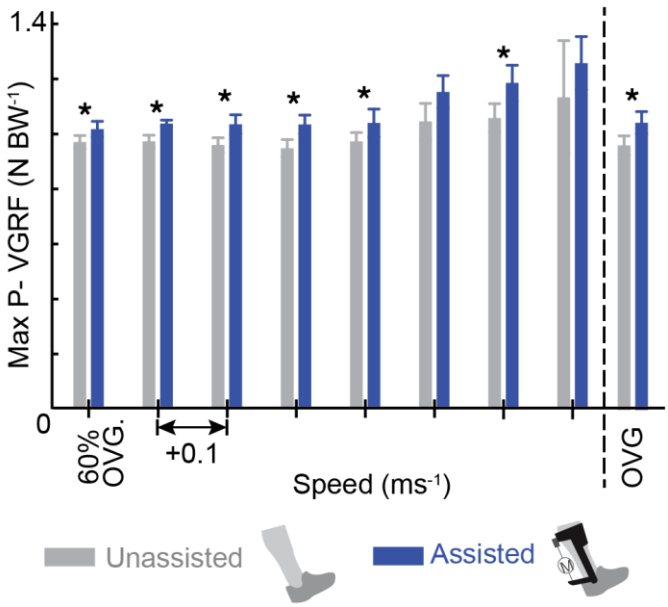


**Figure 2.6**. Peak vertical GRFs.

Increased paretic peak push off vertical GRF in the *Assisted* condition supports suggestion that reductions in TLA encourage the conversion of exoskeleton torque into vertical rather than forward propulsion. The peak paretic vertical GRF during pushoff are plotted with (blue) and without (grey) exoskeleton assistance applied as walking speed increases. To the right of the dashed line peak vertical GRF are averaged at each user's comfortable OVG speed.

## Discussion

The use of ankle-based rehabilitation strategies has increased in popularity in recent years (Awad et al., 2017b; Caputo and Collins, 2014; Collins et al., 2015; Forrester et al., 2016; Koller et al., 2015; Takahashi et al., 2015b). Our controller builds upon the foundation provided by Takahashi et. al. through the inclusion of: (1) a speed-adaptive gain capable of scaling exoskeleton torque with walking speed and (2) an EMG adaptive gain (similar to (Koller et al., 2015)) calculated by the moving average of soleus EMG peaks over five strides to ensure the control is still saturated despite reductions in soleus EMG that can occur while using myoelectric controllers

(Koller et al., 2015). To our knowledge, this is the first study to implement a powered ankle exoskeleton that modulates plantarflexion torque magnitude with walking speed. In the current work we specifically investigated the impact of our novel controller across a range of speeds to elucidate the relationships among ankle assistance, walking speed, and walking performance for persons post-stroke. The results of this study provide a foundation for improved development of future ankle-based rehabilitation technologies capable of adapting to the user and the environment.

In support of our first hypothesis, our speed-adaptive gain performed as intended by increasing assistance with walking speed. This successful assistance modulation provides a new framework by which we can explore and interpret the impact of assistance on walking function across a range of speeds. Our second hypothesis was also supported; peak total paretic ankle power increased with exoskeleton assistance and with speed, and the exoskeleton delivered net positive energy at the paretic ankle proportional to changes in walking speed. Additionally, average net paretic limb power was increased with exoskeleton assistance, suggesting that assistance applied at the ankle transferred energy to the paretic limb as intended. Despite increases in ankle and limb power, our third hypothesis was not supported: average metabolic cost of transport showed no significant reduction with exoskeleton assistance.

Failure to convert exoskeleton assistance to forward propulsion could explain the lack of metabolic benefits seen with exoskeleton assistance in this study as previous studies have shown an inverse relationship between metabolic cost and measures of paretic propulsion (Awad et al., 2017b). Specifically, an exosuit for persons post-stroke reduced the metabolic cost of walking and was accompanied by small increases in percent paretic propulsion in addition to improved joint powers similar to the results here (Awad et al., 2017b). We expected that increased ankle power from exoskeleton assistance would yield an increase in paretic propulsion because the ankle plays

a key role in forward propulsion during healthy walking (Nadeau et al., 1999) . Despite increases in ankle power, paretic propulsion was reduced for the *Assisted* condition compared to the *Unassisted* condition, suggesting that exoskeleton assistance at the ankle was not converted to forward propulsion. Since exoskeleton benefits were apparent in both joint and limb powers but did not translate to forward propulsion, we explored whether overall limb configuration limited the transfer of mechanical energy at the ankle into center of mass propulsion. Reductions in TLA, a commonly used measure of limb configuration, is characteristic of hemiparetic gait. Reduced TLA can further impede the transfer of power from the ankle to propulsion of the COM and reduce long-term walking function (Hsiao et al., 2015). TLA values for the *Unassisted* condition reported here are within the range of TLA reported for persons post-stroke in literature (Awad et al., 2015a). In the *Assisted* condition, TLA was further reduced, bringing the trailing limb closer to vertical and apparently accelerating the COM vertically rather than anteriorly during exoskeleton assistance. Thus, while joint and limb powers were increased, conversion of ankle torque into forward propulsion was limited by suboptimal limb kinematics. The increase in peak vertical GRF during propulsion seen in the *Assisted* condition when compared to the *Unassisted* condition provides further support for the suggestion that decreased TLA encouraged conversion of exoskeleton assistance to vertical rather than forward propulsion. TLA is determined by the interactions of lower limb kinematic properties (Figures S2.1, S2.2, S2.3, and S2.4), but it is not immediately apparent what caused the decrease in TLA for the *Assisted* condition. It is possible that the increase in ankle torque may induce limb instability, such that subjects decrease TLA during assistance as a protective mechanism to maintain stability. Future analyses could more directly examine the interaction between exoskeleton assistance and TLA. Nevertheless, the current study highlights the importance of limb configuration during exoskeleton assistance. Previous examples of

biofeedback and verbal cues demonstrate their potential for improving hemiparetic gait; therefore, future research could address this concern using biofeedback or verbal cues that guide users into optimal limb configurations. Specifically, visual feedback of plantarflexor and dorsiflexor EMG signals during post-stroke walking allowed users to increase their walking speed as well as ankle power generation during pushoff phase of gait (Aiello et al., 2005). Verbal qualitative feedback about walking performance has been shown to improve OVG walking speed (Aiello et al., 2005; Dobkin et al., 2010) and could be leveraged to increase TLA during exoskeleton assistance to increase propulsion. Alternative solutions to suboptimal limb configurations include investigating the timing of exoskeleton assistance or using a multi-joint exoskeleton capable of accounting for TLA during propulsion. Specifically, an exoskeleton providing assistance during the eccentric phase of soleus activity could allow greater tibial progression during stance, increasing the TLA in preparation for the assistance applied during propulsion. Alternatively, exoskeletons or robotic training aids acting across multiple joints (Agrawal et al., 2007; Banala et al., 2009; Krishnan et al., 2012) offer a promising tool for applying assistance and could encourage users into optimal limb configurations during pushoff.

Although altered TLA is most likely responsible for the lack of metabolic changes with exoskeleton assistance, other factors- including acclimation time and assistance timing - are known to impact energy consumption during walking (Awad et al., 2017b; Malcolm et al., 2013; Sawicki and Ferris, 2008). Participants had limited acclimation to exoskeleton assistance in this study. However, previous studies of walking with powered ankle assistance indicate that in healthy subjects, gait adapts to reach steady state neuromotor and metabolic performance after ~30-40 minutes of walking practice (Sawicki and Ferris, 2008). Therefore, it is possible that increased acclimation time could improve metabolic performance. This is a challenge inherent to evaluating

gait performance with exoskeleton assistance in clinical populations, for whom lengthy acclimation periods are more physically demanding and could induce fatigue. The timing and magnitude of exoskeleton assistance is known to impact metabolic costs in healthy controls (Caputo and Collins, 2014). Post-stroke walking performance varies markedly across individuals, thus personalized parameter settings for exoskeleton assistance may be warranted. Recent research supports this consideration, reporting for a group of persons post-stroke that personalized engagement timing when walking with an exosuit improved propulsion and reduced metabolic costs while using the device (Awad et al., 2017b). The timing of exoskeleton assistance in the current work considered the individual participant's timing for both GRFs as well as soleus EMG signal, but it is possible that other assistance timings exist that improve torque delivery.

There are some additional limitations that should be considered. Due to the participant burden and inclusion criteria, we consider a small sample size. We did randomize the order of *Assisted* and *Unassisted* sessions for subjects, however, there was no randomization of walking speed, and therefore it is possible that at higher speeds subjects were better acclimated to exoskeleton assistance. However, as one of our goals was to see if participants could walk at faster speeds with the exoskeleton assistance, randomization of speeds was not possible. Furthermore, because each individual had a different comfortable OVG speed, evaluation speeds at each increment (n01 n02, etc.) differed in magnitude between individuals. It is also possible that one minute was not sufficient for participants to adapt to each speed. Metabolic cost of transport was calculated across the entire 'speed ramp'; however, this approach is subject to end effect errors because metabolic energy requirements at the end of the speed ramp may not affect measurements until sometime later. There was limited acclimation time for familiarizing the participants with exoskeleton assistance, and the exoskeleton limited the degree of freedom of the ankle to flexion.

Any degree of freedom restriction caused by the physical device in other planes (e.g., inversion/eversion) is unlikely to account for differences in metabolic expenditure between the *Assisted* and *Unassisted* conditions because the exoskeleton was worn (unpowered) in the *Unassisted* condition. However, it is possible that wearing the exoskeleton limited rotations in other directions (e.g.: frontal plane) and that this limitation could affect metabolic expenditure when compared to walking without an exoskeleton. Despite this, previous exoskeletons using similar hardware have shown benefits in healthy controls (Collins et al., 2015) and therefore we do not believe range of motion limitations had significant negative impacts. Finally, no instructions were given to participants regarding how to optimize delivery of exoskeleton assistance.

## Conclusions

Our novel speed-adaptive proportional myoelectric controller demonstrates the potential for ankle exoskeletons to be used in rehabilitation interventions for persons post-stroke. Myoelectric controllers offer a user-controlled option for stroke rehabilitation; however, EMG data following a stroke is more variable, especially on the paretic limb where weak signals and abnormal muscle control add complications to typical processing methodology. Alternative exoskeleton controllers may mitigate some of the challenges of implementing proportional myoelectric exoskeletons outside the lab. For example, an impedance based controller capable of reducing metabolic cost of intact human walking (Collins et al., 2015) in healthy controls offers an exciting research area for stroke rehabilitation where human-robot interaction dynamics may be tailored to the individual's physiology. Future studies implementing impedance-based controllers and incorporating verbal cues that guide users into optimal limb configurations could exceed the capabilities of the current work and contribute to reduced metabolic cost of transport for persons post-stroke walking with an ankle exoskeleton.

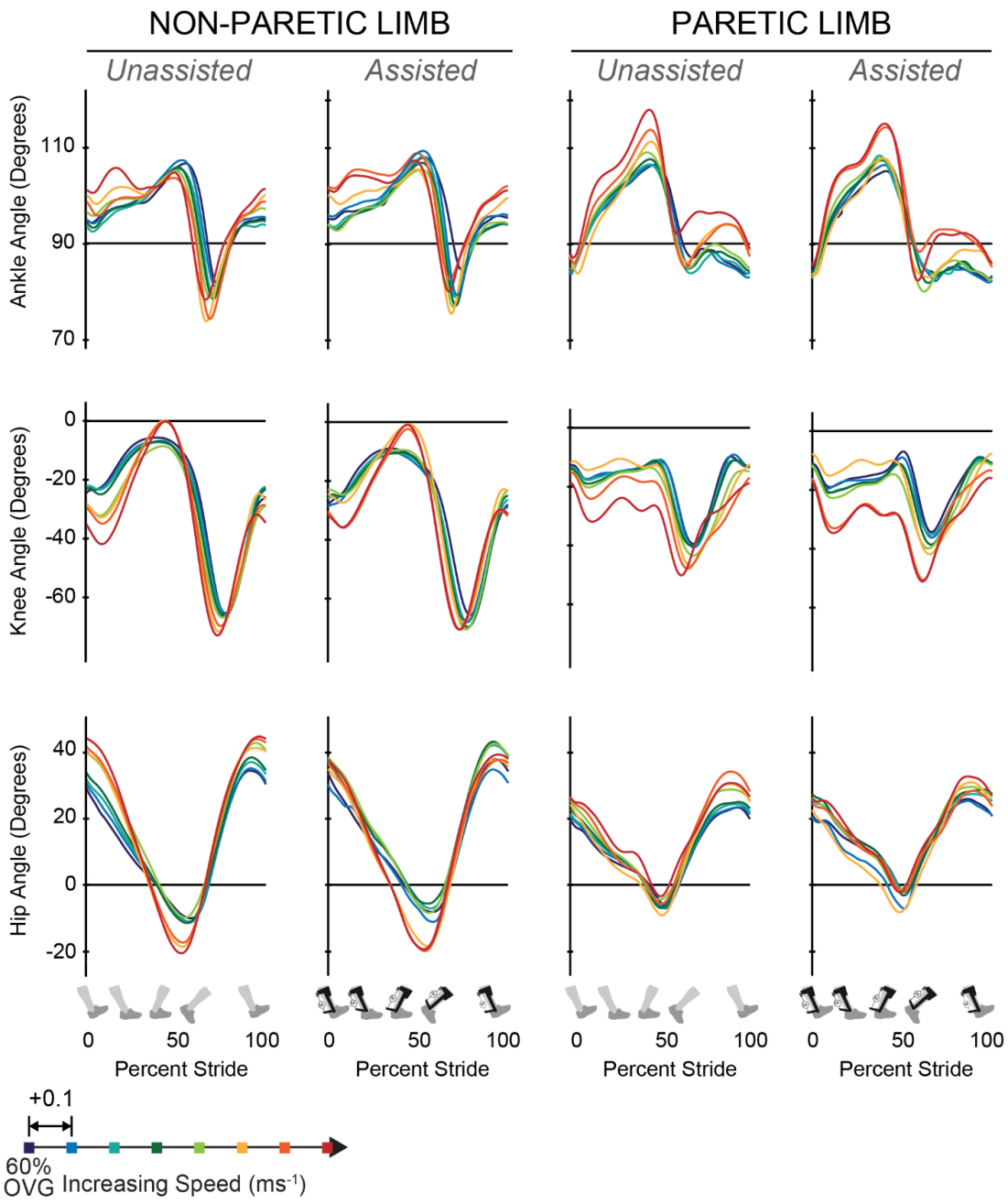


**Figure S2.1.** Joint angles.

Ankle, knee and hip joint angles for non-paretic and paretic limbs with and without exoskeleton assistance. Joint angles are calculated from subject averages and are plotted with percent stride for all walking speeds.

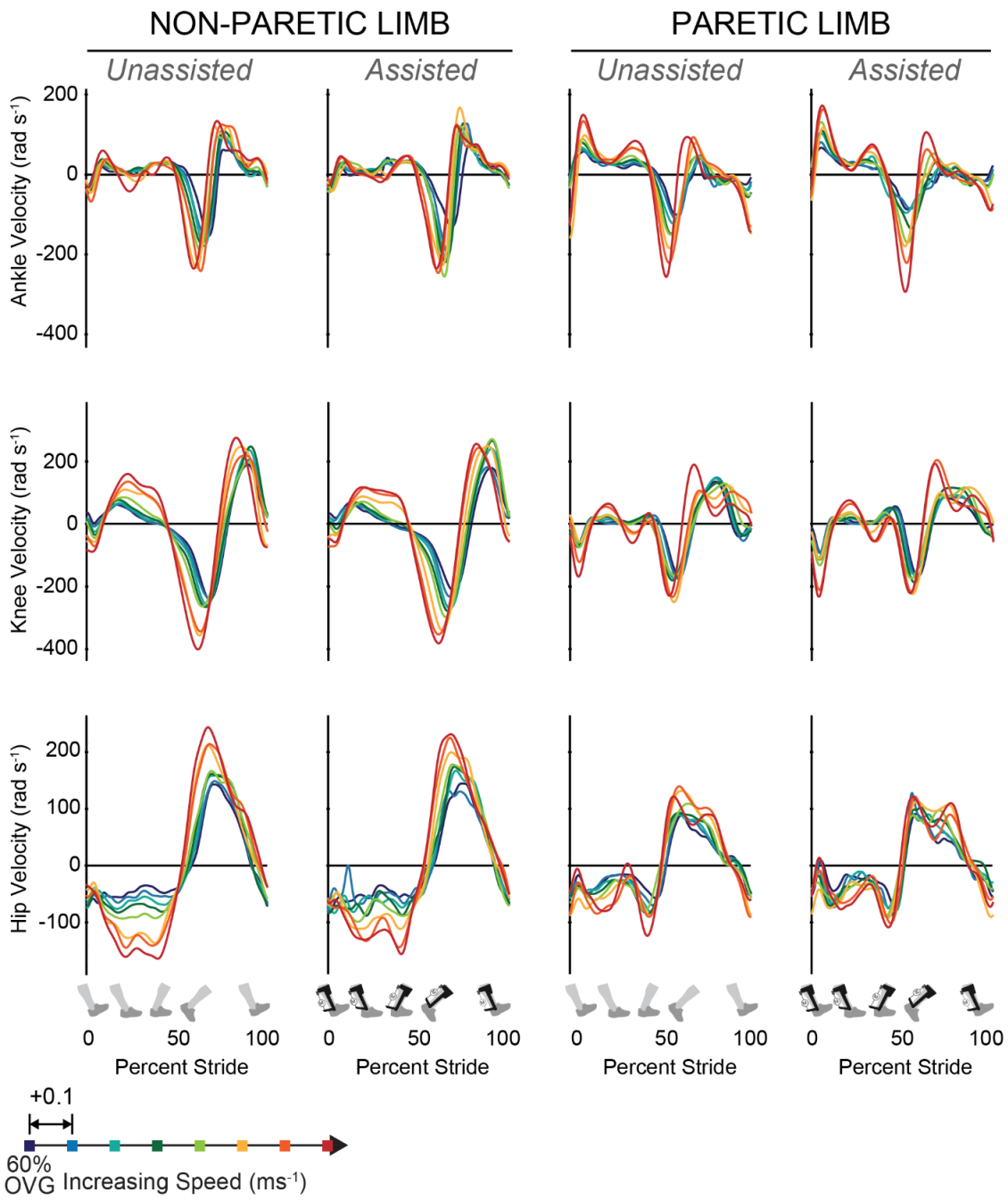


**Figure S2.2.** Joint Velocities.

Ankle, knee and hip joint velocities are shown for the non-paretic and paretic limbs with and without exoskeleton assistance. Joint velocities are calculated from subject averages and are plotted with percent stride for all walking speeds.

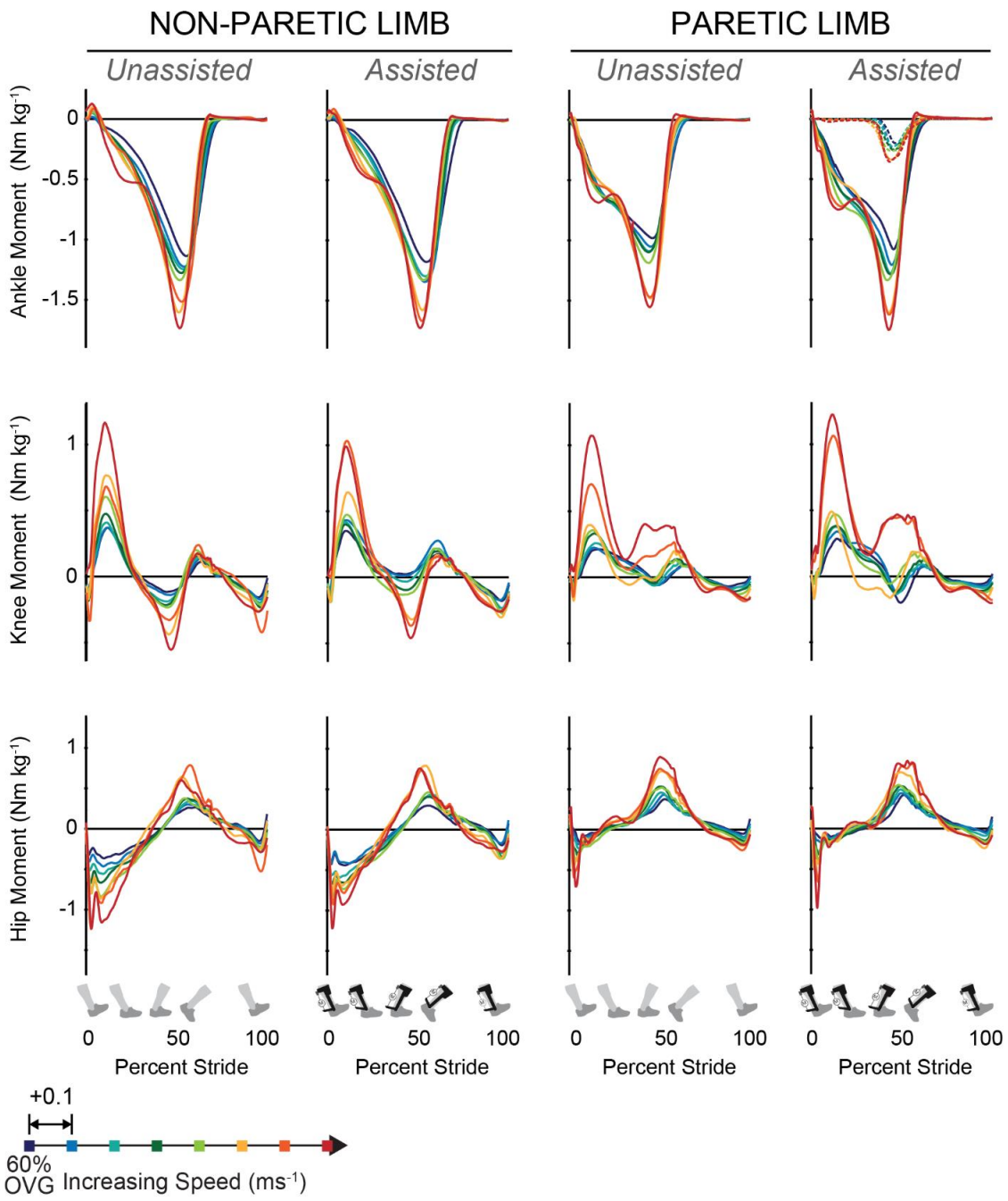


**Figure S2.3.** Joint moments.

Ankle, knee and hip joint moments are shown for the non-paretic and paretic limbs with and without exoskeleton assistance. Joint Moments are calculated from subject averages and are plotted with percent stride for all walking speeds. Exoskeleton torque is dashed.

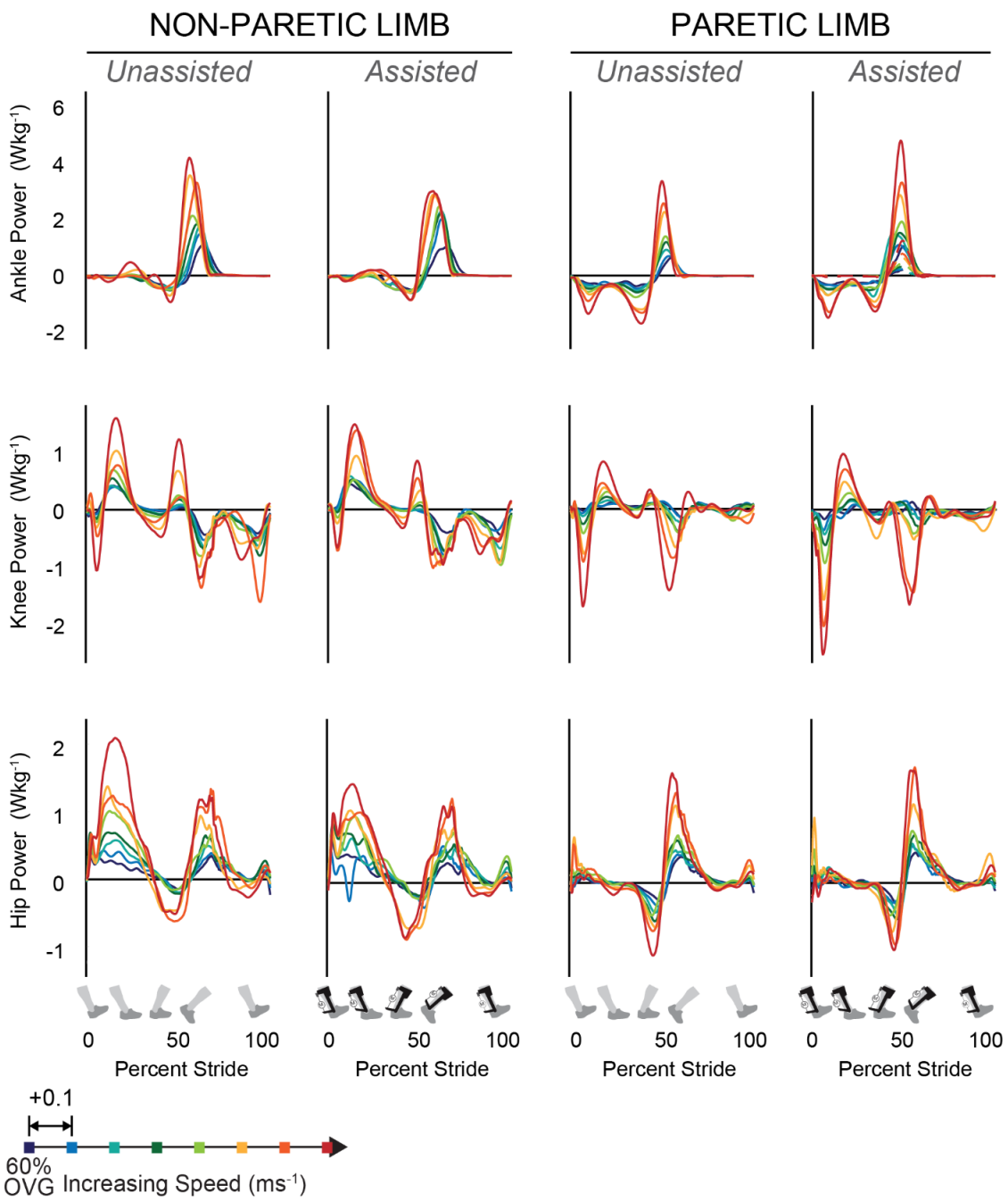


**Figure S2.4.** Joint powers.

Ankle, knee and hip joint powers are shown for the non-paretic and paretic limbs with and without exoskeleton assistance. Joint powers are calculated from subject averages and are plotted with percent stride for all walking speeds.

**Figure S2.5**. Average positive joint powers

Average positive joint powers presented as percentages of total joint contributions demonstrate the largest impact of exoskeleton assistance is increases in total (biological + exoskeleton) ankle power at five speeds when compared to the *Unassisted* condition. Rows of pie charts represent walking speed starting at n00 and increasing until the horizontally dashed line; the top row of pie charts represents positive average joint contributions at comfortable OVG speed. Pie charts represent the ankle (blue), knee (green), and hip (orange) contributions and are organized in the following columns (from left to right): 1) non-paretic joints *Unassisted* (light), 2) non-paretic joints *Assisted* (dark), 3) paretic joints *Unassisted* (light), and 4) paretic joints *Assisted* (dark). The diameter of each pie is scaled by the maximum sum of average positive joint powers (n07, non-paretic, *Unassisted*). Paired t-tests were calculated according to values of average positive joint powers rather than the contribution of a joint to the summed joint powers. Paretic: Total (biological + exoskeleton) positive paretic ankle power was significantly higher at four speeds (*n00:* p=0.038, d=1.78; *n02:* p=0.015, d=1.97; *n03:* p=0.018, d=1.73; *n04:* p= 0.009, d=2.27) as well as at comfortable OVG speed (p=0.007, d=1.46) with exoskeleton assistance. Paretic average biological ankle power was increased significantly at one speed (*n02*: p=0.047, d=1.28) with exoskeleton assistance. Lastly, average positive hip power was increased significantly at one speed (*n00*: p=0.034, d=1.18). No significant change was found in paretic average positive knee power at any speed. Non-Paretic: Average positive non-paretic ankle power increased with exoskeleton assistance at two speeds (*n02*: p=0.023, d=0.42; *n03*: p=0.012, d=0.47), and average positive non-paretic knee power decreased at one speed (*n05:* p=0.044, d=0.426).

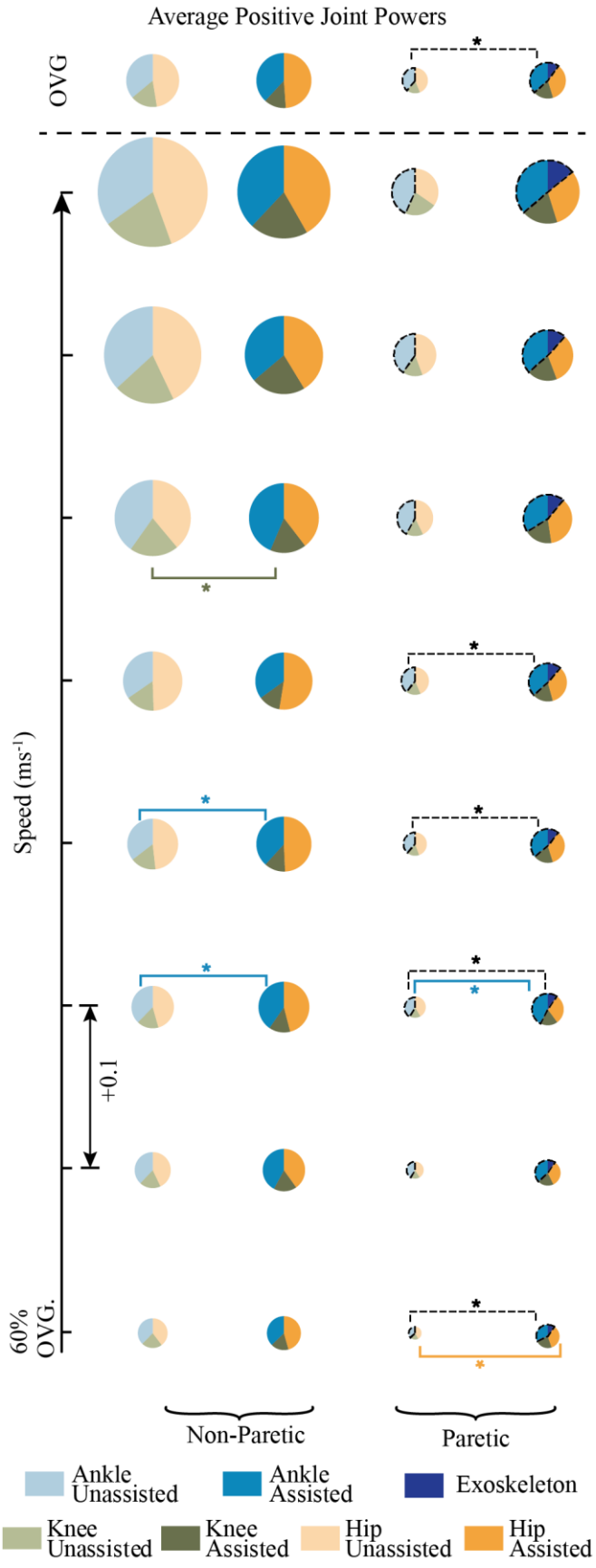
Average Positive Joint Powers
OVG
Speed (ms-1)
+0.1
60% OVG.
Non-Paretic
Paretic
Ankle Unassisted
Ankle Assisted
Exoskeleton
Knee Unassisted
Knee Assisted
Hip Unassisted
Hip Assisted

**Figure S2.6.** Average negative joint powers.

Average negative paretic joint powers showed limited changes with exoskeleton assistance across walking speeds. Pie charts are organized by speed; the first row of pie charts is calculated at 60% of each users comfortable OVG speed (n00) and speed increases each row until the dashed line. After the dashed line average negative joint powers are calculated at each user's comfortable OVG speed. Pie charts represent the ankle (blue), knee (green), and hip (orange) contributions and are organized by the following columns (from left to right): 1) non-paretic joints *Unassisted* (light), 2) non-paretic joints *Assisted* (dark), 3) paretic joints *Unassisted* (light), and 4) paretic joints *Assisted* (dark). Note that the diameters are scaled by dividing the sum of joint contributions for each pie by the maximum sum of average positive joint powers (n07, non-paretic, *Unassisted*). Although the pie charts illustrate percentage contributions from each joint t-tests were performed by comparing values for average negative joint power for the *Unassisted* and *Assisted* conditions. Paretic: The magnitude of average negative knee powers were increased at two speeds for the *Assisted* when compared to the *Unassisted* condition (n05: p=0.044, d=0.76; *OVG*: p=0.031, d=0.47). Non-paretic: The magnitude of average negative ankle power increased at one speed for the *Assisted* when compared to the *Unassisted* condition (*n03*: p=0.026, d=0.74). At a different speed, the magnitude of average negative knee powers increased for the *Assisted* when compared to the *Unassisted* condition (*OVG:* p=0.040, d=0.68).

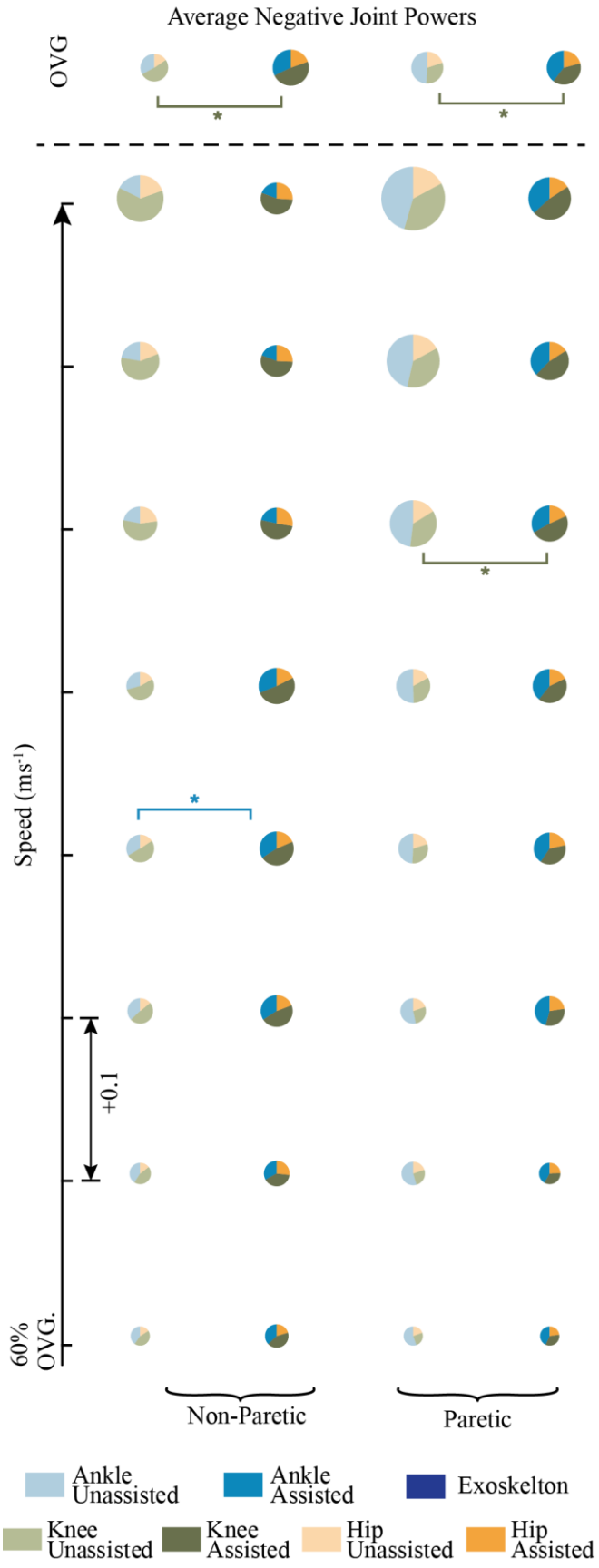
Average Negative Joint Powers
OVG
*
*
*
*
Speed (ms-1)
+0.1
60% OVG.
Non-Paretic
Paretic
Ankle Unassisted
Ankle Assisted
Exoskelton
Knee Unassisted
Knee Assisted
Hip Unassisted
Hip Assisted

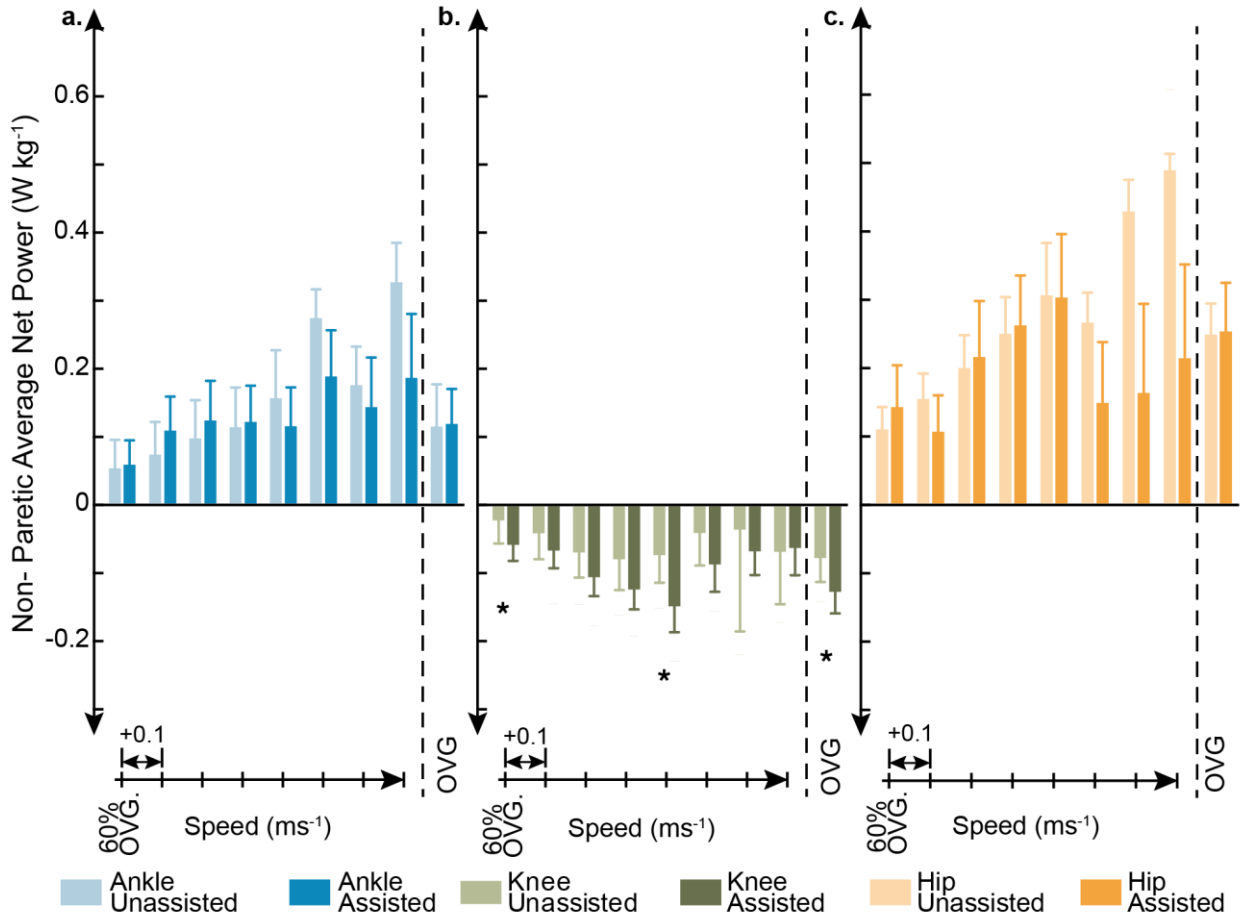


**Figure S2.7.** Non paretic Average Joint powers.

Average net non-paretic knee power was significantly reduced at three walking speeds (*n00*: p = 0.045, d =0.50; *n04*: p = 0.030, d=0.60; *OVG*: p =0.014, d=0.60). Average net non-paretic ankle (A), knee (B), and hip (C) power (± standard error) for the *Unassisted* (light colors) and *Assisted* (dark colors) conditions. All values are calculated from subject averages over five gait cycles. To the right of the dashed line average net powers averaged at each user's comfortable OVG speed are shown.

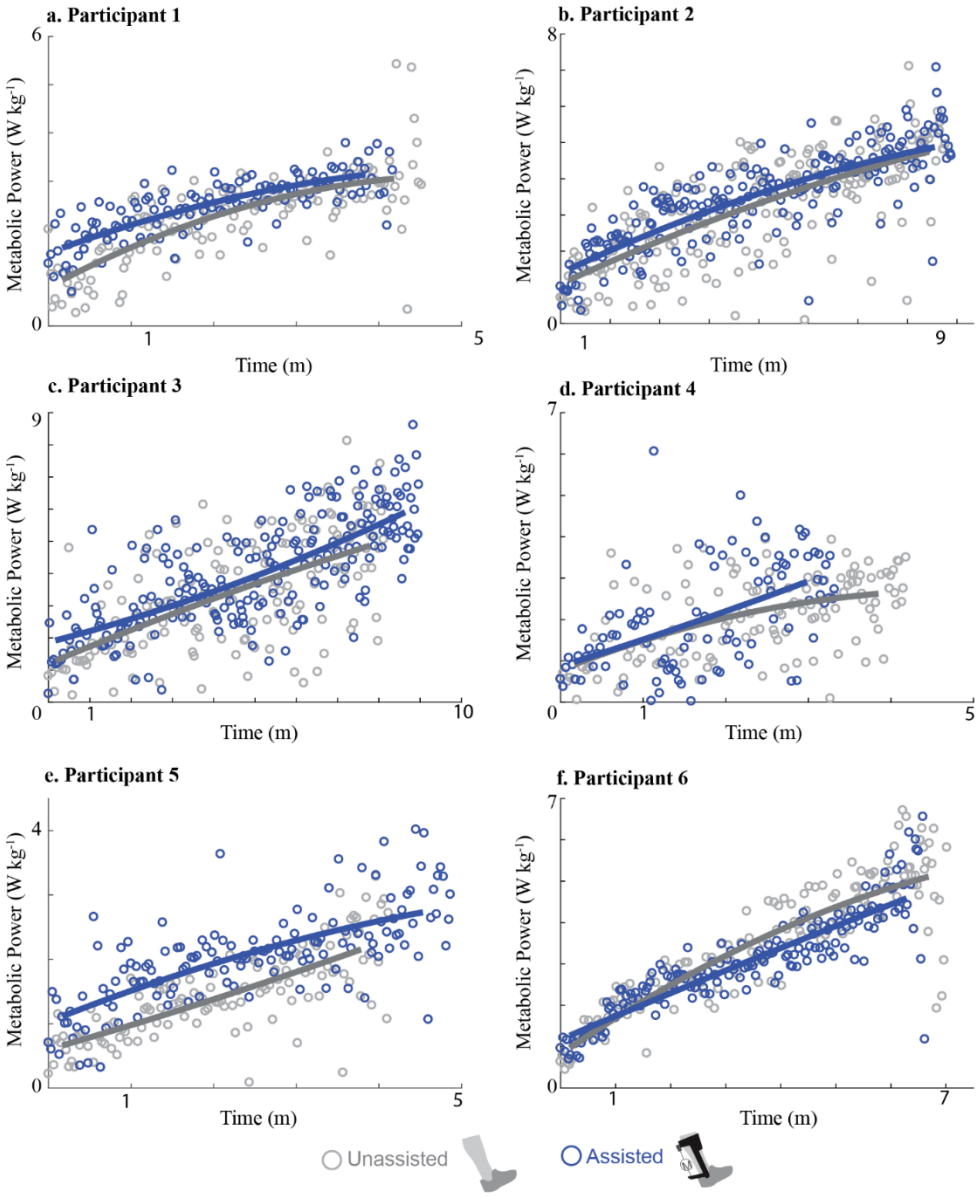


**Figure S2.8:** Participant Metabolic Powers.

Mass normalized metabolic power during each participant's *Assisted* and *Unassisted* data collection sessions. The normalized metabolic power is plotted for participants one (A), two (B), three (C), four (D), five (E), and six (F). Fit lines were generated based on a second order polynomial.

# CHAPTER 3

## Isolating the Energetic and Mechanical Consequences of Imposed Reductions in Ankle and Knee Flexion during Gait. (Published *in Journal of Neuroengineering and Rehabilitation*, 2021).

Emily M. McCain, Theresa L. Libera, Matthew E. Berno, Gregory S. Sawicki, Katherine R. Saul, Michael D. Lewek.

## Abstract

Background: Weakness of ankle and knee musculature following injury or disorder results in reduced joint motion associated with metabolically expensive gait compensations to enable limb support and advancement. However, neuromechanical coupling between the ankle and knee make it difficult to discern independent roles of these restrictions in joint motion on compensatory mechanics and metabolic penalties.

Methods: We sought to determine relative impacts of ankle and knee impairment on compensatory gait strategies and energetic outcomes using an unimpaired cohort (N=15) with imposed unilateral joint range of motion restrictions as a surrogate for reduced motion resulting from gait pathology. Participants walked on a dual-belt instrumented treadmill at 0.8 m s-1 using a 3D printed ankle stay and a knee brace to systematically limit ankle motion (restricted-ank), knee motion (restricted-knee), and ankle and knee motion (restricted-a+k) simultaneously. In addition, participants walked without any ankle or knee bracing (control) and with knee bracing worn but unrestricted (braced).

Results: When ankle motion was restricted (restricted-ank, restricted-a+k) we observed decreased peak propulsion relative to the braced condition on the restricted limb. Reduced knee motion (restricted-knee, restricted-a+k) increased restricted limb circumduction relative to the

restricted-ank condition through ipsilateral hip hiking. Interestingly, restricted limb average positive hip power increased in the restricted-ank condition but decreased in the restricted-a+k and restricted-knee conditions, suggesting that locking the knee impeded hip compensation. As expected, reduced ankle motion, either without (restricted-ank) or in addition to knee restriction (restricted-a+k) yielded significant increase in net metabolic rate when compared with the braced condition. Furthermore, the relative increase in metabolic cost was significantly larger with restricted-a+k when compared to restricted-knee condition.

Conclusions: Our methods allowed for the reproduction of asymmetric gait characteristics including reduced propulsive symmetry and increased circumduction. The metabolic consequences bolster the potential energetic benefit of targeting ankle function during rehabilitation.

## Background

Acute or chronic injuries or diseases including amputations (Adamczyk and Kuo, 2015; Houdijk et al., 2009), osteoarthritis (Creaby et al., 2012; Mills et al., 2013; Shakoor et al., 2003), or stroke (Gao and Zhang, 2008; Patten et al., 2004; Son and Rymer, 2020; Son et al., 2020) can result in unilateral lower limb impairment and lead to walking that is asymmetric (Allen et al., 2011; Little et al., 2020), requires more positive joint work (Detrembleur et al., 2003; Farris et al., 2015), and is metabolically expensive (Michael et al., 2005). Increased metabolic cost may be driven by changes in mechanical work requirements resulting from compensations for impairment of the ankle and knee (Farris et al., 2015). For example, reduced ankle function following a stroke limits propulsion (Allen et al., 2014) which may impact swing phase mechanics (Dean et al., 2020) and correlate with decreased long-term walking function (Awad et al., 2015a; Chen et al., 2005c). Alternatively, reduced knee flexion - the cornerstone of “stiff-knee gait” - results in compensatory

mechanisms including hip hiking and circumduction (Lewek et al., 2012), which can lead to reduced walking speeds and altered joint power distribution (Kerrigan et al., 2001; Stoquart et al., 2012a). Perhaps most importantly, induced weakness at both the ankle (Olney et al., 1991) and knee (Waters and Mulroy, 1999) is reported to increase the energetic cost of walking.

Therefore, a common objective of gait interventions is to alter the underlying mechanics and reduce additional work that may be associated with metabolic penalties (Awad et al., 2017b; Chen et al., 2005a; McCain et al., 2019). Unilateral impairments following a stroke are particularly challenging to treat because the impairment due to joint contractures and reduced muscle flexibility limit joint motion across multiple joints (Boffeli and Collier, 2014; Leung et al., 2014; Mulroy et al., 2010; Ong et al., 2019). *Thus, the independent roles of ankle and knee motion on compensatory mechanics and energetic cost are difficult to discern because ankle and knee motion are interrelated.* For example, persons with stiff-knee gait also present with reductions in ankle excursion and ankle power during push-off (Kerrigan et al., 2001) that limit knee joint velocity at toe-off and knee flexion during swing (Anderson et al., 2004; Piazza and Delp, 1996). Additionally, impaired limb advancement could result from either ankle or knee weakness post-stroke and lead to compensatory circumduction of the foot (Little et al., 2014; Little et al., 2018; Stanhope et al., 2014).

Understanding the metabolic penalties resulting from reduced motion at individual joints would provide insight into which rehabilitation or therapeutic interventions are likely to be metabolically advantageous. Changes in coordination patterns in persons post-stroke (Clark et al., 2010) make coaching a participant with hemiparesis to walk with ‘improved’ function of a joint impossible. Additionally, isolating the metabolic consequence of reduced joint function in persons post stroke is further complicated because the changes in motor control and muscle weakness that

result in joint impairment are difficult to manipulate. Instead, previous research has applied an ankle (Huang et al., 2015; Vanderpool et al., 2008; Wutzke et al., 2012) or knee (Akbas et al., 2019b; Lewek et al., 2012) brace in unimpaired participants to target reductions in a single joint's range of motion (ROM) to experimentally isolate the specific impacts of reduced ankle versus knee function. Bracing at the ankle resulted in the redistribution of power from the braced ankle to the ipsilateral and contralateral hips and an increase in metabolic cost (Wutzke et al., 2012). Those authors postulated that the increase in metabolic cost resulted from the transfer of power away from the ankle joint which is suited for efficient energy storage and return through the Achilles tendon (Sawicki et al., 2009). Similarly, research investigating unilateral knee bracing to simulate stiff-knee gait found increases in limb circumduction achieved through hip hiking and increased whole-body metabolic energy cost (Akbas et al., 2019b; Lewek et al., 2012).

Individually limiting ankle or knee ROM is known to be metabolically costly, but it is not clear which restriction is more detrimental, or how these restrictions interact. A synthesis of the literature suggests that restricting the ankle may be more metabolically costly than restricting the knee for several reasons. First, the ankle is responsible for more positive joint power than the knee during unimpaired walking (McGowan et al., 2008; Sawicki et al., 2009), and therefore limitations at the ankle are likely to require larger increases in positive joint power elsewhere. Second, in contrast to the ankle, during the stance phase the knee is primarily responsible for power absorption which is accomplished through negative muscle work. Because negative muscle work has a higher efficiency than positive muscle work, it is unlikely that compensations for reduced power absorptions will be as metabolically detrimental (Margaria, 1976). During swing, we expect impaired ankle and knee motion will both result in the inability to flex the limb and induce similar compensations and penalties. Finally, due in part to the elastic energy storage of the Achilles

tendon, the ankle is a more efficient producer of positive power when compared to the knee or hip (Sawicki et al., 2009; Zelik et al., 2014). Therefore, redistributing power away from the ankle to other joints is likely to increase the total cost of positive power more than redistribution from the knee to other joints (Wutzke et al., 2012). Overall, with ample research suggesting the importance of the ankle in energetic efficiency, it is reasonable to hypothesize a restriction of the ankle should result in larger increases in metabolic cost than restriction of the knee. Though previous research has begun to address metabolic impacts of restricting joints individually, no research has examined the isolated versus combined effects of reduced unilateral ankle and knee ROM on mechanical or metabolic outcomes.

The purpose of this study is to provide insight into the individual and combined effects of reduced ankle and knee range of motion on gait adaptations and metabolic consequences. We used a custom 3D printed ankle stay and knee brace to isolate the impacts of reduced unilateral ankle, knee, and ankle+knee ROM on joint and limb-level compensations and the resulting metabolic consequences. Based on findings from previous literature, we hypothesized that: (**h1**) Limiting ankle ROM would attenuate peak ankle power at pushoff, reduce peak limb propulsion and require bilateral increases in sagittal hip power to compensate, (**h2**) Limiting knee ROM would decrease knee flexion velocity at toe off, impair swing limb advancement and require increased circumduction via ipsilateral increases in frontal plane hip power, and (**h3**) the metabolic cost of compensatory mechanics resulting from restricting ankle ROM would be larger than the cost of compensations from restricting knee ROM.

## Methods

### Data Collection

The institutional review board (IRB) at the University of North Carolina at Chapel Hill approved all procedures, and all participants signed an IRB approved consent form prior to data collection. Data were recorded for 15 (7M/8F) healthy participants (age: 24.2±3.0 yrs.; height: 1.75±0.13 m; mass: 75.5±15.7 kg) walking at 0.8 m $s^{-1}$ on an instrumented split-belt treadmill (Bertec, Columbus, OH, USA). We selected this speed because it is within the range of speeds reported for persons post-stroke (Mahon et al., 2015; McCain et al., 2019), allowed ambulation with bracing restricting both the ankle and knee of simultaneously, and was sufficiently fast to allow for the detection of potential metabolic differences between conditions. Participants completed five conditions, each lasting seven minutes, including: (1) control [***control***]: no brace worn, (2) braced [***braced***]: knee brace worn but unrestricted, and three restricted conditions: (3) unilaterally restricted ankle [***restricted-ank***], (4) unilaterally restricted knee [***restricted-knee***], and (5) unilaterally restricted ankle + knee [***restricted-a+k***]. Joint bracing was achieved with a custom 3D printed ankle stay placed on the dorsum of the foot/ankle and a donJoy T-ROM knee brace (DJO Global, Inc, Vista, CA, USA). Knee bracing was worn unrestricted on both limbs in the *braced* and *restricted-ank* conditions. In the *restricted-knee* and *restricted-a+k* conditions, knee bracing was worn on both limbs but only restricted unilaterally. We applied lightweight ankle stays unilaterally for the *restricted-ank* and *restricted-a+k* conditions and removed them for all other walking conditions. The order of the *braced, restricted-ank, restricted-knee,* and *restricted-a+k* conditions was randomized, but the *control* condition was performed last to prevent the need for multiple marker placements per data collection. Participants wore a fall harness with no body weight support and the only instruction provided to participants was to avoid using handrails when

possible. Any use of the handrails was noted by the data collection team and walking data from that timeframe was excluded from the analysis. During all conditions, we recorded rates of oxygen consumption and carbon dioxide production using a portable metabolic system (K5, Cosmed, Chicago, IL). Prior to walking trials, we collected five minutes of quiet standing to obtain baseline metabolic energy consumption. An eight-camera motion capture system (Vicon, Oxford, UK), sampling at 120 Hz, recorded the positions of 42 reflective markers attached to the pelvis and lower limb (similar marker set to (Farris et al., 2015; McCain et al., 2019)). Marker locations in 3D space were filtered with a 6 Hz Butterworth filter in OpenSim software (Delp et al., 2007). We recorded ground reaction forces (GRFs) recorded at 1200 Hz using the fully instrumented dual-belt treadmill. GRFs were filtered using a second order low pass Butterworth filter with a cutoff frequency of 25 Hz.

**Data Processing**

Data were post-processed and initial kinematic and kinetic analyses were performed in OpenSim using a full-body model (Rajagopal et al., 2016) adapted to represent the lower limb and scaled to each participant's anthropometry using marker locations taken during a static trial. The resulting model had six degrees of freedom describing the pelvis and six degrees of freedom per leg including three degrees of freedom at the hip, and one degree of freedom at the knee, ankle, and subtalar joints. We determined lower limb joint angles and pelvic list from filtered marker data and individual models using an inverse kinematics algorithm (Thelen and Anderson, 2006). The inverse dynamics and analysis tools in OpenSim were used to determine joint angular velocities, moments, and powers in the sagittal and frontal plane for the hip, in the sagittal plane for the knee and ankle and in the frontal plane for the subtalar joint. We calculated joint range of motion (ROM) across the gait cycle as the difference between maximum and minimum joint angle values (Wutzke

et al., 2012). The max anterior GRF between 40 and 70% of gait cycle was identified as the peak propulsive force and normalized by participant mass. We calculated limb circumduction as the maximum lateral deviation from the path of progression of the foot during swing (Chen et al., 2005c; Tyrell et al., 2011). Sections of anteriorly directed GRFs were integrated using the trapezium method for both limbs; propulsive symmetry was determined by dividing the contribution from the restricted limb by the sum of unrestricted and restricted limb integrated anterior GRFs. In the *braced* condition, we used the left limb in place of the restricted limb so that for any condition 50% propulsive symmetry would indicate symmetry (McCain et al., 2019; Peterson et al., 2010b). We determined joint kinematics and kinetics, pelvic list, circumduction, peak propulsion, and propulsive symmetry for 10 gait cycles, then averaged across gait cycles for each participant and trial. Pelvic list was found over the 10 gait cycles of the restricted limb for all restricted conditions, and for the left limb in the *braced* condition. Gait cycles were consecutive and selected from the last two minutes of walking in each condition by identifying and removing gait cycles bordering crossover steps and selecting the 10 consecutive gait cycles closest to the end of the two minutes from the remaining data.

We calculated average positive and negative joint mechanical power at the ankle, knee and hip as described previously (Farris et al., 2015; McCain et al., 2019). Briefly, the time series lower-limb joint mechanical power (watts vs. time) for each lower-limb joint was integrated in positive and negative intervals over ten gait cycles to determine mechanical work over a cycle for ankle, knee and hip (J). Gait cycle average positive and negative joint powers (W $kg^{-1}$) were calculated by dividing the work (J) by the corresponding stride time interval (s) and normalized to each participant's mass (kg). To isolate the impact of the brace conditions, we calculated the difference in average powers (Δaverage positive joint power) for restricted conditions relative to the *braced*

condition. The total average positive joint powers were determined by summing joint powers from both limbs per gait cycle. Again, to isolate the impact of the brace conditions, we calculated the difference in total average positive joint power (Δtotal average positive joint power) for the restricted conditions relative to the *braced* condition.

We calculated metabolic powers from rates of oxygen consumption and carbon dioxide production during the last two minutes of each condition and quiet standing using a standard approach (Brockway, 1987). The net metabolic rate was determined by subtracting metabolic power of quiet standing from the metabolic power of each condition and normalizing by participant mass. To isolate the impact of the bracing conditions, we analyzed the change in metabolic rate (Δnet metabolic rate) relative to the *braced* condition. In order to evaluate the relationship between the metabolic and mechanical impacts of limiting joint ROM, the delta efficiency of positive work was computed as the linear relationship between Δnet metabolic rate and Δtotal average positive joint mechanical powers (Farris et al., 2015).

**Statistical Analyses**

We performed one-way (walking condition) repeated measures (participants) reduced maximum likelihood (REML) analysis using the PROC MIXED method in SAS statistical modeling software to determine if the walking condition was a significant factor for each outcome. In the absence of missing values, this method gives the same P values and multiple comparisons tests as repeated measures ANOVA. We inspected the normality of the residuals using a Q-Q plot generated by the SAS model described above. For any outcome measures without clearly discernable linear trends in the Q-Q plot we further investigated the normality of the residuals using Shapiro-Wilkes analysis using the PROC UNIVARIATE method. Only one outcome measure was not normally distributed. To remedy this, we used the PROC ROBUSTREG method

is SAS to test for outliers, and after removing one outlier we performed another Shapiro Wilkes analysis to confirm normality and ran paired t-tests. For outcome measures that are presented relative to the *braced* condition (Δsagittal plane average positive hop power, Δfrontal plane average positive hip power, Δmetabolic cost, and Δtotal average positive joint power) we made three comparisons including: 1) *locked-ank* vs *locked-knee*, 2) *locked-ank* vs *locked-a+k*, and *3*) *locked-knee* vs *locked-a+k*. For all other data, we made the following six comparisons: 1) *braced* vs *locked-ank*, 2) *braced* vs *locked-knee*, 3) *braced* vs *locked-a+k*, 4) *locked-ank* vs *locked-knee*, 5) *locked-ank* vs *locked-a+k*, and 6) *locked-knee* vs *locked-a+k* conditions. We corrected used a Bonferroni correction for multiple comparisons. We determined the significance of a linear correlation between using Pearson's linear correlation coefficient only after confirming normality of the variables plotted.

## Results

We first sought to establish whether restricting joint ROMs had the intended effect on the target joints. We subsequently assessed each respective hypothesis regarding the effect of ankle and knee restriction on compensatory mechanics. Finally, we evaluated our final hypothesis regarding Δnet metabolic rate in response to imposed joint restrictions.

**Locked Limb Ankle Angle, Velocity, and Power**: Walking condition significantly impacted restricted limb ankle range of motion (ROM), restricted limb ankle minimum velocity during pushoff, and peak restricted limb ankle power (all $p<0.001$). (1): Ankle ROM (Figure 3.1A, Figure S3.1) was significantly reduced in the restricted-ank, (16.9787°±3.59°; $p<.0001$), restricted-knee (17.96°±3.67°; $p<.0001$), and restricted-a+k (14.61°±3.78°; $p<.0001$) conditions when compared to the braced (24.11°±5.06°) condition. We also found significant reductions in ankle ROM for the restricted-a+k condition when compared to the restricted-knee ($p=0.002$) condition.

(2) Minimum restricted limb ankle velocity during pushoff (Figure 3.1B, Figure S3.2) was significantly reduced in the restricted-ank, (-145.43±43.06 deg s-1; p<.0001) restricted-knee (-152.40±41.55 deg s-1; p<.0001), and restricted-a+k (-130.38±37.68 deg s-1; p<.0001) conditions when compared to braced (-215.73± 46.78 deg s-1) condition. (3) Peak restricted limb ankle power: We observed significant reductions in peak restricted limb ankle power (Figure 3.1C, Figure S3.4) in the restricted-ank (1.31±0.53 W kg-1) when compared to the restricted-knee (1.66 ±0.64 W kg-1; p=0.012) or braced (1.94±0.69 W kg-1; p<.0001) conditions. Peak restricted limb ankle power was also reduced in the restricted-a+k (1.35±0.53 W kg-1) when compared to the restricted-knee (p = 0.038) or braced (p <0.0001) conditions.

**Figure 3.1.** Ankle and knee joint angles, velocities, and powers.

Bracing at the ankle and knee limits subject average (N=15) joint ROM, velocity, and mechanical power. Conditions with any restriction of joint motion (*restricted-ank, restricted-knee, restricted-a+k)* show (A) reduced ankle ROM and (B) reduced magnitudes of peak ankle velocity during pushoff when compared to the *braced* condition. In the *restricted-a+k* condition ankle ROM decreased in comparison to the *restricted-knee*. (C) Peak ankle power decreased in all conditions with ankle restriction (*restricted-ank, restricted-a+k)* when compared to other conditions (*braced, restricted-knee)*. (D) Knee ROM decreased in all conditions with restriction of joint motion (*restricted-ank, restricted-knee, restricted-a+k)* when compared to the *braced* condition, and was further reduced in conditions bracing the knee (*restricted-knee, restricted-a+k)* when compared to the *restricted-ank* condition. All conditions with knee bracing had reduced knee joint velocity at toe off (E) when compared to the *braced* and *restricted-ank* conditions, and the magnitude of peak knee joint power absorption (F) at pushoff was decreased in the *restricted-knee* condition when compared to *restricted-ank* and *braced* conditions. Asterisks indicate a statistically significant difference (post-hoc paired t-test with Bonferroni correction for multiple comparison, $p < 0.05$).

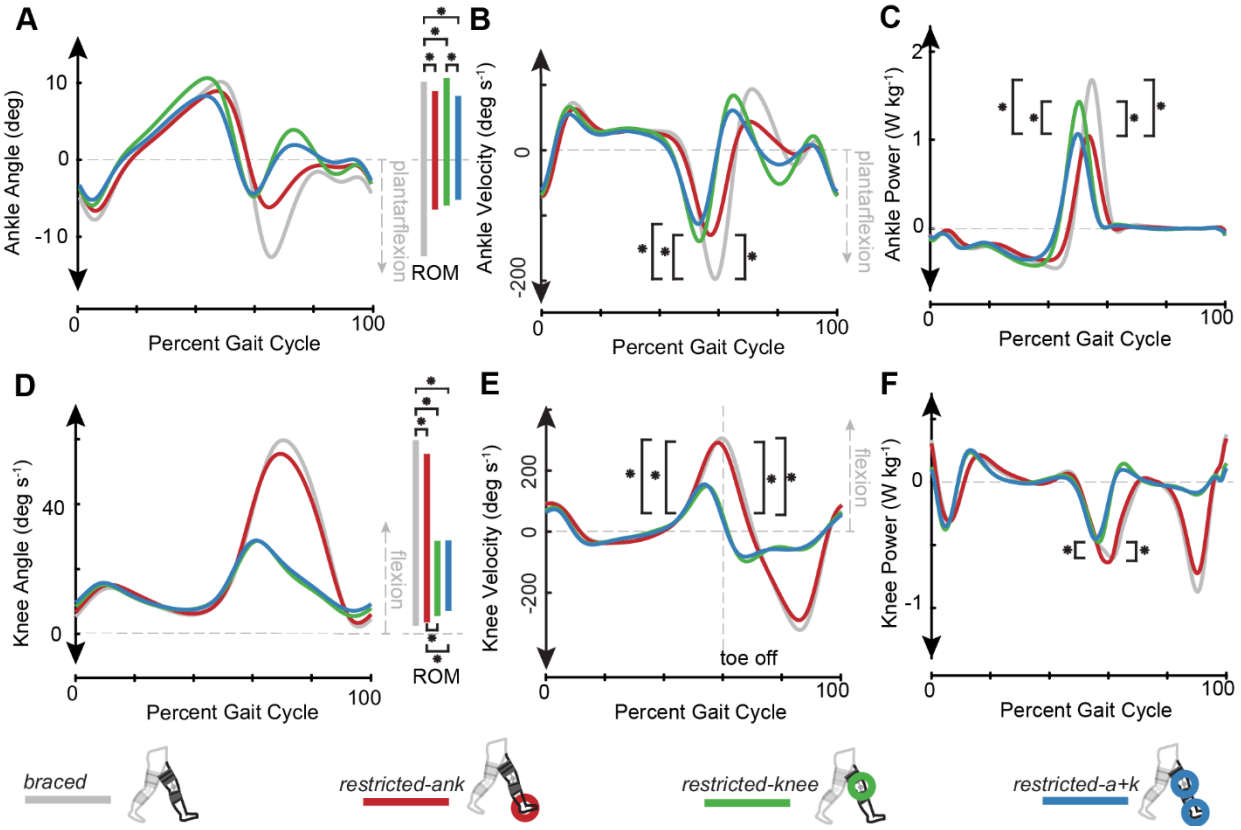
A
Ankle Angle (deg)
10
0
-10
0
100
Percent Gait Cycle
plantarflexion
ROM
B
Ankle Velocity (deg s-1)
0
-200
0
100
Percent Gait Cycle
plantarflexion
C
Ankle Power (W kg-1)
2
1
0
0
100
Percent Gait Cycle
D
Knee Angle (deg s-1)
40
0
0
100
Percent Gait Cycle
flexion
ROM
E
Knee Velocity (deg s-1)
200
0
-200
toe off
0
100
Percent Gait Cycle
flexion
F
Knee Power (W kg-1)
0
-1
0
100
Percent Gait Cycle
braced
restricted-ank
restricted-knee
restricted-a+k

**Locked Limb Knee Angle, Velocity, and Power.** Walking condition had a significant effect on restricted limb knee joint ROM ($p<0.0001$), restricted limb knee flexion velocity at toe off ($p<0.0001$), and restricted limb knee power absorption during pushoff ($p=0.0004$). We found significant reductions in (1) restricted limb knee ROM (Figure 3.1D, Figure S3.1) in all three braced conditions (restricted-ank:53.23°±5.66°, $p=0.01$, restricted-knee: 4.84°±4.14°, $p<0.0001$, restricted-a+k: 24.22°±5.82°; $p<0.0001$) when compared to the braced condition (58.55°±3.85°). Further, reductions in restricted limb knee ROM were present in the restricted-knee and restricted-a+k conditions ($p<0.001$) when compared to the restricted-ank condition. We found significant reductions in (2) restricted limb knee flexion velocity at toe off (Figure 3.1E, Figure S3.2) in the restricted-knee (48.34±58.88 deg s-1, $p<0.0001$) and restricted-a+k (33.03±82.86 deg s-1, $p<0.0001$) conditions when compared to the braced (305.25±44.16 deg s-1) condition. When compared to the restricted-ank (278.48 ± 48.19 deg s-1) condition, we found significant reductions in restricted limb knee flexion velocity at toe off in the restricted-knee ($p<0.0001$) and restricted-a+k ($p<0.0001$) conditions. (3) restricted limb knee power absorption (Figure 3.1F, Figure S3.4) during pushoff was larger in the braced (-0.7681±0.23 W kg-1, $p=0.020$) and restricted-ank (-0.825±0.200 W kg-1, $p=0.0003$) conditions when compared to the restricted-knee condition (-0.6433±0.18 W kg-1). All joint angles, velocities, moments, and powers are reported in Figs. S1, S2, S3, and S4, respectively.

**Peak restricted Limb Propulsion:** Walking condition had a significant effect on peak propulsion of the restricted limb ($p<0.0001$) (Figure 3.2A). Post-hoc analysis revealed restricted limb peak propulsion was significantly decreased in the restricted-ank (1.45±0.25 N kg-1, $p=0.0011$) and restricted-a+k (1.52±0.20 N kg-1, $p=0.040$) conditions when compared to the

braced (1.68±0.16 N kg-1) condition. Although limb propulsion decreased in the restricted-knee condition (1.54±0.18 N kg-1) when compared to braced, this change was not significant (p=0.094).

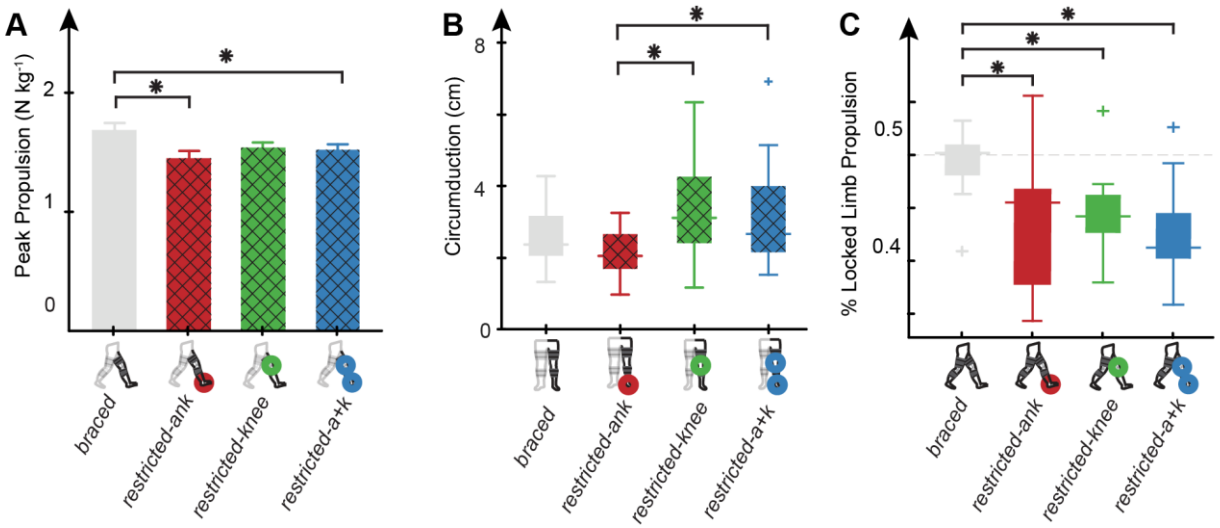


**Figure 3.2.** Peak limb propulsion, circumduction and %Locked limb propulsion.

Joint level restrictions propagated to limb-level changes in peak propulsion, circumduction, and %locked limb propulsion. Conditions with ankle restriction (*restricted-ank, restricted-a+k)* show decreased (A) subject averaged (N=15) peak propulsion on the restricted limb when compared to the *braced* condition. Error bars are mean+s.e.m.. Limited knee flexion in the *restricted-knee* and *restricted-a+k* conditions resulted in increased (B) subject averaged (N=15) circumduction when compared to the *restricted-ank* condition. Error bars are mean±s.d. Any restriction of joint motion (*restricted-ank, restricted-knee, restricted-a+k)* resulted in a reduction in (C) subject averaged (N=15) propulsive symmetry when compared to the *braced* condition. Error bars are mean±s.d. Black hatched lines were used for data calculated on the restricted limb in one of the three restricted conditions. Asterisks indicate a statistically significant difference (post-hoc paired t-test with Bonferroni correction for multiple comparison, $p < 0.05$).

**Propulsive Symmetry**: Walking condition had a significant effect on propulsive symmetry (Figure 3.2C, $p<0.0001$). We found that all restricted conditions (restricted-ank: 44.1±6.6 %, $p=0.0002$; restricted-knee: 44.4±3.8 %, $p=0.0006$; restricted-a+k: 42.3±4.43 %, $p<.0001$) exhibited a reduction in the propulsive symmetry compared to the braced (49.5 ± 2.92%) condition.

**Locked Limb Circumduction:** On the restricted limb, the braced conditions had a significant effect on circumduction values ($p=0.0032$). restricted limb circumduction (Figure 3.2B) was significantly higher in the restricted-knee (3.35±1.29 cm, $p=0.005$) and restricted-a+k (3.19±1.50 cm, $p = 0.02$) conditions when compared to the restricted-ank (2.10±0.65 cm). There was no significant difference between the braced condition and any of the restricted conditions. Walking condition did not have a significant effect on the unrestricted limb's circumduction ($p=0.715$).

**ΔAverage Positive Hip Joint Power**: Walking condition had a significant effect ($p =0.0003$) on restricted limb sagittal Δaverage positive hip power. We found significant increases in sagittal Δaverage positive hip power (Figure 3.3A) in the restricted-ank (0.009±0.017 W kg-1) condition when compared to the restricted-knee (-0.030±0.034 W kg-1, $p=0.001$) or the restricted-a+k (-0.025±0.031 W kg-1; $p=0.003$) conditions. Walking condition did not have a significant effect ($p=0.83$) on restricted limb frontal Δaverage positive hip power. Walking condition did not have a significant effect on unrestricted limb sagittal ($p = 0.19$) or frontal plane ($p=0.062$) Δaverage positive power. While there was no significant change between conditions, the Δaverage positive frontal plane hip power (Figure 3.3B) on the unrestricted limb was negative for all conditions.

**Pelvic List:** Walking condition had a significant effect ($p<0.001$) on minimum pelvic list in early swing (55-70% of gait cycle). We found a significant decrease in minimum pelvic list magnitude (Figure 3.3C) during swing in the restricted-knee (-2.92±2.35°) condition when

compared to the braced (-5.30±3.08°;p=0.0008) and restricted-ank (-4.18±2.51°;p=0.010) conditions. Similarly, minimum pelvic list magnitude decreased in the restricted-a+k (-2.07±2.64°) condition when compared to the restricted-ank (p=0.0001) and braced (p<0.0001) conditions.

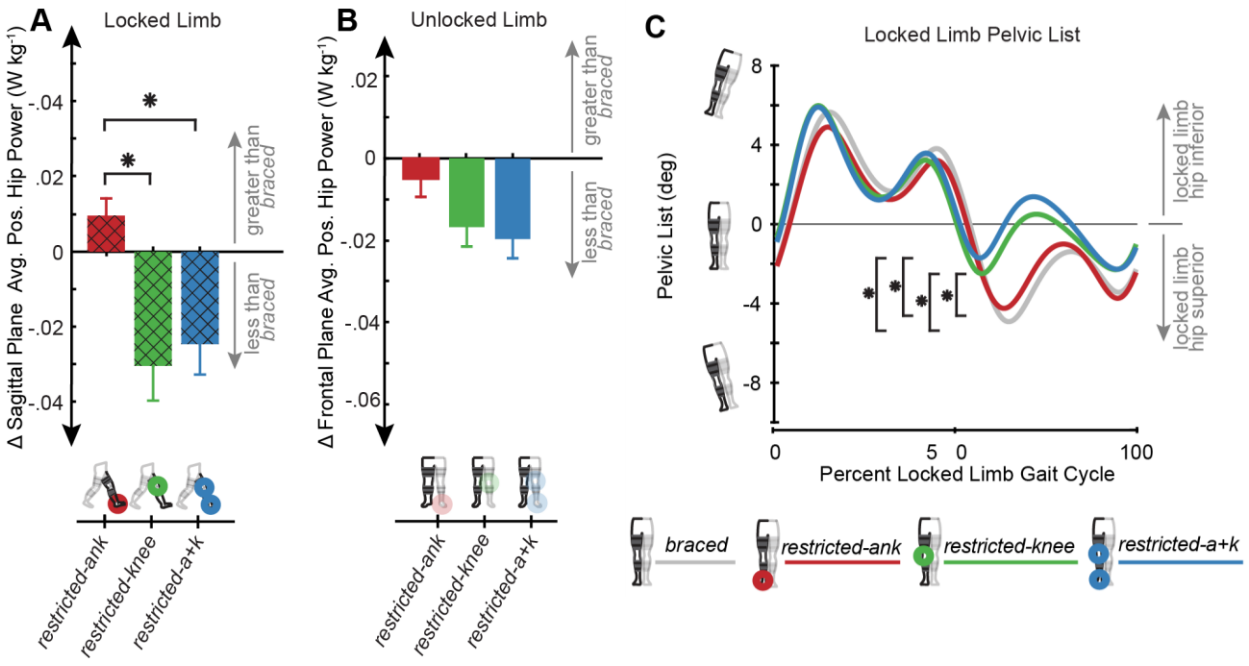


**Figure 3.3.** ΔSagittal and ΔFrontal plane hip powers and pelvic list \

Significant impact of joint restrictions on Δsagittal plane average positive hip power and pelvic list. In the sagittal plane we see increases in (A) subject averaged (N=15) restricted limb Δaverage positive hip powers in the *restricted-ank* condition compared to the *restricted-knee* and *restricted-a+k* conditions. Error bars are mean ± s.e.m. In the frontal plane of the unrestricted limb we saw a decreased (B) subject averaged (N=15) Δaverage positive hip power values in all conditions. Error bars are mean ± s.e.m. (C) subject averaged (N=15) pelvic list was shifted upward in the swing phase in the *restricted-knee* and *restricted-a+k* conditions when compared to the when the knee was immobilized to accomplish foot circumduction without increasing frontal plane hip power. Black hatched lines were used for data calculated on the restricted limb in one of the three restricted conditions. Asterisks indicate a statistically significant difference (post-hoc paired t-test with Bonferroni correction for multiple comparison, $p < 0.05$).

**Net Metabolic Rate:** Walking condition had a significant effect on net metabolic rate (Figure 3.4A, $p<.0001$). We determined the restricted-ank (3.59±0.81 W kg-1, $p=0.0006$) and restricted-a+k (3.77±0.71 W kg-1, $p<0.0001$) conditions were significantly more metabolically expensive than the braced condition (3.13±0.72 W kg-1), and the restricted-a+k was significantly more expensive than the restricted-knee (3.59±0.81 W kg-1, $p=0.0092$). Walking condition also had a significant ($p = 0.0018$) effect on Δnet metabolic rate (Figure 3.4B). Δnet metabolic rate in the restricted-a+k (0.64±0.46 W kg-1) condition was significantly higher than restricted-knee (0.28±0.28 W kg-1, $p =.001$) condition. The Δnet metabolic rate in the restricted-ank (0.46±0.61 W kg-1) condition was not significantly different from the restricted-knee condition ($p=0.17$).

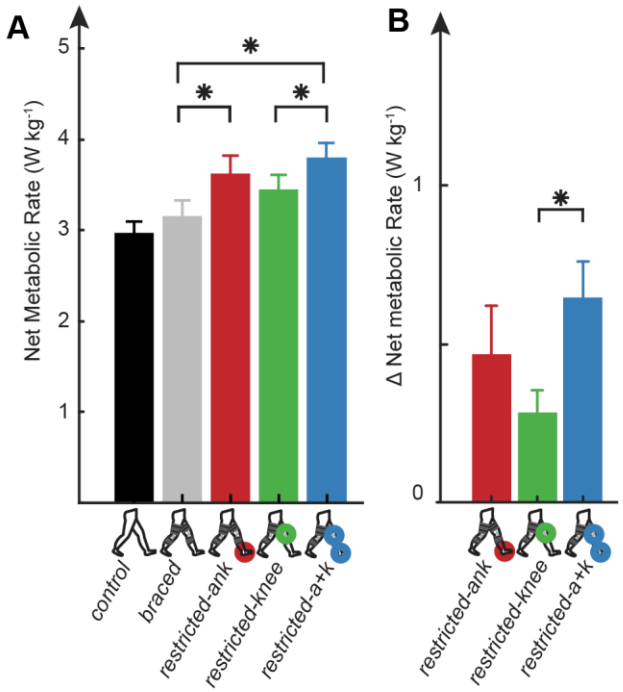


**Figure 3.4.** Net metabolic rate and Δnet metabolic rate.

Ankle restriction increases net metabolic rate and Δnet metabolic rate. (A) The subject averaged (N=15) net metabolic rate increased in all conditions with ankle restriction when compared to the *braced* condition, and the simultaneous restriction of the ankle and knee was more expensive than the restriction of the knee in isolation. The subject averaged (N=15) (B) Δnet metabolic rate increased significantly in the *restricted-a+k* condition when compared to the *restricted-knee* condition. All (A,B) error bars are mean ± s.e.m. Asterisks indicate a statistically significant difference (post-hoc paired t-test with Bonferroni correction for multiple comparison, $p < 0.05$).

**Total Average Positive Joint Power:** Walking condition had a significant effect on total average positive joint power (Figure 3.5A, p=0.0008). The total average positive joint power was significantly lower in the restricted-knee (0.848 ± 0.22 W kg-1; p=0.003) and restricted-a+k (0.832 ± 0.22 W kg-1 ;p=0.0002) conditions when compared to the braced (0.917 ± 0.215 W kg-1)

condition. Further, we found a reduction in total average positive joint powers in the restricted-a+k condition compared to the restricted-ank (0.89 ± 0.22 W kg-1, p=0.024) condition. The distribution of positive and negative joint powers for all conditions are included in Figure S3.5.

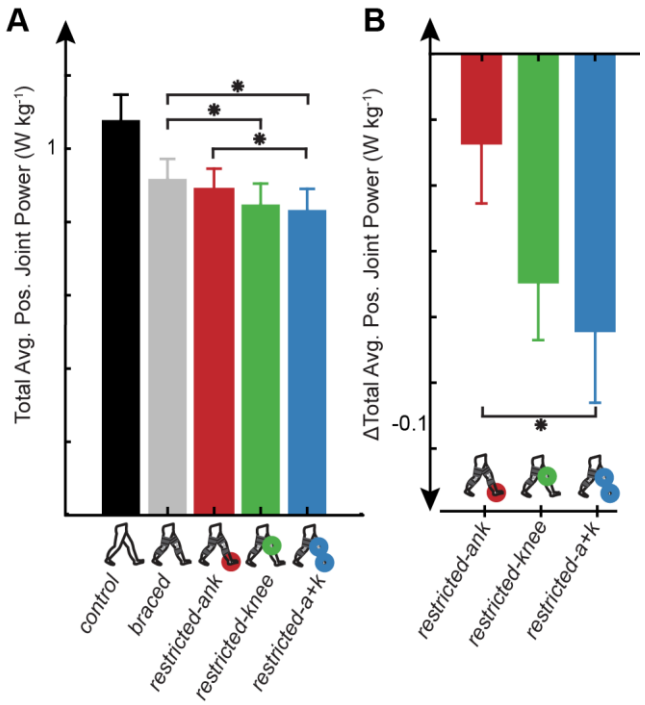


**Figure 3.5**. Total average positive joint power and Δtotal average positive joint power.

Total average positive joint power tends to decrease and Δtotal average positive joint power. Restriction of the knee (restricted-knee, restricted-a+k) resulted in reduced (A) subject averaged (N=15) total average positive joint power compared to the braced condition, `and the restricted-a+k condition was significantly reduced in comparison to the restricted-ank condition. The (B) subject averaged (N=15) Δtotal average positive joint power in the restricted-a+k condition was significantly more negative than the Δtotal average positive joint power in the restricted-ank condition. All (A,B) error bars are mean ± s.e.m. Asterisks indicate a statistically significant difference (post-hoc paired t-test with Bonferroni correction for multiple comparison, $p < 0.05$).

**ΔTotal Average Positive Joint Power**: Walking condition also had a significant effect on the Δtotal average positive joint power (Figure 3.5B, p =0.041). The Δtotal average positive joint power was significantly more negative in the *restricted-a+k* (-0.085 ± 0.083 W kg$^{-1}$; p=0.01) condition when compared to the *restricted-ank* (-0.028 ± 0.69 W kg$^{-1}$) condition.

**Correlation between ΔTotal Average Joint Power and ΔNet Metabolic Power:** No significant correlation (p = 0.143) was found between the Δnet metabolic power and Δtotal average positive joint power (Figure 3.6).

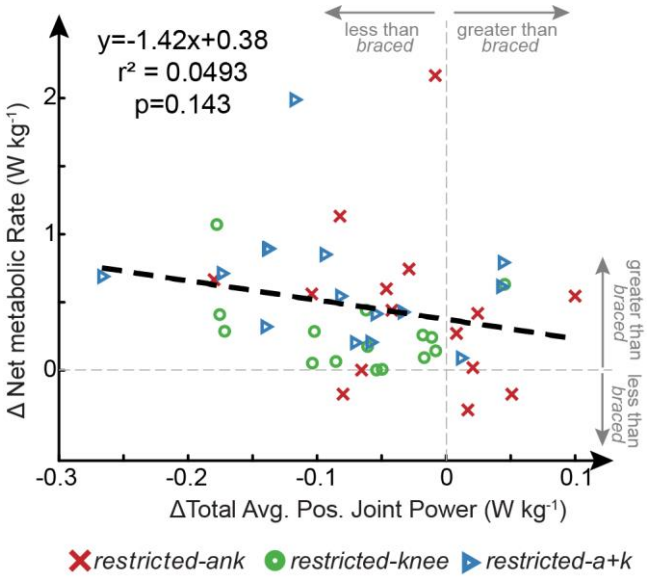


**Figure 3.6**. ΔTotal average positive joint power versus Δnet metabolic rate.

The subject averaged (N=15) Δnet metabolic rate and Δtotal average joint power show no statistically significant correlation and appear to have a negative correlation indicating that positive work is not an appropriate estimate of metabolic cost in atypical gait. No significant linear correlation was found using Pearson's linear correlation coefficient.

## Discussion

Our approach successfully achieved unilateral, joint-specific restrictions in range of motion (ROM) in an isolated fashion at the ankle, knee, and ankle+knee simultaneously. This framework allowed us to separate the relative impact of ankle versus knee restriction and understand their interaction on mechanical compensations and the resultant energetic penalties during walking. This research builds upon previous studies in which the ankle (Wutzke et al., 2012) or knee (Lewek et al., 2012) were braced independently. These results can help optimize future designs of rehabilitative techniques and technology by providing insight into trade-offs of intervening at one lower-limb joint versus another.

In support of our first hypothesis, the use of our custom 3D-printed ankle stay produced a reduction in ankle ROM, which in turn attenuated peak ankle power at pushoff (Figure 3.1 A,C) and reduced peak restricted limb propulsion (Figure 3.2A). Specifically, when the ankle was restricted, with or without locking the knee, we observed reductions in both peak ankle power and peak limb propulsion. In contrast, locking the knee did not lead to a reduction in peak propulsion (Figure 3.2A), providing further evidence that ankle impairments alone may be responsible for commonly observed propulsive deficits in pathologic gait.

We hypothesized that reductions in propulsion resulting from limited ankle mobility would necessitate sagittal plane compensations at both hips; however, Δsagittal plane average positive hip power only increased on the restricted limb when comparing the restricted ankle condition to the restricted knee and combined ankle+knee conditions (Figure 3.3 A,B). ΔSagittal plane average positive hip power did not increase whenever the knee was locked, suggesting that the additional restriction at the knee prevented a sagittal plane hip compensation. It is possible that the restriction

at the knee made foot clearance a priority or limited the hip flexor's capacity to initiate passive knee flexion, thereby reducing motivation for in-plane compensation.

With respect to our second hypothesis, the restriction of knee ROM, with or without the ankle restriction, contributed to an increase in circumduction when compared to only locking the ankle (Figure 3.2B). Interestingly, the increases in circumduction observed in knee-restricted conditions were not significantly larger than the *braced* condition, and the circumduction values found in the *braced* condition were larger than values reported with the ankle locked, although not significantly. We cannot attribute this finding to wearing unrestricted knee braces because knee braces were worn in all conditions except the control. It is possible that bracing the ankle and the resulting increases in sagittal plane hip power limited hip motion in the frontal plane.

We must reject part of our second hypothesis, as we did not observe the increases in frontal plane hip power that we hypothesized would facilitate circumduction of the foot (Figure 3.3B). Instead, we found that participants opted to hip hike (i.e., decrease pelvic list) during restricted limb swing to enable circumduction when the knee was restricted (Figure 3.3C). Interestingly, all restricted conditions had negative Δhip power in the frontal plane, indicating that any bracing reduced hip power generation when compared to the *braced* condition (Figure 3.3B). This finding contrasts with the previously observed increases in frontal plane non-paretic hip power reported for persons-post stroke (Farris et al., 2015). It is possible that the isolated bracing in our study left pelvic list as the simplest compensation for our participants, whereas individuals post-stroke typically are contending with alterations in motor control and activation in addition to stroke-induced weakness.

Our approach of restricting motion at a joint mimicked many gait characteristics of post-stroke walking (Figure S3.1-4). Locking the ankle resulted in reductions in ankle ROM comparable

to paretic ankle ROM values reported in literature (McCain et al., 2019). Reductions in knee joint velocity at pushoff induced by knee restriction were within the range of velocity values reported in stiff-knee literature (Campanini et al., 2013). The peak ankle powers were within the range of values seen previously in stroke survivors walking at similar speeds (McCain et al., 2019). Propulsive symmetry decreased in all of the restricted conditions when compared to the unrestricted condition and peak restricted limb propulsion values for conditions with restricted ankle motion were within, (Awad et al., 2017b; Awad et al., 2014b) but generally on the higher end of values seen in post-stroke literature (Awad et al., 2015a; Awad et al., 2014b; Peterson et al., 2010a). When the knee was locked, we observed increases in circumduction and decreases in peak knee flexion that were very similar to values reported in the literature for persons post-stroke (Akbas et al., 2019b; Akbas and Sulzer, 2019; Campanini et al., 2013; Chen et al., 2005c; Dean et al., 2020; Tyrell et al., 2011).

Despite our success in inducing gait characteristics common to post-stroke, our metabolic results did not support our third hypothesis that restricting the ankle would be more expensive than restricting the knee joint (Figure 3.4B). Nevertheless, our results suggested an energetic impact due to ankle restriction. Specifically, our data indicated that combined restriction of the ankle and knee was more metabolically detrimental (i.e., larger positive Δmetabolic cost) than restriction of just the knee. Furthermore, all conditions that restricted the ankle (i.e., *restricted-ankle* and *restricted-a+k*) were more metabolically costly than the *braced* condition, suggesting that regardless of restrictions in knee ROM, any direct restriction on the ankle was metabolically detrimental. These results provide support for the potential of ankle-based rehabilitative techniques or technologies in persons post-stroke or other lower extremity joint deficits to provide a metabolic

benefit (Awad et al., 2017a; Kesar et al., 2010; Kesar et al., 2011; McCain et al., 2019; Takahashi et al., 2015a).

We anticipated that the increases in metabolic cost during the restricted conditions would be attributed to altered joint power requirements, consistent with findings from post-stroke gait (Detrembleur et al., 2003; Donelan et al., 2002; Farris et al., 2015; Stoquart et al., 2012b). In particular, we expected that greater metabolic cost would be due to a combination of the concurrent transfer of power from more to less efficient joints, thereby requiring more metabolic energy to achieve the same mechanical power output and increased total average positive joint power (Lewek et al., 2012; Wutzke et al., 2012). Specifically, we anticipated a bilateral increase in hip power would accompany an ankle restriction, indicating that joint power requirements were transferred from the highly efficient ankle to the less efficient hips. Instead, we only observed an increase in average positive hip power for the restricted limb in the *restricted-ank* condition when compared to the *braced* condition (Figure 3.3A). Further, an increase in total positive joint powers does not appear to explain the increased energetic requirements because whereas metabolic cost tended to increase across all restricted conditions (Figure 3.4), the average positive work tended to decrease compared to the unrestricted condition (Figure 3.5). This contradicts prior work on mechanics and energetics of walking in persons post-stroke which has suggested that increases in net metabolic power are accompanied by increases in total average positive joint power without a change in the efficiency of positive mechanical work (Detrembleur et al., 2003; Donelan et al., 2002; Farris et al., 2015; Stoquart et al., 2012b). Additionally, we did not observe a significant correlation between Δtotal average positive joint power and Δnet metabolic power (Figure 3.6). Overall, changes in total average positive joint power were a poor indicator of changes in net metabolic power study-wide (Figure 3.4-6, Fig S5). Thus, in general, it need not be true that

changes in metabolic cost are driven by changes in positive mechanical power under conditions with restricted joint ROM. It is possible that this discrepancy in findings is due to the inherent differences in mechanically-induced joint restrictions used here and the unilateral muscle weakness and altered muscle control present after stroke. Specifically, while our study was able to reproduce 'stroke-like' gait by restricting joint kinematics, we do not reproduce neural changes altering muscle-level coordination complexity (Clark et al., 2010), changes in muscle reflex coupling (Akbas et al., 2019a), or changes in muscular contraction efficiency (Son and Rymer, 2020) that exist post-stroke. These results warn that the use of positive joint power as a proxy for metabolic demand when analyzing atypical walking may be tenuous (Quesada et al., 2016). Other factors, such as muscle activation and effort, may be more relevant to mechanisms driving metabolic cost (Beck et al., 2018; Carrier et al., 2011).

There are limitations to this work that require consideration. While bracing at the ankle and knee restricted ankle excursion and knee velocity to values within the range reported for persons post-stroke, we cannot account for the neuromechanical changes that accompany a stroke (see above). We recognize that participants may have used the trunk and upper extremity to compensate for restricted lower limb motion, and the way in which the upper limb was used may also affect the lower limb mechanics reported here. If we had these data, our regression analysis of total average joint powers may be a stronger predictor of metabolic cost. As we look to generalize these results to impaired populations it is important to note that neurological injury could restrict upper limb compensations and have possible effects on measured lower limb function. Additionally, as part of a larger study examining bilateral vs. unilateral restriction, our participants' knee braces were worn bilaterally (albeit unrestricted on one side in all conditions) and may have altered gait when compared to the unbraced *control*. We attempted to account for this limitation by comparing

the restricted conditions to the *braced* condition, during which the knee braces were both worn unrestricted. Our choice to compare to the *braced* condition was made to eliminate the impact of the additional mass of the knee braces. An ankle stay was added onto the participant before the *restricted-ank* and *restricted-a+k* conditions and removed following the conditions so it is also possible that the added mass of the ankle stay could have impacted outcomes; however, the ankle stay was 3D printed out of PLA and weighed less than 3 ounces, and therefore we do not believe the risk of mass-related impacts to be significant. While the exact amount of time needed to acclimate to unilateral bracing is unclear, we attempted to mitigate this limitation by analyzing walking trials from the last two minutes of each seven minute condition. The participants of this study were on average significantly younger than the average person post-stroke, which may impact generalizing our results to older populations. Comfortable overground walking speed in persons post-stroke can also be significantly less than 0.8 m $s^{-1}$, the speed participants walked in this research. However, the walking speed chosen here was designed to be fast enough to challenge the walkers and elicit metabolic changes, but slow enough for them to complete the braced trials. Lastly, we cannot generalize our results to a situation where existing joint or limb limitations led participants to reduce walking speed; future research could investigate the impact of joint restriction on gait compensations and metabolic consequences across walking speeds.

## Conclusions

This work provides insight into the relative contributions of the ankle versus knee on walking mechanics and energetics to better inform how to target interventions for rehabilitation of gait post-stoke. We successfully employed ankle and knee braces to isolate the effects of limited ankle motion versus knee motion, as well as examine the combined effects of simultaneously restricted ankle and knee motion. Our approach reproduced many mechanical features of

hemiparetic gait at the joint and limb levels including reduced ankle power, reduced knee velocity, reduced restricted limb peak propulsion and increased restricted limb circumduction. Unilaterally restricted ankle function induced biomechanical compensations that were particularly detrimental to metabolic demand, bolstering the argument that ankle-centric rehabilitation has the potential to improve walking energetics post-stroke. Interestingly, the large increases in metabolic cost observed with both ankle and knee restricted simultaneously were accompanied by a decrease rather than an increase in total average positive joint power relative to the *braced* condition. This result raises questions about the utility of a work-efficiency approach for understanding mechanics and energetics of gait that has atypical coordination and suggests the need to explore force or activation-based proxies for energetic demand. Finally, restricting kinematics to achieve atypical gait patterns may not capture the complicated changes in coordination that drive changes in mechanics and energetics in populations with neural impairments. Future work is warranted to understand links between neuro-mechanics and energetics, that is, how changes in motor coordination rather than mechanics *per se*, influence metabolic cost of walking.

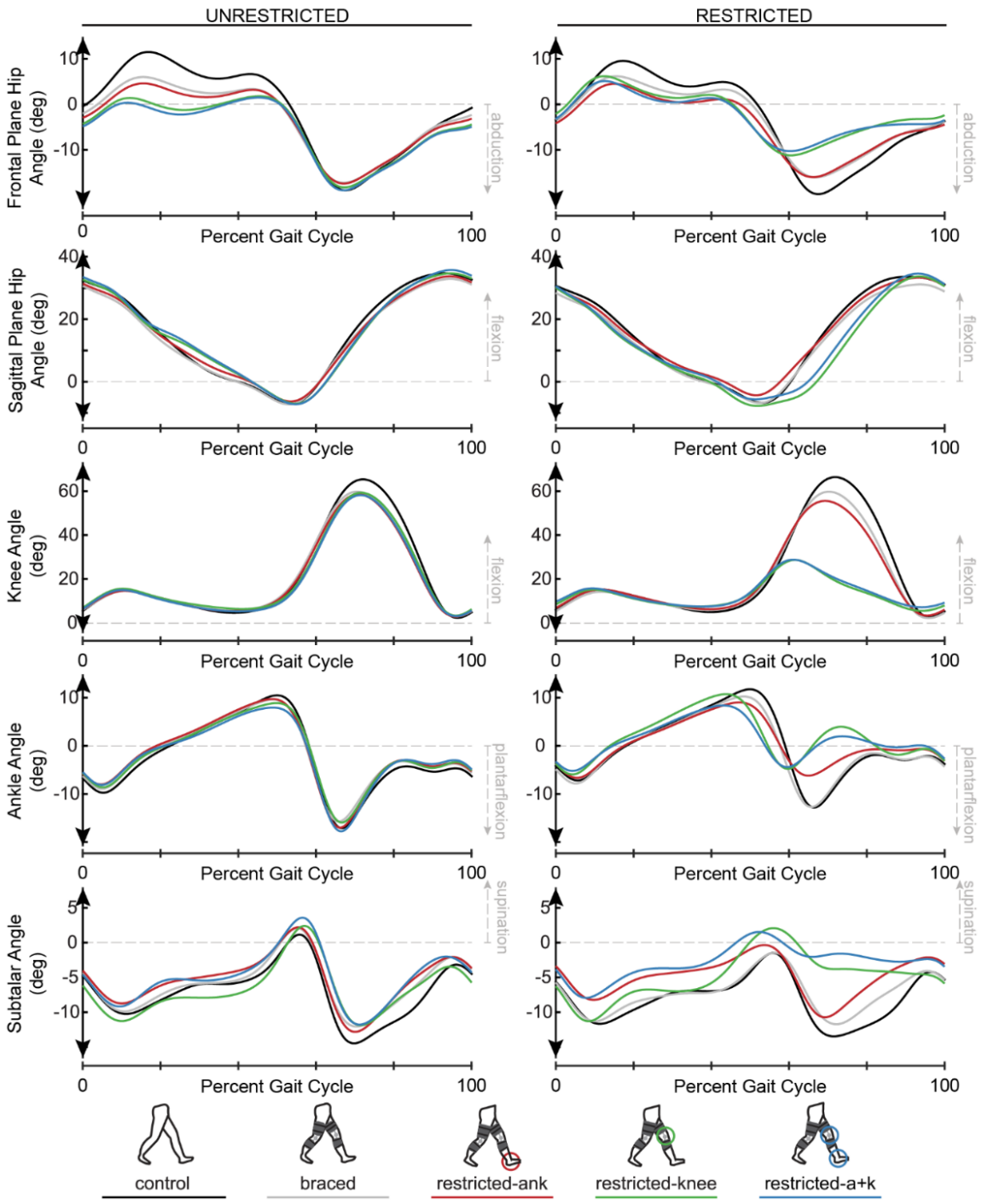


**Figure S3.1:** Subject average joint angles.

Subject average (N=15) joint angles for the *control*, *braced* and all restricted conditions for the unrestricted limb (left column) and the restricted limb (right column).

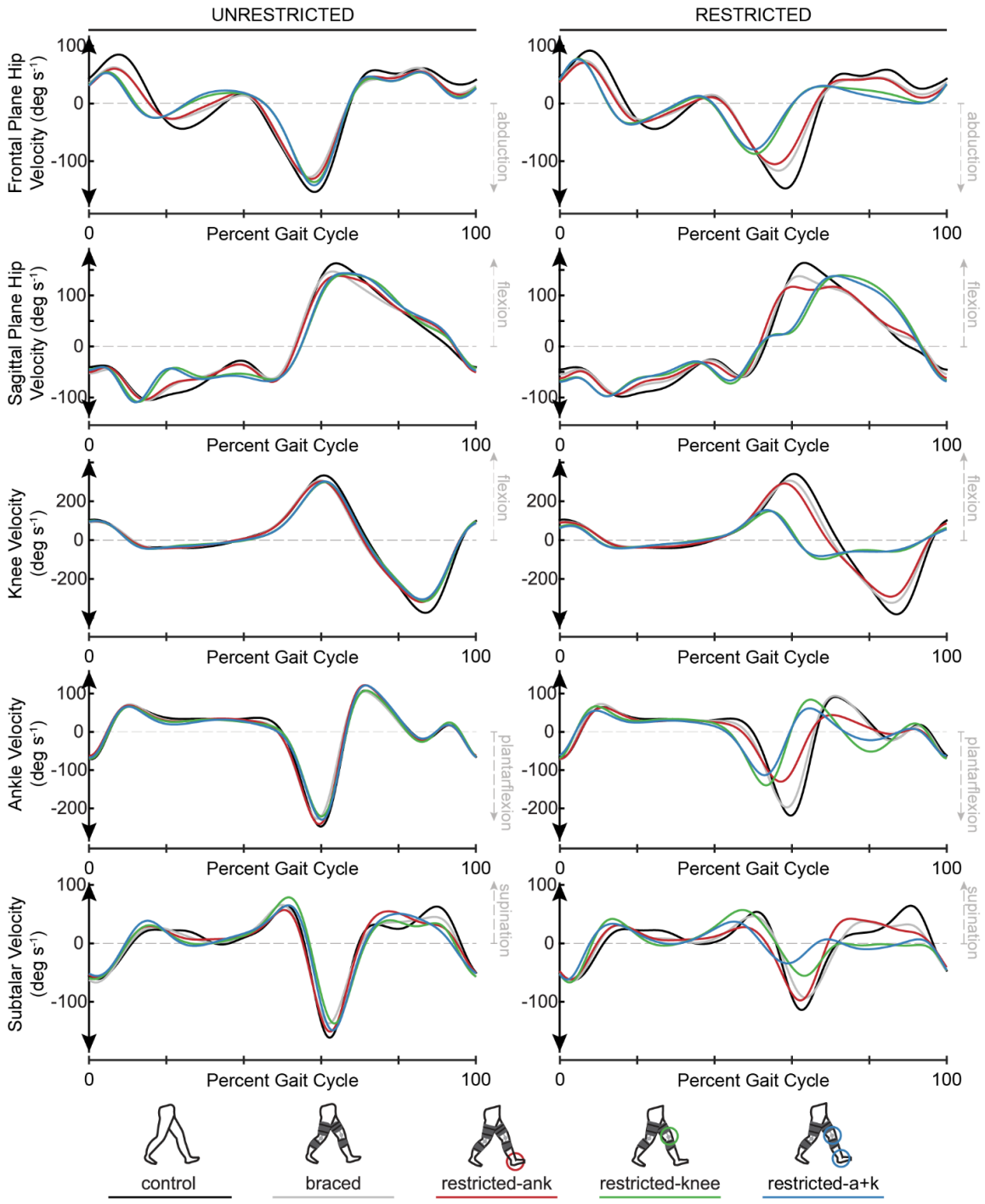


**Figure S3.2:** Subject average joint velocities.

Subject (N=15) average joint velocities for the *control*, *braced* and all restricted conditions for the unrestricted limb (left column) and the restricted limb (right column).

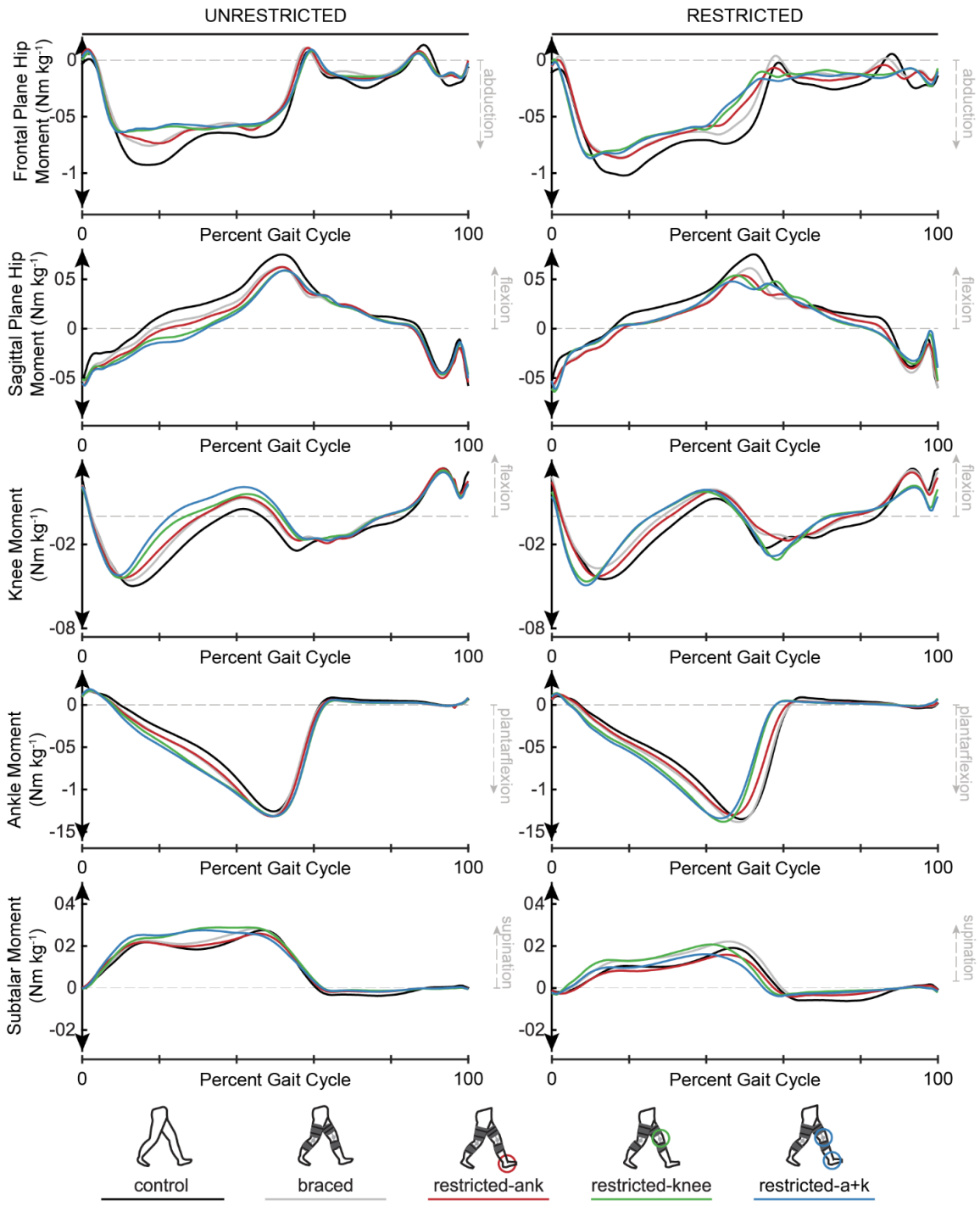


**Figure S3.3:** Subject average joint moments.

Subject average (N=15) joint moments for the *control*, *braced* and all restricted conditions for the unrestricted limb (left column) and the restricted limb (right column).

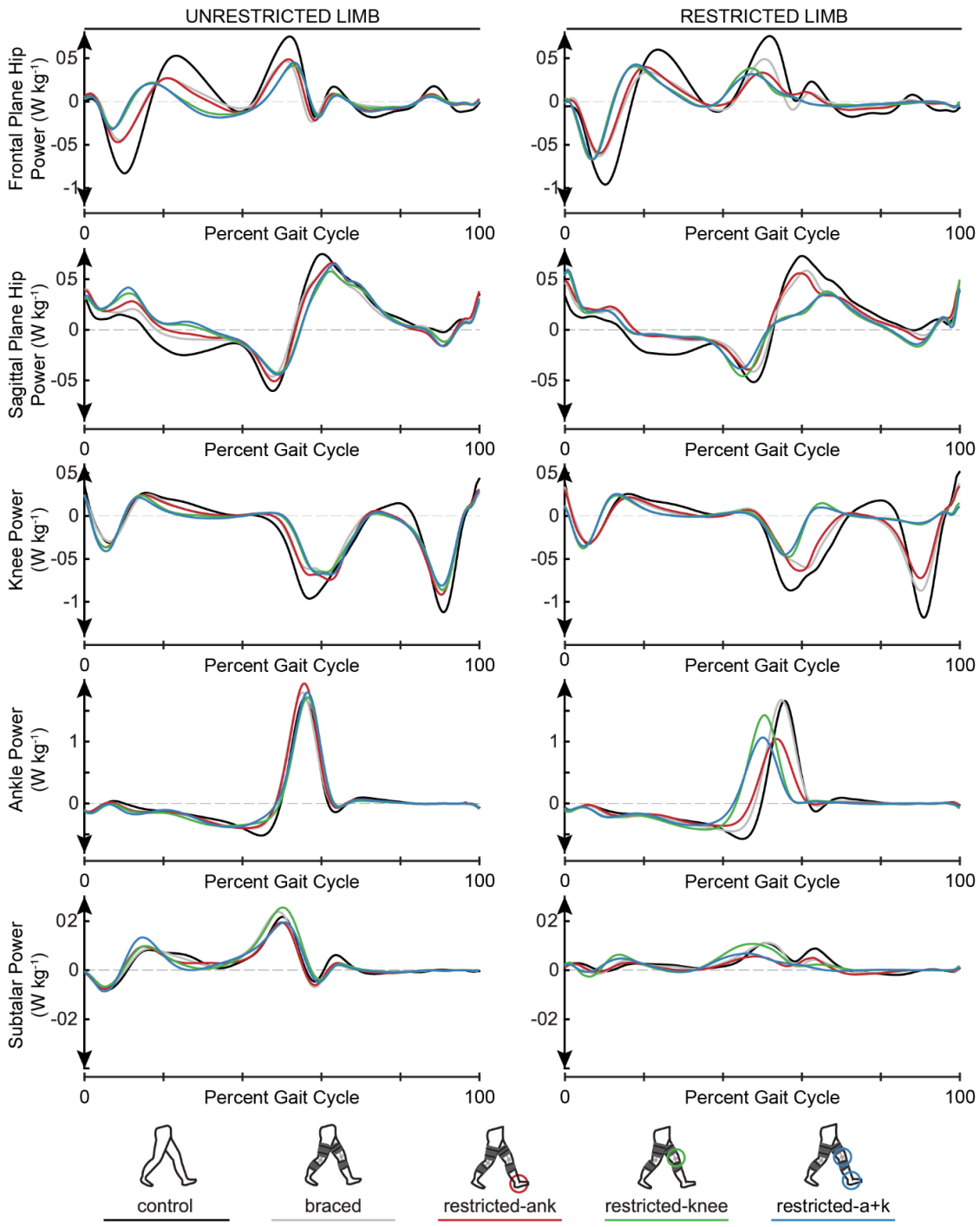


**Figure S3.4**: Subject average joint powers**.**

Subject average (N=15) joint powers for the *control*, *braced* and all restricted conditions for the unrestricted limb (left column) and the restricted limb (right column).

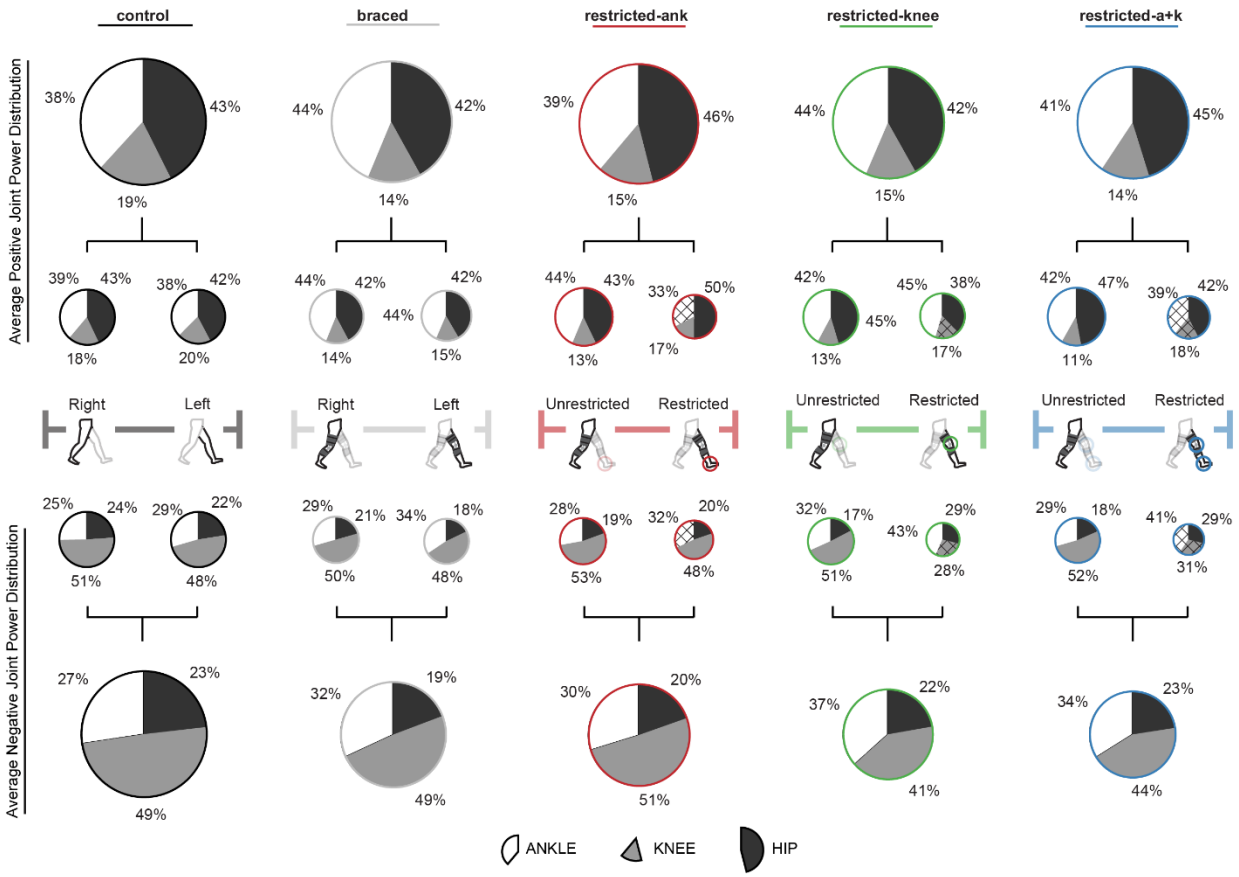


**Figure S3.5**. Average positive (top) and negative (bottom) joint power distribution.

Average positive (top) and negative (bottom) joint power distribution. Sections of pie chart represent the subject averaged (N=15) ankle (white), knee (light grey), and hip (dark grey) contributions and are organized by the following columns (from left to right): 1) *control, braced, restricted-ank, restricted-knee, and restricted-a+k.* Average positive joint powers were summed across both limbs in the top row, and average negative joint powers were summed across both limbs on the bottom row. The distribution of positive and negative power within each limb were indicated in the pie charts in the second and third row of the figure, respectively. Note that the diameters were scaled by dividing the sum of joint contributions for each pie by the maximum sum of average positive or negative joint powers (*control*) and that hatch patterns were used to indicate joints locked.

# CHAPTER 4

**Reduced joint motion supersedes asymmetry in explaining increased metabolic demand during walking with mechanical restriction.** (Submitted to *Journal of Biomechanics*, 2021)

Emily M. McCain, Matthew E. Berno, Theresa L. Libera, Michael L. Lewek, Gregory S. Sawicki, Katherine R. Saul.

## Abstract

Recent research has highlighted the complex interactions among chronic injury- or disease-induced joint limitations, walking symmetry, and increased metabolic cost. Determining the specific metabolic impacts of asymmetry or joint impairment in clinical populations is difficult because of concurrent neurological and physiological changes. This work investigates the metabolic impact of gait asymmetry and joint restriction by unilaterally (asymmetric) and bilaterally (symmetric) restricting ankle, knee, and combined ankle and knee ranges of motion in unimpaired individuals. We calculated propulsive asymmetry, temporal asymmetry, and step-length asymmetry for an average gait cycle; metabolic rate; average positive center of mass power using the individual limbs method; and muscle effort using lower limb electromyography measurements weighted by corresponding physiological cross-sectional areas. Unilateral restriction caused propulsive and temporal asymmetry but less metabolically expensive gait than bilateral restriction. Changes in asymmetry did not correlate with changes in metabolic cost. Interestingly, bilateral restriction increased average positive center of mass power compared to unilateral restriction. Further, increased average positive center of mass power correlated with increased energy costs, suggesting asymmetric step-to-step transitions did not drive metabolic changes. The number of restricted joints reduces available degrees of freedom and may have a larger metabolic impact than gait asymmetry, as this correlated significantly with increases in

metabolic rate for 7/9 participants. These results emphasize symmetry is not by definition metabolically optimal, indicate that the mechanics underlying symmetry are meaningful, and suggest that available degrees of freedom should be considered in designing future interventions.

## Introduction

Asymmetric walking is common after acute or chronic injuries or diseases, including amputations (Adamczyk and Kuo, 2015; Houdijk et al., 2009), knee or hip osteoarthritis (Creaby et al., 2012; Mills et al., 2013; Shakoor et al., 2003), hip arthroplasty (Lugade et al., 2010), and stroke (Brouwer et al., 2009; Chen et al., 2005b; Patterson et al., 2010; Wonsetler and Bowden, 2017). Gait asymmetry is quantified by spatiotemporal (Isakov et al., 1997; Nolan et al., 2003) and propulsive characteristics, and is accompanied by increased energetic requirements (Detrembleur et al., 2003; Mattes et al., 2000; Stoquart et al., 2012b) thought to result from expensive and badly coordinated step-to-step transitions (Houdijk et al., 2009; Mahon et al., 2015). Specifically, the energetic increases are thought to derive from reduced impaired limb propulsion leading to reduced peak instantaneous center of mass (COM) power (Awad et al., 2015a; Awad et al., 2014b; Farris et al., 2015; Lewek and Sawicki, 2019; Peterson et al., 2010a). Decreased instantaneous COM power may require expensive compensations like increased collision work during double support or increased contralateral work in unimpaired single support (Donelan and Kram, 2001; Donelan et al., 2002; Soo and Donelan, 2010). Therefore, researchers have proposed that restoring walking symmetry may reduce energetic requirements (Finley and Bastian, 2017; Mahon et al., 2019).

However, the interaction between walking asymmetry and metabolic cost is inconsistently characterized in the literature. This relationship is further obscured by the innumerable methods for quantifying asymmetry (propulsive, spatial, temporal) and by the diversity of interventions that target symmetry. Ankle-based exoskeletons (Awad et al., 2017b) and prosthetic emulators

(Quesada et al., 2016) can improve impaired limb propulsion but do not consistently reduce metabolic cost. Using feedback to guide unimpaired participants, researchers have induced step-length asymmetry (Nguyen et al., 2020) or step-time asymmetry (Ellis et al., 2013) and observed metabolic increases relative to participants' unaltered gait. However, others demonstrated step-time (Stenum and Choi, 2020) and step-length asymmetry (Sánchez et al., 2020) can be energetically optimal when unimpaired participants walk on a split-belt treadmill at different belt velocities. Repeated sessions of training on a split-belt treadmill (Reisman et al., 2013b) or walking with functional electrical stimulation (Awad et al., 2015b) improved step-length asymmetry in clinical populations, and improved asymmetry correlated with reduced metabolic cost (Awad et al., 2015b). However, in longitudinal studies, metabolic improvements could result from other benefits that accompany gait training including increased preferred walking speed (Reisman et al., 2013a; Tyrell et al., 2011) and muscle strength (Bohannon, 2007). Further, while some found a significant correlation between improved step-length (Awad et al., 2015b) or foot placement (Finley and Bastian, 2017) symmetry and reduced metabolic cost, others observed that improved stance *time* asymmetry was moderately correlated with metabolic cost (Ryan et al., 2020). Additional research found no metabolic benefit to single-session reductions in step-length asymmetry (Nguyen et al., 2020; Padmanabhan et al., 2020; Sánchez and Finley, 2018). Characterizing the relationship between improved gait asymmetry and metabolic reductions requires further investigation.

Injury or disease-induced anatomical (Quesada et al., 2016) or physiological (Attias et al., 2016; Ong et al., 2019) changes that can unilaterally constrain joint and limb function make investigating the interactions among altered joint function, walking asymmetry, and metabolic cost especially challenging. Therefore, ankle (Huang et al., 2015; Wutzke et al., 2012) and knee (Lewek

et al., 2012) bracing were previously used to limit joint range of motion (ROM) and induce gait asymmetry in unimpaired participants. This approach allows investigators to isolate the biomechanical and energetic impacts of reduced joint ROM and walking asymmetry from the impacts of concurrent anatomical or physiological changes in clinical populations. However, asymmetry accompanied by joint restriction still makes it difficult to identify whether outcomes are a result of the asymmetry per se or a consequence of joint restriction. To isolate the metabolic impact of reduced joint ROM and induced asymmetry, we used knee braces and custom 3D-printed ankle stays to restrict ankle ROM, knee ROM, and ankle+knee ROM unilaterally and bilaterally. We hypothesize (h1a) that induced asymmetry will be more metabolically expensive than induced symmetry (bilaterally restricted joints) (h1b) due to energetically expensive step-to-step transitions. If increased metabolic cost in asymmetric gait indeed results from badly coordinated step-to-step transitions, then restoring symmetry with bilateral bracing should also eliminate expensive transitions. However, researchers have reported that simultaneous ankle and knee restriction is more metabolically expensive than ankle restriction (McCain et al., 2021), possibly because restricting additional joints or degrees of freedom (DOFs) lessens redundancy and restricts compensation. Thus, we hypothesized (h2) that as a proxy for available DOFs, the number of joints restricted will correlate with a metabolic increase in asymmetric and symmetric conditions.

## Methods

### Data Collection

UNC-Chapel Hill institutional review board approved procedures and consent forms signed prior to data collection by nine healthy adult participants (5M/4F, 25.22±0.30years, 1.77±0.13m, 78.34±15.9kg). We recruited healthy adults without a history of surgery for lower extremity musculoskeletal injury or a lower extremity musculoskeletal injury in the past two years. Participants walked on an instrumented split-belt treadmill (Bertec, Columbus, OH, USA) for eight conditions, each lasting 7 minutes, including: (1) *control*: no braces worn, (2) *braced*: knee braces worn unrestricted bilaterally; unilaterally restricted conditions: (3) *uni-ank:* unilaterally restricted ankle, (4) *uni-knee:* unilaterally restricted knee, and (5) *uni-a+k:* unilaterally restricted ankle+knee; and bilaterally restricted conditions: (6) *bi-ank*: bilaterally restricted ankles, (7) *bi-knee:* bilaterally restricted knees, and (8) *bi-a+k:* bilaterally restricted ankles+knees simultaneously. Our approach allowed reduction of available DOFs both symmetrically (**0**: *control*, *braced*; **2:** *bi-ank*, *bi-knee* **4**: *bi-a+k*) and asymmetrically **(1**: *uni-ank*, *uni-knee*; **2**: *uni-a+k*). Walking speed (0.8m/s) was chosen to accommodate the increased challenge associated with the *bi-a+k condition.* 3D-printed ankle stays secured to the foot/ankle dorsum restricted ankle ROM, and lockable donJoy T-ROM knee braces (DJO Global, Inc, Vista, CA, USA) restricted knee ROM. We only applied ankle stays unilaterally for *uni-ank* and *uni-a+k* conditions, and bilaterally for *bi-ank* and *bi-a+k* conditions. Knee braces were worn bilaterally for all conditions except the *control* condition. The *control* condition was performed last to eliminate additional static captures, and other conditions were performed in a random order. In *braced*, *uni-ank,* and *bi-ank* conditions knee ROM was unrestricted, in *uni-ank* and *uni-a+k* conditions knee ROM was unilaterally restricted, and in *bi-knee* and *bi-a+k* conditions knee ROM was bilaterally restricted.

We recorded rates of oxygen consumption and carbon dioxide production with a portable metabolic system (K5, Cosmed, Chicago, IL) for five minutes of quiet standing before walking and during walking conditions. The positions of 42 reflective markers attached to the pelvis and lower limb (McCain et al., 2019) were recorded using an eight-camera motion capture system (Vicon, Oxford, UK) sampling at 120Hz; marker positions were filtered within OpenSim software (Delp et al., 2007) using a 6Hz Butterworth filter. Ground reaction forces (GRFs) were recorded at 1200Hz, then filtered with second-order low-pass Butterworth filter (cutoff frequency: 25Hz). We collected surface electromyography (EMG) (Trigno, Delsys) at or above 1200Hz bilaterally for tibialis anterior, soleus, lateral gastrocnemius, medial gastrocnemius, vastus lateralis, and biceps femoris. We filtered EMG with a $4^{th}$ order bandpass filter (30Hz/450Hz), found the rolling root mean square (50ms), smoothed data with a moving average (50ms), and normalized EMG by representative EMG peaks.

**Data Processing**

We used an OpenSim full-body model (Rajagopal et al., 2016) altered to represent the lower limb and scaled according to participant anthropometry. Filtered marker data and personalized models were input into a inverse kinematic algorithm (Thelen and Anderson, 2006) to determine joint angular velocities and moments. We determined heel strike and toe-off timing with a custom MATLAB script using GRF data. Propulsive asymmetry (PA), temporal asymmetry (TA), step-length asymmetry (SLA), average positive COM power and weighted muscle effort were calculated as described below over 10 gait cycles for each limb and averaged across gait cycles for each subject and condition. We removed gait cycles bordering crossover steps and selected ten consecutive gait cycles nearest the end of the last two minutes of data collection to ensure metabolic steady state. To isolate the impact of joint ROM restriction from that of bracing

mass, we calculated Δmetabolic cost, ΔPA, ΔTA, Δaverage positive COM power, and Δweighted muscle effort for restricted (*uni* & *bi)* conditions relative to the *braced* condition.

**Measures of Asymmetry:** We calculated asymmetry measures as the ratio of maximum contribution (between legs) to summed contribution (both legs) such that 0.5 indicates symmetry and larger values indicate increased asymmetry (Lewek et al., 2018). This ratio was calculated from integrated anteriorly directed GRFs for PA, from the percent gait cycle spent in single limb support for TA, and from average step-lengths for SLA. Step-lengths were determined from the sagittal distance in calcaneus marker locations at heel strikes.

**Metabolic Rate**: We calculated metabolic power from rates of oxygen consumption and carbon dioxide production measured during five minutes of quiet standing before the first condition and during the last two minutes of each condition (Brockway, 1987). The net metabolic rate was determined as the difference in metabolic power for each walking condition and metabolic power of quiet standing, normalized by participant mass.

**Average Positive COM Power**: We calculated instantaneous external mechanical limb powers using individual limbs method (Donelan et al., 2002) in a custom MATLAB script. We calculated COM velocity for each gait cycle by integrating COM acceleration, determined from external forces and body mass, with integration constants determined such that sagittal velocity equaled treadmill speed and average vertical and medial COM velocities were zero. The dot product of COM velocity and each limb's mass normalized GRF gave instantaneous limb power. To obtain average positive COM power for a gait cycle we summed average positive limb power for each limb, where average positive limb powers for each limb and gait cycle were determined by integrating periods of positive instantaneous power and dividing by average corresponding gait cycle duration.

**Weighted muscle effort**: We determined average integrated muscle activity ($a_m^{\text{int}}$) by integrating normalized muscle activities and dividing by the number of gait cycles. Weighted muscle activity was found with the equation $\sum_{m=1}^{N_{muscles}} \left( \left( a_m^{\text{int}} * PCSA_m \right) / a_m^{MAX} \right) * 100$ where $PCSA_m$ is muscle physiological cross-sectional area (Rajagopal et al., 2016), $a_m^{MAX}$ is the subjects max average integrated muscle activity for all conditions, and $N_{muscles}$ is the total number of muscles included bilaterally.

**Statistical Analyses**

We performed a one-way (factor levels: braced, bi-ank, bi-knee, bi-a+k) repeated measures reduced maximum likelihood (REML) analysis in SAS Statistical Software (SAS Institute, Cary, NC, USA) on asymmetry measures to ensure there was no significant differences in asymmetry among the braced, *bi-ank*, *bi-knee*, and *bi-a+k* conditions. Then we performed two-way repeated measures REML analysis in SAS to determine whether restriction symmetry (factor 1 levels: unilateral/bilateral) or restriction joint (factor 2 levels: ankle, knee, ankle+knee) were significant ($p_{REML}<0.05$) factors outcome measures (PA, TA, SLA, average positive COM power, metabolic rate, weighted muscle effort, Δmetabolic rate, Δaverage positive COM power, Δweighted muscle effort). We visually inspected residuals in Q-Q plots for normality, and Grubb's test was used to determine and remove one outlier value in the metabolic data (participant P9, condition: *bi-knee*). Post-hoc analyses to determine significance between factor levels ($p_{ph<}0.05$) included t-tests with Bonferroni corrections for multiple comparisons (*uni-ank* vs *bi-ank, uni-knee* vs. *bi-knee, uni-a+k* vs *bi-a+k)* We used a custom MATLAB script to determine the Pearson correlation coefficient (r) and significance ($p_{p<}0.05$), calculate the coefficient of determination ($R^2$), and perform a simple linear regression analysis.

## Results

**Measures of Symmetry**: Joint restrictions induced propulsive (Figure 4.1A, $p_{REML}$ =0.02) and temporal (Figure 4.1B, $p_{REML}$<0.01) asymmetry in unilaterally compared to bilaterally restricted conditions. Furthermore, TA increased in *uni-knee* (TA=0.53±0.01) and *uni-a+k* (TA=0.53±0.01) conditions when compared to *bi-knee* (TA=0.51±0.01, $p_{ph}$<0.01) and *bi-a+k* (TA=0.51±2e$^{-3}$, $p_{ph}$<0.01) conditions, respectively. Restriction location significantly affected TA ($p_{REML}$<0.01), and we found increased TA with knee ($p_{ph}$=0.02) or ankle+knee ($p_{ph}$<0.01) restrictions compared to ankle restriction. Post-hoc analysis did not find statistically significant differences between factor levels for propulsive asymmetry. Step-length asymmetry was not significantly affected by either factor (Figure 4.1C). We analyzed the braced and bilaterally restricted conditions and found no significant change in asymmetry measures.

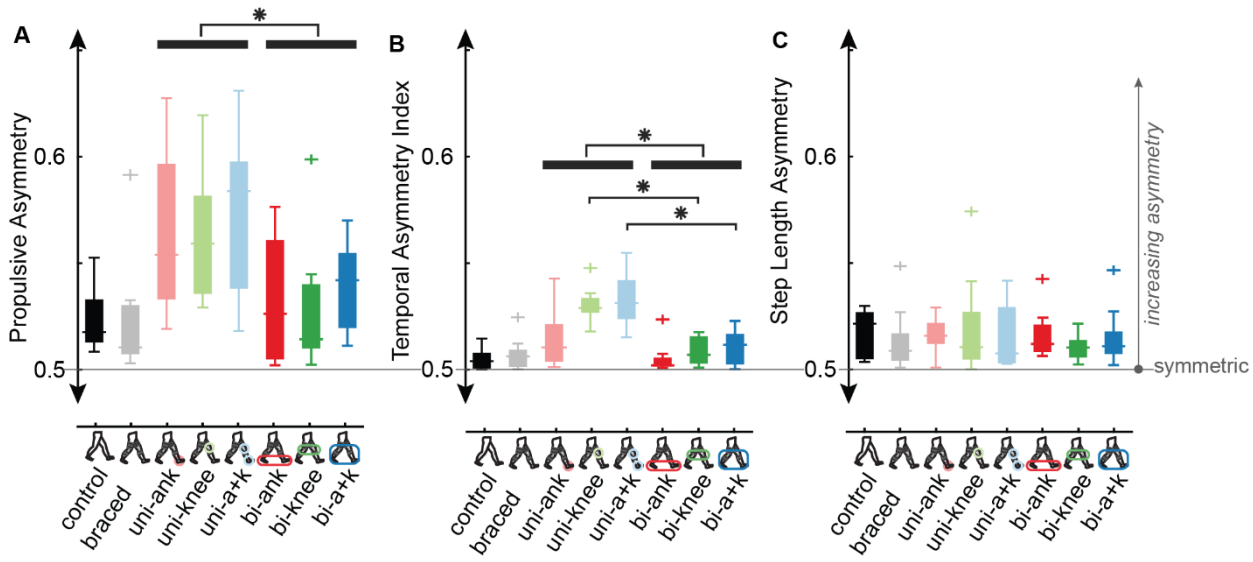


**Figure 4.1** Walking asymmetry measures.

Group (A) propulsive asymmetry, (B) temporal asymmetry, and (C) step-length asymmetry across conditions. Single asterisks (*) above horizonal bars indicate that the symmetry (unilateral/bilateral) nature of restriction had as significant effect on corresponding asymmetry values. Single asterisks above brackets indicate significant differences between specific conditions.

**Metabolic Rate:** ΔMetabolic rate (Figure 4.2B) was also significantly affected by restriction symmetry ($p_{REML}<0.01$) and by joints restricted ($p_{REML}<0.01$), and there was a significant interaction between these factors ($p_{REML}<0.01$). Symmetric knee restriction in *bi-knee* (0.71±0.38 W/kg) and *bi-a+k* (1.21±0.48 W/kg) conditions was more metabolically expensive than asymmetric knee restriction in *uni-knee* (0.13±0.20 W/kg; $p_{ph}<0.01$) and *bi-a+k* (0.40±0.33 W/kg; $p_{ph}<0.01$) conditions, respectively. ΔMetabolic rate did not significantly correlate with Δpropulsive asymmetry (Figure 4.2C, $p_p=0.89$) or Δtemporal asymmetry (Figure 4.2D, $p_p=0.92$).

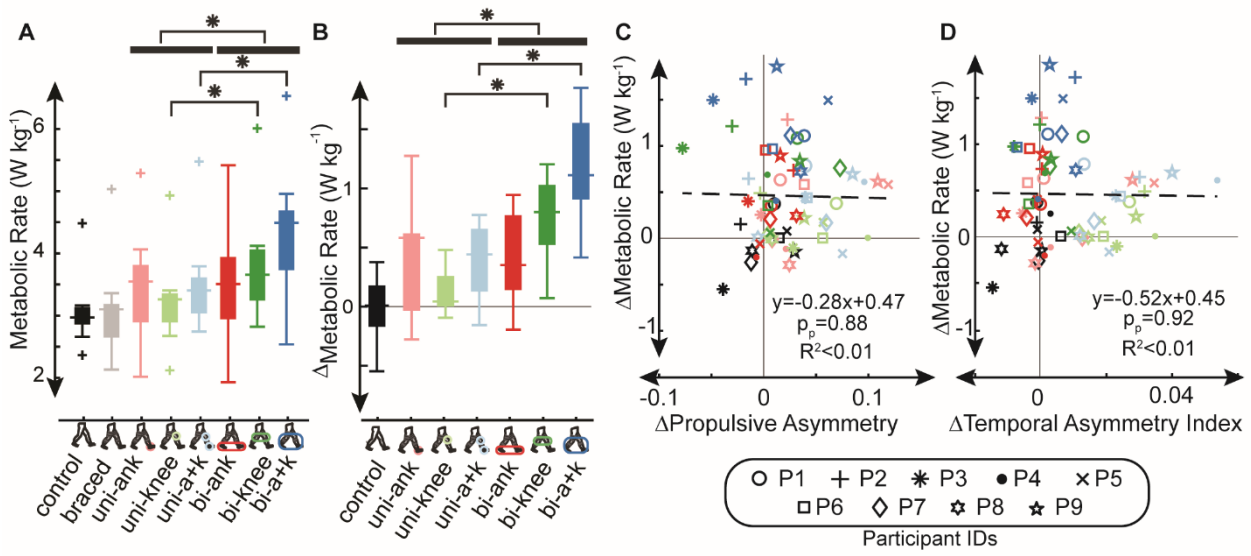


**Figure 4.2.** Metabolic rate and Δmetabolic rate versus walking asymmetry.

Group (A) metabolic rate and (B) Δmetabolic rate for all conditions. Single asterisks (*) above horizonal bars indicate that the symmetry (unilateral/bilateral) nature of restriction had as significant effect on corresponding asymmetry values. Single asterisks above brackets indicate significant differences between specific conditions. Subject specific Δmetabolic rates plotted with (C) Δpropulsive asymmetry and (D) Δtemporal asymmetry showing resulting linear correlations with Pearson coefficient p-values.

**Average Positive COM Power**: Restriction symmetry had a significant effect on Δaverage positive COM power (Figure 4.3B, $p_{REML}$=0.03) as bilaterally restricted conditions had increased Δaverage positive COM power compared to unilaterally restricted conditions. Further, *bi-a+k* Δaverage positive COM power (0.04±0.06 W/kg) was significantly increased compared to *uni-a+k* Δaverage positive COM power (-0.02±0.05 W/kg, $p_{ph}$=0.03). We found a significant ($p_p$<0.01, $R^2$=0.12) positive correlation between Δaverage positive COM power and Δmetabolic cost (Figure 4.3C). Average positive and negative limb power during both double support periods and average

instantaneous mechanical power of each limb normalized for a gait cycle were calculated and included for additional context (Figure S4.1).

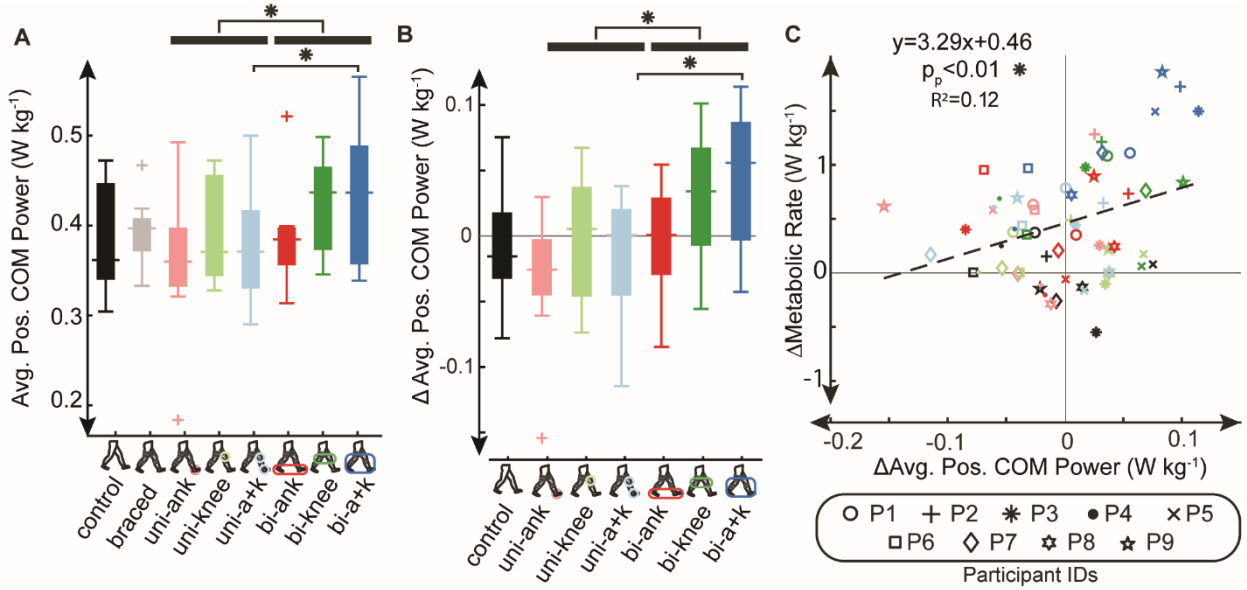


**Figure 4.3** Average positive COM power and its metabolic impacts.

Group (A) average positive COM power and (B) Δaverage positive COM power for all conditions. Single asterisks (*) above horizonal bars indicate that the symmetry (unilateral/bilateral) nature of restriction had as significant effect on corresponding asymmetry values. Single asterisks above brackets indicate significant differences between specific conditions. Subject specific Δmetabolic rates plotted with (C) Δaverage positive COM work and single asterisk (*) indicates significant correlation.

**Weighted Muscle Effort**: ΔWeighted muscle effort (Figure 4.4B, $p_{REML}$=0.048) was significantly affected by the joint restricted, but not affected by restriction symmetry. Further, when the ankle and knee were restricted simultaneously, we found a significant increase in Δweighted muscle effort ($p_{ph}$=0.04) compared to ankle restriction alone. ΔWeighted muscle effort was not significantly correlated with Δmetabolic cost (Figure 4.4C).

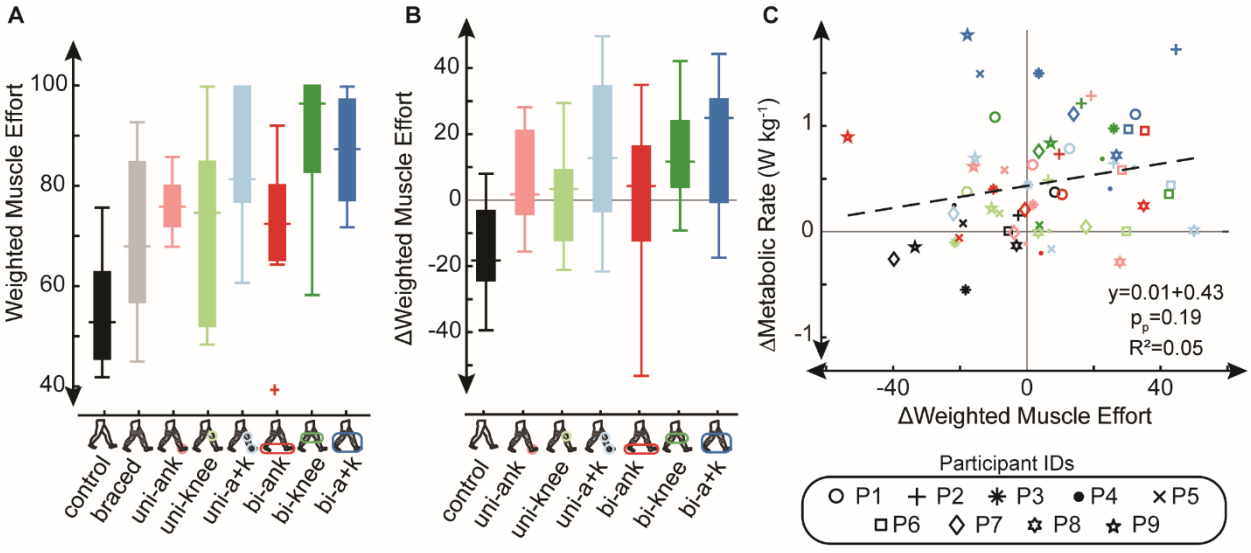


**Figure 4.4** Weighted muscle effort and metabolic impacts.

Group (A) weighted muscle effort and (B) Δweighted muscle effort for all conditions. Single asterisks (*) above solid bars indicate that the symmetry of restriction had as significant effect on corresponding asymmetry values. Single asterisks above brackets indicate significant differences between specific conditions. Subject specific Δmetabolic rates plotted with (C) Δweighted muscle effort.

**Correlation Between ΔMetabolic Cost and Restricted Degrees of Freedom**: The number of constrained DOFs was significantly corelated with the Δmetabolic cost for seven participants (Figure 4.5, P1, P2, P3, P6, P7, P8, P9; $p_p<0.02$). The $R^2$ values for these seven participants were $0.63<R^2<0.96$.

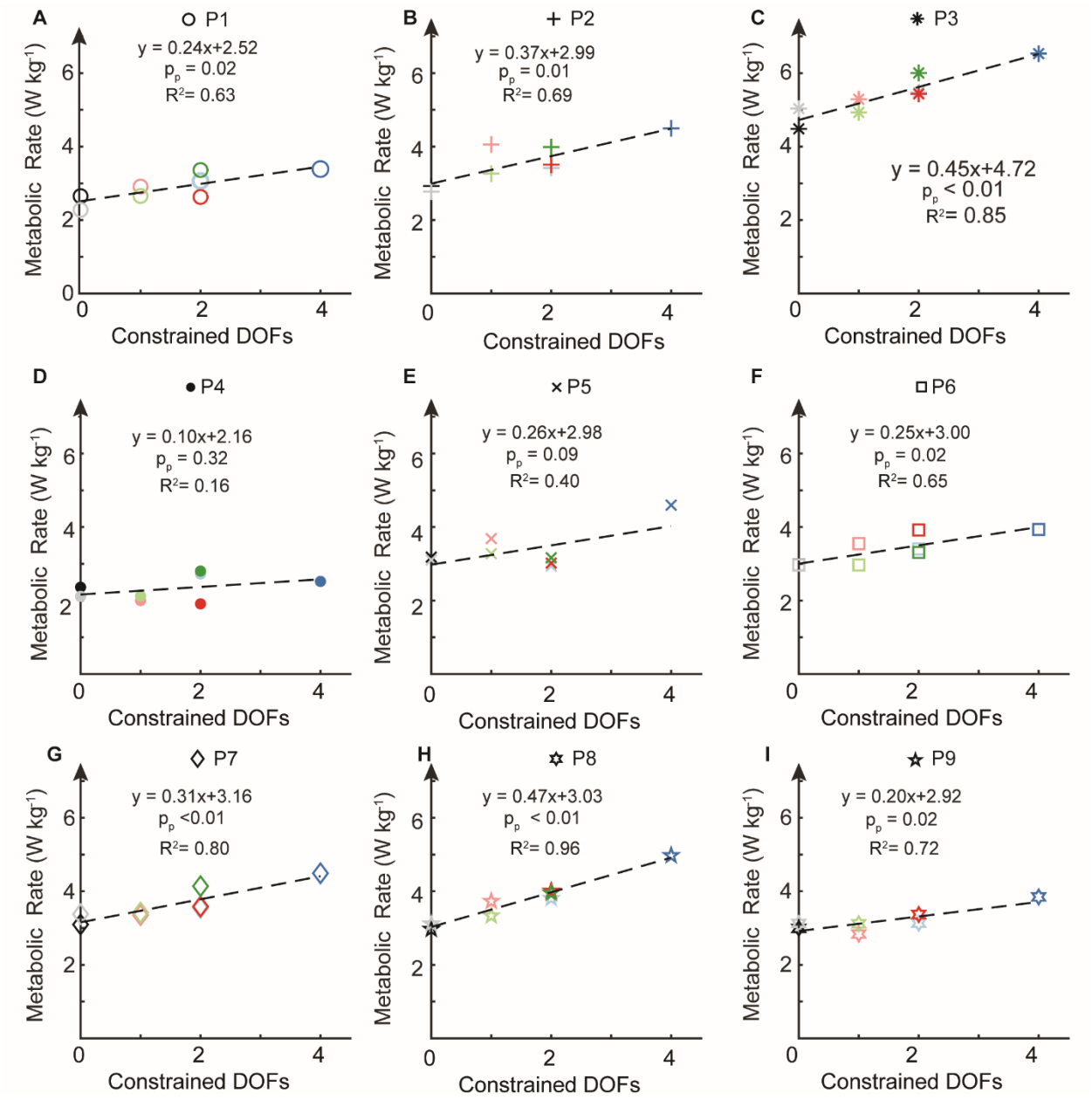


**Figure 4.5.** Metabolic impact of constrained DOFS.

The number of constrained DOFs is plotted with metabolic rate for all participants (A:I). A single asterisk indicates a significant Pearson correlation.

## Discussion

We investigated the metabolic consequences of gait asymmetry and reduced DOFs using joint-specific restrictions with unimpaired participants. This builds upon previous work (Lewek et al., 2012; McCain et al., 2021; Wutzke et al., 2012) by applying multiple joint restrictions unilaterally and bilaterally to explore the metabolic impacts of asymmetry and joint restriction. Our approach elicited asymmetric and symmetric gait and demonstrated that asymmetry in and of itself does not drive increased energy requirements. Instead, we found the number of restricted DOFs had the strongest correlation with metabolic rate. Our results suggest that rather than targeting walking symmetry, assistive technology or rehabilitative strategies that mitigate limb or joint impairments - thereby increasing functional DOFs - may have greater potential to reduce metabolic requirements.

Our approach successfully induced temporal and propulsive walking asymmetry, but induced asymmetry did not result in metabolic increases as hypothesized. Specifically, we found asymmetrically restricted conditions were *less* metabolically costly than symmetrically restricted conditions, and no significant correlation existed between Δmetabolic cost and asymmetry measures (ΔPA, ΔTA). These results reinforce that symmetry is not always metabolically optimal (Roemmich et al., 2019; Sánchez and Finley, 2018; Sánchez et al., 2019) and suggest that walking asymmetrically with one restricted limb is more economical than walking symmetrically with two restricted limbs (Browne et al., 2021). Interestingly, any knee restriction had a larger impact on TA than did ankle restriction, indicating knee restriction may promote increased temporal asymmetry (Figure 4.1B). It is possible that a knee restriction makes foot clearance a priority, with the resulting compensations, such as foot circumduction (McCain et al., 2021), impacting the duration of single limb support. Despite changes in TA and PA, we did not see any significant

change in SLA. Unimpaired controls may compensate for restriction with temporal gait adaptations alone, whereas clinical populations may have less capacity to manipulate underlying gait parameters (Hak et al., 2013).

Despite our success in creating propulsive asymmetries, energetically expensive asymmetric step-to-step transitions were not at the root of metabolic increases as we hypothesized. Instead, we found symmetric conditions had larger total average positive COM power and correspondingly higher metabolic rates. It is possible that a decrease in gait cycle duration in the symmetrically restricted conditions could account for the larger average positive COM power. Likewise, we did not measure arm movement, which is known to increase with greater bilateral propulsion needs (Lewek et al., 2010), and has the potential to impact the COM work rate (Collins et al., 2009). However, we note the correlation observed between Δmetabolic cost and Δaverage positive COM power (Figure 4.3C) had a small R-squared value, and thus explains little variability in the metabolic data.

Additional muscle-level metabolic impacts could explain why Δaverage positive COM power does not account for variability of this dataset, as muscle contractions not resulting in motion are not accounted for by COM power. Qualitatively, correlation between Δweighted muscle effort and Δmetabolic cost (Figure 4.4C) is similar to the correlation between Δaverage positive COM power and Δmetabolic cost and is a better predictor of Δmetabolic cost than ΔPA or ΔTA. It is possible that inclusion of upper limb EMG measurements to account for arm movement needed to conserve angular momentum or back muscles used for trunk stability would improve this correlation; alternatively, muscles surrounding the hip may have been crucial to understand kinematic compensations and could strengthen the predictive quality of this

relationship (Stenum and Choi, 2016). Future research could employ musculoskeletal simulation to investigate contributions of muscles difficult to measure experimentally.

Our results suggest metabolic increases may be driven by the number of restricted DOFs. We found that for seven of nine participants, metabolic rate and restricted DOFs were significantly correlated, and the number of restricted DOFs accounted for between 63% and 96% of the metabolic variability. These results echo previous research suggesting that reducing available DOFs limits compensatory strategies (Clark et al., 2010) the resulting gait may require increased metabolic cost (Mahon et al., 2015). This may explain inconsistencies in previous literature examining relationships between gait asymmetry and metabolic consequences. Specifically, improvement in paretic ankle DOF performance resulting from increased muscle strength may drive decreased energy requirements observed with repeated gait training (Awad et al., 2015b); this would explain why the same benefits do not accompany single-session gait training that addresses symmetry but does not increase available DOFs (Sánchez and Finley, 2018).

Our results echo that asymmetry can be less metabolically expensive than symmetry (Browne et al., 2021; Sánchez et al., 2020), and suggest rehabilitative interventions targeting specific improvement in affected limb DOFs function rather than improvement in specific symmetry metrics may have more potential to reduce energy requirements. In this work, bilaterally restricted DOFs resulted in symmetric and energetically expensive gait; similarly, when instructed to improve symmetry, clinical populations may reduce the unaffected limb's performance, limiting available DOFs, and creating symmetric and metabolically detrimental gait. While counterintuitive, this may be the only achievable manner for individuals with large intralimb functional discrepancies walk symmetrically. While the intention of targeting symmetry in patient populations is to improve impaired limb function to match unimpaired limb function, the method

for restoring symmetry is not ensured. For example, limb symmetry is frequently used for return-to-play decisions following anterior cruciate ligament injury (Wellsandt et al., 2017). This metric can overestimate knee function (Wellsandt et al., 2017), possibly because athletes opt to reduce unimpaired limb function to expedite their return-to-play, again creating symmetric, but undesirable, performance. In addition, recent work suggests transfemoral amputees have individualized, metabolically-optimal, levels of walking asymmetry such that any deviation is metabolically detrimental (Mahon et al., 2019). We suggest energetically optimal asymmetry may maximize impaired limb function such that increasing symmetry would require restricting the unimpaired limb, thereby reducing available DOFs.

There are several limitations to this work. On average, study participants were significantly younger than many patient populations which may impact generalization of these results. However, we note that our asymmetry measures were similar to reports for clinical populations in the literature (Allen et al., 2014; Awad et al., 2017b; Little et al., 2020). Reported values for average positive COM power are slightly larger than values reported in previous ILM analysis for persons post-stroke and unimpaired participants (Farris et al., 2015). The asymmetry ratios we present do not indicate which limb contributes to asymmetry in unilateral conditions. However, we note that they allow us to calculate the magnitude of asymmetry consistently across unilaterally and bilaterally restricted conditions. Restricting ankle motion was accomplished using a 3D printed polylactic acid ankle stay for ankle restricted conditions and otherwise removed; while results could be affected by added mass, the ankle stays weighed <3 ounces. Our participants wore knee braces bilaterally for all restricted conditions so the added mass of knee bracing was consistent across conditions and thus should not impact outcomes. Walking asymmetry and restricted DOFs are related in this work and their metabolic impact cannot be completely decoupled. However, our

approach allowed for both symmetric and asymmetric DOFs reduction and therefore can provide insight into the relative metabolic impact of asymmetry and DOFs. In addition, we acknowledge that the chosen gait speed is slower than our participants typically walk; however, this speed was selected to ensure that participants would be challenged enough to elicit a metabolic impact while allowing participants to complete all braced conditions. The predictive power of weighted muscle effort and Δweighted muscle effort metrics would likely be improved by a more extensive set of EMG measurements. We identified the metabolic data for one participant and trial as an outlier (P9, *bi-knee);* because much of our analyses related metabolic data to other outcomes, we removed that one data point (P9, *bi-knee)* from all analyses. Our correlation analysis did not account for participants as a random variable, and it is possible that if we had, the predictive power of the analyses could have increased. Further, a larger sample size may have allowed us to detect additional relationships.

In summary, we investigated the metabolic impacts of asymmetry and available DOFs using joint restriction unilaterally and bilaterally in unimpaired controls. We elicited increased asymmetry with unilateral compared to bilateral restrictions. Interestingly, symmetric restriction was more mechanically and metabolically expensive than asymmetric restriction, and changes in symmetry did not correlate with changes in metabolic cost. Further, we found the average positive COM power to be larger in the energetically expensive, symmetrically restricted conditions than in conditions with unilateral restrictions, suggesting asymmetric step-to-step transitions do not drive metabolic outcomes. Increased energetic requirements correlated significantly with changes in Δaverage positive COM power and tended to correlate, although insignificantly, with weighted ΔEMG effort. Interestingly, we found a significant correlation between metabolic rate and the number of DOFs restricted for most participants, suggesting reducing available DOFs has a larger

metabolic impact than asymmetry. These findings are not intended to discourage restoration of walking symmetry, but instead should emphasize importance of how symmetry is restored and suggest the inclusion of DOFs availability as a metric guiding future interventions.

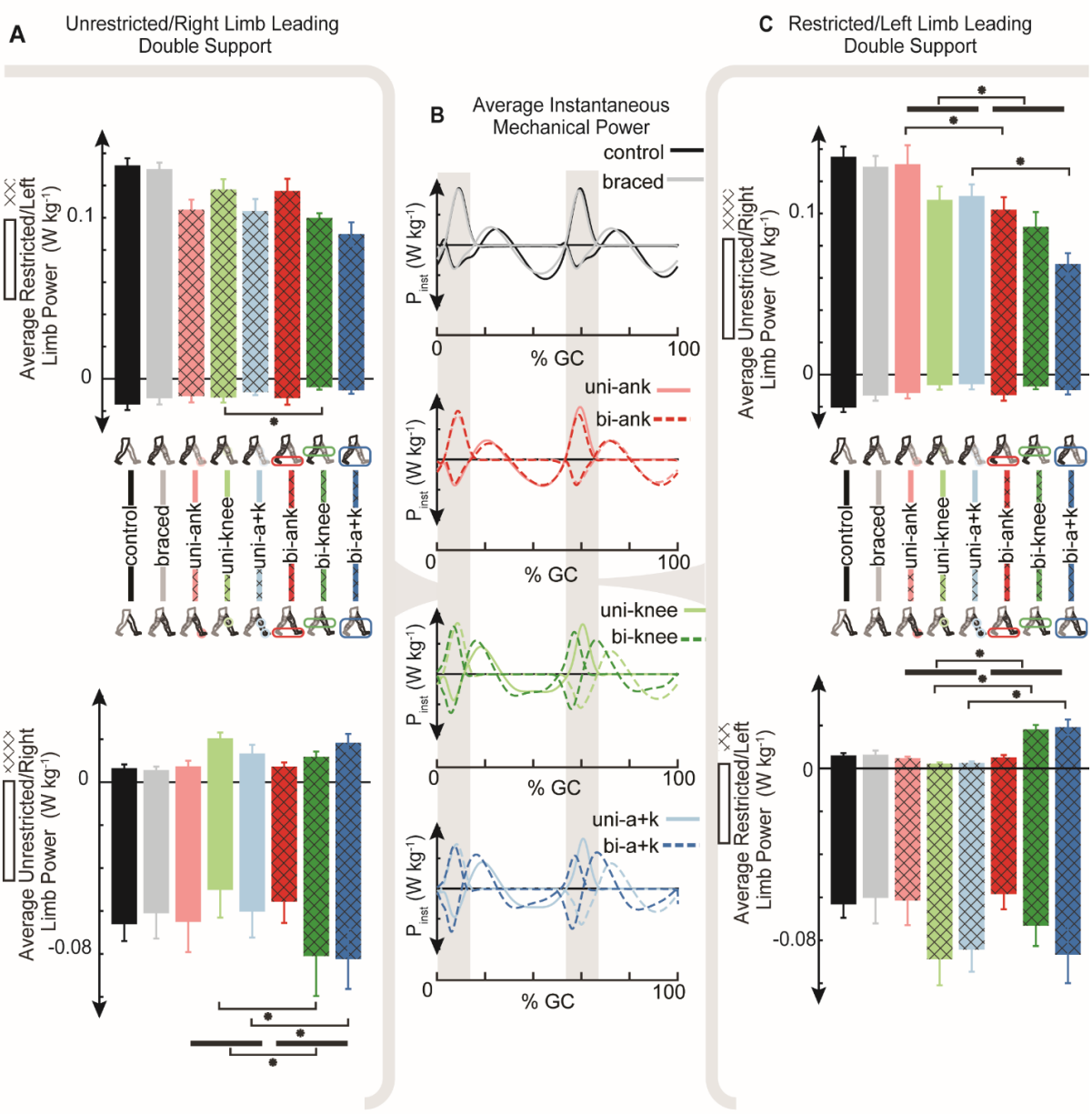


**Figure S4.1.** Individual Limbs Method Analysis

The Group average±standard error positive and negative average limb powers during (A) unrestricted/right limb leading and (C) restricted/left limb leading double support periods is plotted normalized by gait cycle time; hatched fill indicates that the limb was restricted in this condition. The (B) average instantaneous mechanical power of each limb is plotted normalized by gait cycle for all conditions

# CHAPTER 5

**The influence of induced gait asymmetry on joint reaction forces.** (In preparation for the *Journal of Biomechanics*, 2021)

Emily M. McCain, Morgan J. Dalman, Matthew E. Berno, Theresa L. Libera, Michael L. Lewek, Gregory S. Sawicki, Katherine R. Saul.

## Abstract

Chronic injury- or disease-induced joint or limb impairments result in asymmetric gait deviations that may precipitate changes in joint loading associated with joint pain and osteoarthritis. Understanding the impact of gait deviations on joint reaction forces is challenging because of concurrent neurological and/or anatomical changes and because joint reaction forces cannot be experimentally measured without medically invasive instrumented implants. Instead, researchers can simulate walking kinematics with musculoskeletal models and calculate joint reaction forces. We sought to determine the impact of joint motion limitations and induced asymmetry on the ankle, knee, and hip joint reaction forces. Data were recorded as 8 unimpaired participants walked with custom ankle stays and knee braces to unilaterally (uni) and bilaterally (bi) restrict ankle (*uni-ank, bi-ank)*, knee (*uni-knee*, *bi-knee*), and combined ankle and knee (*uni-a+k, bi-a+k*) motion. Personalized models, experimentally determined kinematics, and ground reaction forces were used with the computed muscle control tool to determine simulated muscle activations guided by electromyography-driven timing constraints. A joint force analysis probe determined ankle, knee, and hip joint reaction forces along the long axis of the talus, tibia, and femur, respectively. Knee restriction increased ground reaction force peak and loading rate ipsilaterally but decreased peak ground reaction forces contralaterally when compared to the *braced* condition. Bilateral joint restrictions resulted in increased ground reaction force peak and

loading rate compared to the contralateral limb of unilaterally restricted conditions. Despite changes in ground reaction forces, joint reaction forces were relatively unchanged because of a reduction in muscle forces during loading response. Our research demonstrates bracing at a joint results in increased limb loading; however, reductions in muscle forces counteract changes in limb loading such that joint reaction forces were relatively unchanged.

## Introduction

Unilateral impairments resulting from chronic injury or illness - including lower limb amputation (Mahon et al., 2019), injury to the anterior cruciate injury (Chaudhari et al., 2008), Parkinson's disease (Frazzitta et al., 2013), or stroke (Allen et al., 2011; Allen et al., 2014) - result in walking patterns that are asymmetric. Gait asymmetry ratios compare impaired and unimpaired limbs with regard to a variety of spatiotemporal, kinematic, and kinetic measures (e.g. step-length (Allen et al., 2011), step-time (Ellis et al., 2013) and limb propulsion (Xergia et al., 2013)). Of note, the presence of asymmetric walking patterns is thought to be associated with increased joint reaction forces (Andriacchi and Mündermann, 2006; Maly, 2008). Changes in joint reaction forces have been implicated in the increased incidence of comorbidities including osteoarthritis (OA) (Chaudhari et al., 2008) and joint pain (Hendershot and Wolf, 2014) in patient populations who frequently display asymmetric gait. Rehabilitative efforts that target improved impaired limb or joint function (Awad et al., 2017b) or reduced spatiotemporal/propulsive asymmetry (Awad et al., 2015b) may restore limb loading to decrease the likelihood of developing comorbidities including joint pain and OA.

Understanding the relationship among impaired limb or joint function, walking asymmetry, and joint reaction forces is difficult because joint reaction forces can only be experimentally measured by expensive, medically invasive, instrumented implants (Fregly et al., 2012). As this

instrumentation is typically implanted after OA development or injury, measurements may be impacted by altered gait kinematics (Bytyqi et al., 2014) or changes in muscle strength (Loureiro et al., 2018). Therefore, the impact of altered joint function or walking asymmetry on joint loading is often quantified by joint moments or ground reaction forces as a proxy for joint reaction forces (Shakoor et al., 2003; Tateuchi et al., 2017). Using these proxy measures, researchers have provided some evidence for the influence of asymmetry on altered limb loading. For example, split-belt treadmill training to reduce step-length asymmetry resulted in concurrent reduction in ankle joint moment asymmetry in persons post-stroke (Betschart et al., 2020). In addition, ankle exoskeletons applying torque to the paretic ankle can increase the ankle joint moments (Takahashi et al., 2015c). Lastly, powered ankle-foot prosthetics have been shown to decrease the unaffected limb resultant peak vertical ground reaction forces in unilateral transtibial amputees (Grabowski and D'Andrea, 2013).While these results indicate that improving joint function or spatiotemporal walking asymmetry may influence joint moments and ground reaction forces, these measures do not account for joint loading due to internal forces from muscles, and thus represents an incomplete analysis of the problem.

Musculoskeletal modeling simulations can calculate joint reaction forces due to all loads placed on the model (Steele et al., 2012) including contributions from applied external, inertial, and calculated muscle forces (Imani Nejad et al., 2020; Shao et al., 2009). For example, researchers have applied musculoskeletal modeling techniques to simulate clinical gait (Akbas et al., 2019a; Gerus et al., 2013; Marra et al., 2015) and the shape and timing of contact force profiles measured with implanted instrumentation (Manal and Buchanan, 2013). More recently EMG-driven simulations have been used to predict joint reaction forces in other clinical populations including persons post-stroke (Marrocco et al., 2016) or post ACL reconstructive surgery (Wellsandt et al.,

2015). EMG-driven musculoskeletal simulation therefore has the potential to characterize the relationship between altered joint function and walking asymmetry on lower limb joint reaction forces.

After chronic injury- or disease- induced impairments, concurrent anatomical or physiological changes make isolating the impacts of reduced joint range of motion and walking asymmetry on joint reaction forces difficult. Previous research has successfully used joint bracing unilaterally (Lewek et al., 2012; McCain et al., 2019; Wutzke et al., 2012) and bilaterally at lower limb joints to restrict joint motion and engender asymmetric and symmetric gait in unimpaired participants. The purpose of this work is to extend this approach to investigate the impact of altered joint function and the resulting walking (a)symmetry on joint reaction forces.

We used EMG-informed musculoskeletal modeling simulations of unimpaired participants walking with restricted ankle range of motion, knee range of motion, and ankle+knee range of motion unilaterally and bilaterally. With imposed joint restriction, decreased impaired limb cushioning during heel strike may result in increased in joint loading ipsilaterally (Shih et al., 2019); therefore, we hypothesized (h1a) unilateral joint restrictions will result in increased ipsilateral knee and hip joint reaction force loading rate and first peak value. Restricting joint motion has been shown to reduce ipsilateral propulsion (McCain et al., 2019) requiring increased collision during step to step transition to redirect the center of mass (Donelan and Kram, 2001; Mahon et al., 2015). that may result in larger contralateral joint reaction forces. Therefore, we hypothesized (h1b) that unilateral joint restrictions will result in increased contralateral knee and hip joint reaction force loading rate and first peak value. Secondly, we hypothesized that (h2) unilateral restriction of the ankle and knee simultaneously will result in larger ipsilateral joint reaction force peak and loading rate when compared to unilateral restriction of the ankle or knee

because of reduced limb compliance. Lastly, (h3) symmetric (bilateral) joint restrictions will restore symmetric propulsion, thereby reducing JRF peaks and loading rates when compared to the unrestricted limb with asymmetric (unilateral) restrictions.

## Methods

### Data Collection

All procedures were approved by the institutional review board at UNC-Chapel Hill. Eight healthy adult participants signed approved consent forms prior to data collection. During data collection, participants walked on an instrumented split belt treadmill at 0.8 $ms^{-1}$ for eight data collection conditions, each lasting 7 minutes, including: (1) *control*: no braces worn, ( 2) *braced*: knee braces worn unrestricted bilaterally; unilaterally restricted conditions: (3) *uni-ank:* unilaterally restricted ankle, (4) *uni-knee:* unilaterally restricted knee, and (5) *uni-a+k:* unilaterally restricted ankle+knee; and bilaterally restricted conditions: (6) *bi-ank*: bilaterally restricted ankles, (7) *bi-knee:* bilaterally restricted knees, and (8) *bi-a+k:* bilaterally restricted ankles+knees simultaneously. This joint restriction protocol allowed us to investigate (1) the impact of a specific joint restriction (*braced* vs *uni-ank*, *uni-knee*, *uni-a+k*) and (2) the impact of induced asymmetry vs symmetry by comparing unilateral to bilateral restriction. We used custom 3D printed ankle stays to restrict ankle motion and a lockable DonJoy T-Rom knee brace to restrict knee motion (McCain et al., 2021). Ankle stays were applied unilaterally (*uni-ank, uni-a+k)* and bilaterally (*bi-ank, bi-a+k*) then removed for all other conditions. Knee bracing was worn bilaterally for all conditions except the *control* condition which was performed last to prevent multiple static captures. Knee bracing was set to restrict knee motion unilaterally (*uni-knee, uni-a+k)* and bilaterally (*bi-knee, bi-a+k*) but unrestrictive in all other conditions. The *braced, uni-ank, uni-knee, uni+k, bi-ank, bi-knee, bi-a+k* conditions were randomly ordered.

We recorded the positions of 43 reflective markers attached to the lower limb and pelvis (McCain et al., 2019) using an eight-camera system (Vicon, Oxford, UK) sampling data at 120 Hz; recorded marker positions were filtered with a 6Hz Butterworth filter in OpenSim software (Delp et al., 2007). Ground reaction forces (GRFs) were recorded at 1200 Hz, then filtered with a $2^{nd}$ order low pass Butterworth filter (25Hz). Surface electromyography (EMG) (Trigno, Delsys) was recorded at or above 1200Hz bilaterally on the tibialis anterior, soleus, lateral gastrocnemius, medial gastrocnemius, vastus lateralis, and biceps femoris. EMG data were filtered using a $4^{th}$ order bandpass filter (30Hz/450Hz), then the rolling root mean square was taken (50ms) before data was smoothed using a moving average (50ms) and normalized by representative peaks.

**Musculoskeletal Simulations**

We adapted an existing OpenSim full-body model (Rajagopal et al., 2016) to represent the lower-limb and scaled the model to each user's anthropometry using static data captures. The inverse kinematics algorithm was used to determine joint kinematics from individualized models and filtered marker data (Delp et al., 2007). The residual reduction algorithm tool was used to improve the dynamic consistency of the model and generate sets of smoothed kinematics that were input into the computed muscle control optimization tool (Thelen and Anderson, 2006); we ran RRA separately for the *control* condition, to account for added mass of knee bracing. Processed and normalized EMG signals were used to define CMC constraints to ensure muscle activation timing was consistent with recorded data (McFarland et al., 2019). Specifically, using the six muscle recordings, we constrained the timing of ten representative muscles (Table 5.1) to be consistent with recorded normalized EMG. We ran CMC simulations for 10 stance phases bilaterally. Stance phases were selected to be from 10 consecutive gait cycles during the last two minutes of data collected for each trial to ensure maximum adaptation time. The gait cycles were

chosen from that time frame by identifying and removing any time periods with crossover steps then selecting the 10 consecutive gait cycles closest to the end of the data. Heel strike and toe off timing determined from GRFs using a custom MATLAB script.

**Table 5.1:** EMG recordings and corresponding model constraints

| EMG recorded Muscles | Model Muscles Constrained |
|---|---|
| Tibialis Anterior | Tibialis Anterior |
| Lateral Gastrocnemius | Lateral Gastrocnemius |
| Medial Gastrocnemius | Medial Gastrocnemius |
| Soleus | Soleus |
| Bicep femoris | Bicep femoris long head<br>semimembranosus<br>semitendinosus |
| Vastus lateralis | vastus lateralis<br>vastus intermedius<br>vastus medialis |

**Data Processing**

**Joint reaction analysis.** A joint analysis probe (Steele et al., 2012) was incorporated into the CMC algorithm to calculate the joint reaction forces (JRFs) at the ankle in the talus body frame, at the knee in the tibia body frame and at the hip in the femur body frame. We considered JRFs along the y-axis of the body frame and normalized force by subject weight. Peak JRFs at each joint were calculated as the maximum of the first 50% of stance phase and JRF loading rates were determined as the maximum gradient between heel strike and 1$^{st}$ peak JRF timing (Morgenroth et al., 2014). JRF peak and loading rates were averaged for each limb across subjects for each condition.

**Ground Reaction Force Analysis**. We considered the vertical ground reaction forces across all conditions. Ground reaction forces were normalized to subject mass, and peak ground reaction forces were found as the maximum force during the first half of stance phase (Grabowski

and D'Andrea, 2013). The GRF loading rate was determined as the maximum gradient of the GRF between heel strike and peak GRF timing. GRF peaks and loading rates were averaged for each limb across subjects for each condition.

**Summed Ankle, Knee, and Hip Muscle Forces.** A muscle analysis probe was included in the CMC algorithm to calculate the force generated in all included model muscles. To investigate the role of muscle forces on ankle, knee, and hip joint reaction forces we summed time-varying curves of forces corresponding muscles responsible for ankle plantarflexion/dorsiflexion, knee flexion/extension, and hip flexion/extension, respectively (Table 5.2). Time-varying ankle, knee, and hip joint muscle force curves were integrated with time during double support to quantify the role of muscle forces 1$^{st}$ peak and loading rates of joint reaction forces. Summed ankle, knee and hip muscle forces for each limb were averaged across subjects for each condition.

**Table 5.2**: Simulated muscles included in total joint muscle force calculation.

| Ankle | | Knee | | Hip | |
|---|---|---|---|---|---|
| Plantarflexion | Flexor digitorum longus | Flexion | lateral gastrocnemius | Flexion | Adductor brevis |
| | Flexor digitorum longus | | medial gastrocnemius | | Adductor longus |
| | lateral gastrocnemius | | Biceps femoris long head | | Gluteus minimus (anterior) |
| | medial gastrocnemius | | Biceps femoris short head | | Iliacus |
| | Flexor digitorum longus | | Gracilis | | Psoas |
| | Flexor digitorum longus | | Sartorius | | Rectus femoris |
| Dorsiflex | Extensor hallucis longus | | Semimembranosus | | Sartorius |
| | Extensor hallucis longus | | Semimembranosus | | Tensor fascia latae |
| | tibialis anterior | Extension | Vastus lateralis | Extension | Adductor longus |
| | | | Vastus medialis | | Adductor magnus (distal) |
| | | | Vastus intermedius | | Adductor magnus (ischial) |
| | | | Rectus femoris | | Adductor magnus (middle) |
| | | | | | Adductor magnus (proximal) |
| | | | | | Biceps femoris long head |
| | | | | | Gluteus Medius (anterior) |
| | | | | | Gluteus Medius (middle) |
| | | | | | Gluteus Medius (posterior) |
| | | | | | Gluteus maximus (anterior) |
| | | | | | Gluteus maximus (middle) |
| | | | | | Gluteus maximus (posterior) |
| | | | | | Gluteus minimus (posterior) |
| | | | | | Semimembranosus |
| | | | | | Semimembranosus |

**Statistical analysis**

We performed a one-way (factor levels: braced, uni-ank, uni-knee, uni-a+k) repeated measures reduced maximum likelihood (REML) analysis in SAS Statistical Software (SAS Institute, Cary, NC, USA) to determine significant ($p_{reml}^{uni}$<0.05) impacts on first peak and loading rates for ground reaction forces, joint reaction forces, and total joint muscle forces. To investigate the significance ($p_{ph}$<0.05) in h1a, h1b, and h2, we performed t-tests with Bonferroni multiple comparisons (h1a/h1b: *braced* vs *uni-ank, braced vs uni-knee;* h2: *uni-ank vs uni-a+k, uni-a+k vs uni-a+k)* on GRFs, JRFS, and total joint muscle forces for the ipsilateral (h1a/h2) and contralateral (h1b) limbs, respectively. We performed a two-way repeated measures REML analysis to determine whether outcome measures (GRFs, JRFs, total joint muscle force) were significantly ($p_{reml}^{bi}$<0.05) affected by walking asymmetry (factor 1 levels: unilateral/bilateral) or restriction joint (factor 2 levels: ankle, knee, ankle+knee).

## Results

Outputs from model scaling, inverse kinematics, reduced residuals algorithm, and computed muscle control were determined to be withing OpenSim best practices (Delp et al., 2007). Subject averaged joint angles determined from CMC simulations are plotted over stance phase (Figure S5.1). CMC determined simulated muscle activity represented some features of measured muscle activity for the restricted limb of *unilaterally restricted* conditions (Figure S5.2), unrestricted limb of the *unilaterally restricted* conditions (Figure S5.3), and *bilaterally restricted* conditions (Figure S5.4). Unconstrained simulated muscle activity for the rectus femoris, biceps femoris short head, psoas, and iliacus muscles are provided over stance phase all conditions (Figure S5.5).

**Ground Reaction Forces.** On the ipsilateral limb, unilaterally restricted limb (Figure 5.1a) first peak ($p_{reml}^{uni}$=0.04) and loading rate ($p_{reml}^{uni}$<0.01) for vertical GRFs were significantly affected by walking trials. Peak GRF increased significantly in the *uni-a+k* (11.16±0.51 N BW$^{-1}$, $p_{ph}$=0.05) condition compared to the *braced* condition (10.82±0.53 N BW$^{-1}$). Loading rate was significantly increased in the *uni-a+k* (171.29±25.58 N BWs$^{-1}$, $p_{ph}$<0.01) condition when compared to the *braced* condition (108.49±12.89 N BWs$^{-1}$). In the *uni-a+k* (197.13±25.75 N BWs$^{-1}$) GRF loading rate increased significantly when compared to the *uni-ank* (128.21±18.97 N BWs$^{-1}$, $p_{ph}$<0.01) condition. In the *uni-ank* condition we saw no significant increase in peak GRF (10.89 ± 0.49 N BW$^{-1}$) or GRF (128.21 ± 18.97 N BW$^{-1}$) loading rate when compared to the *braced* condition. On the contralateral unrestricted limb, peak GRF ($p_{reml}^{uni}$=0.02) and GRF loading rate ($p_{reml}^{uni}$=0.01) were significantly impacted by the walking trials. Peak GRF decreased significantly in the *uni-a+k* (10.48 ± 0.45 N BW$^{-1}$, $p_{ph}$=0.05 ) condition when compared to the *braced* condition, and GRF loading rate increased significantly in the *uni-a+k* (146.54±24.86 N BWs$^{-1}$) when compared to the *uni-ank* (134.72±27.58 N BWs$^{-1}$, $p_{ph}$= 0.04) conditions. We saw no significant change in peak GRF or GRF loading rate in the *uni-ank* condition when compared to the *braced* or *uni-a+k* conditions. When considering unilaterally vs bilaterally restricted conditions, peak GRF was significantly affected by symmetry of restriction ($p_{reml}^{uni}$<0.01) and symmetrically restricted conditions had higher GRF peaks than unrestricted conditions. Joint restriction did not significantly affect the GRF, but there was also a significant interaction between joint restriction and the symmetry of restriction ($p_{reml}^{bi}$=0.05). GRF loading rate was significantly affected by the symmetry of restriction ($p_{reml}^{bi}$<0.01) and the joint restriction ($p_{reml}^{bi}$ <0.01), and there was a significant interaction between joint restriction and symmetry of restriction ($p_{reml}^{bi}$<0.01).

Symmetrically restricted conditions had significantly larger GRF loading rates than asymmetric conditions.

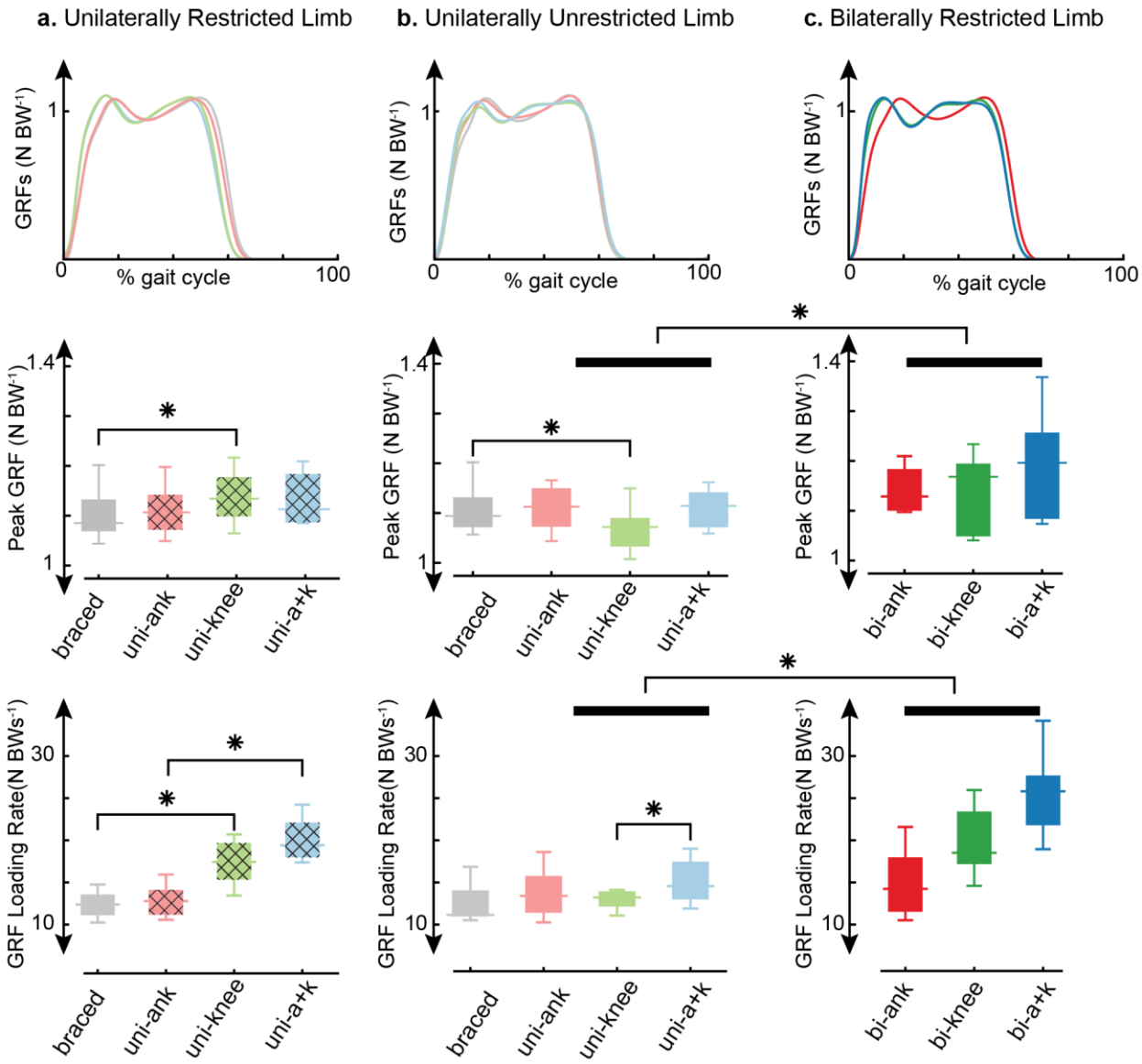


**Figure 5.1.** Vertical GRFS over a gait cycle, peak GRF and GRF loading rates.

Vertical GRFs normalized over a gait cycle, median ± standard deviation peak GRF, and median ± standard deviation GRF loading rate are plotted for the (**a**) restricted limb in the *braced* and *unilaterally* restricted conditions, (**b**) unrestricted limbs in the *braced* and *unilaterally* restricted conditions, and for the (**c**) *bilaterally* restricted conditions.

**Joint reaction forces.** We plotted subject averaged values from the *braced* and unilaterally restricted conditions ipsilateral limb (Figure 5.2a) and contralateral limb (Figure 5.2b); subject averaged JRF values from one limb over stance phase are plotted for the bilaterally restricted conditions (Figure 5.2c). We provided subject average ± standard deviation for peak JRF (Table 5.3) and JRF loading rates (Table 5.4). On the ipsilateral limb in unilaterally restricted and braced conditions, ankle peak JRFs and JRF loading rates were not significantly affected walking condition. We found ipsilateral peak knee JRF was significantly affected by walking condition ($p_{reml}^{uni}$ =0.01). Post hoc analysis found peak knee JRF (Figure 5.3.a) was significantly decreased in the *uni-ank* (0.37±0.56 N BW$^{-1}$) condition when compared to the *braced* (3.84±0.44 N BW$^{-1}$, $p_{ph}$=0.01) and *uni-a+k* (3.77±0.47 N BW$^{-1}$, $p_{ph}$=0.05) conditions. Knee JRF loading rate was not significantly affected by walking condition. Ipsilateral hip peak JRFs and JRF loading rates were not significantly affected walking condition. On the contralateral limb, we found walking condition (levels: *braced, uni-ank, uni-knee, uni-a+k)* did not significantly affect JRF peak or JRF loading rate at any of the joints. When comparing unilaterally vs bilaterally restricted conditions with two factors (joint, restrictions symmetry), we found neither factor significantly affected JRF peak or JRF loading at the ankle, knee, or hip.

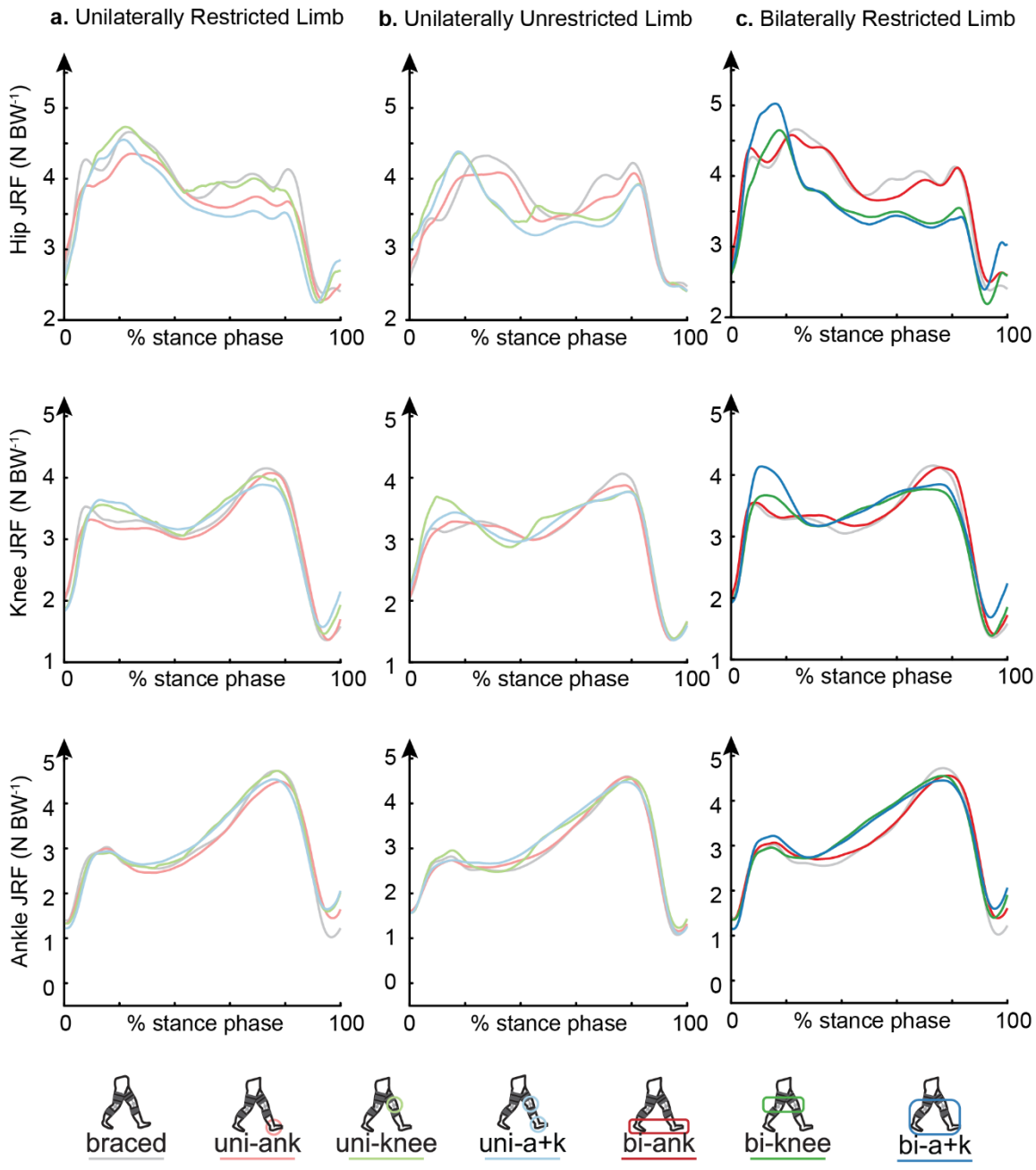


**Figure 5.2.** Subject averaged joint reaction forces

Joint reaction forces at the ankle, knee, and hip joint are plotted over stance phase for the (**a**) restricted limb in the *braced* and *unilaterally* restricted conditions, (**b**) unrestricted limbs in the *braced* and *unilaterally* restricted conditions, and for the (**c**) *bilaterally* restricted conditions.

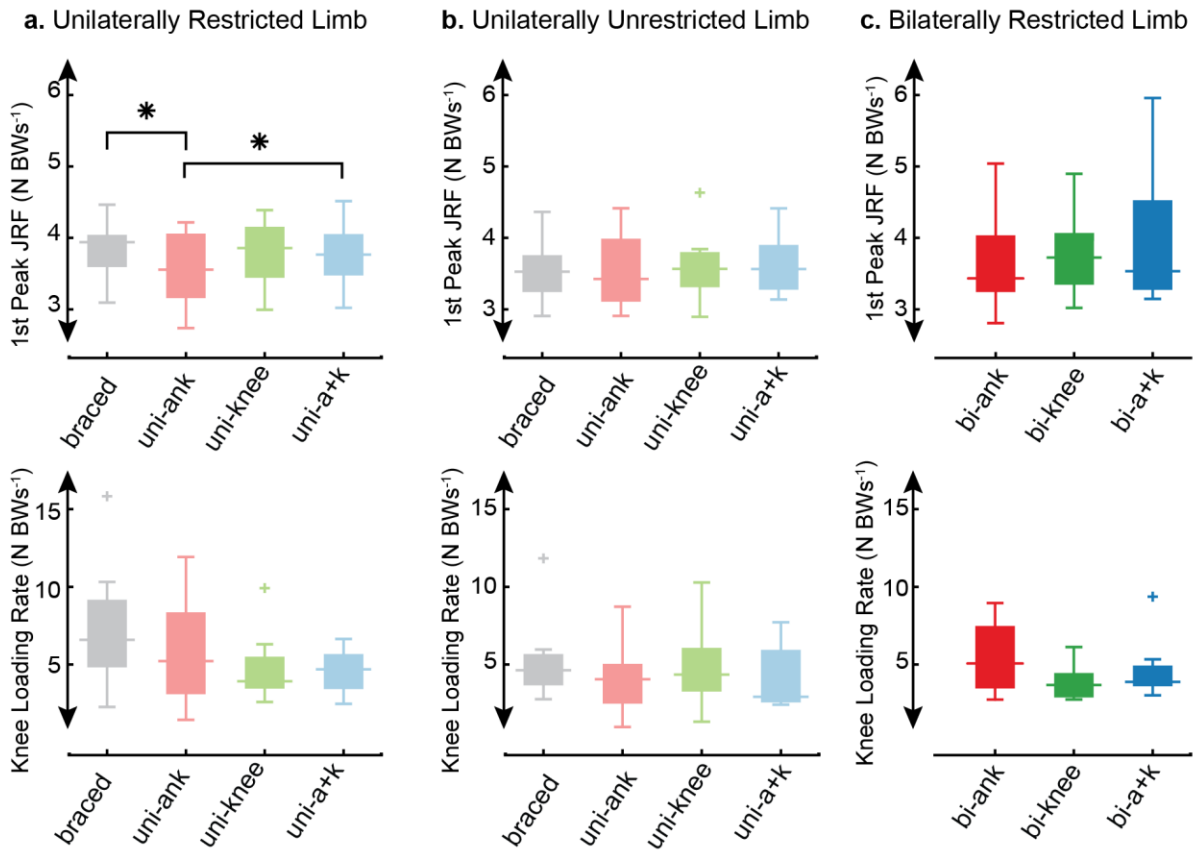


**Figure 5.3**. Peak knee JRF, and JRF knee loading rate.

Peak knee JRF and JRF loading rates are plotted for the (a) *braced* and *unilaterally* restricted conditions, (b) unrestricted limbs in the *braced* and *unilaterally* restricted conditions, and for the (c) bilaterally restricted conditions. Centerline refers to median and error bars are ± standard deviation.

**Table 5.3.** Group peak joint reaction forces (mean ± std; N BW$^{-1}$)

| Condition | Restricted Limb | | | Unrestricted Limb | | |
|---|---|---|---|---|---|---|
| | Ankle | Knee | Hip | Ankle | Knee | Hip |
| control | 3.45±0.42 | 3.92±0.61 | 5.46±0.88 | 3.13±0.41 | 3.73±0.58 | 4.99±0.82 |
| braced | 3.39±0.36 | 3.84±0.44 | 5.08±0.93 | 3.12±0.33 | 3.54±0.45 | 4.49±0.83 |
| uni-ank | 3.36±0.58 | 3.56±0.56 | 4.61±0.85 | 3.19±0.41 | 3.55±0.55 | 4.38±0.72 |
| uni-knee | 3.32±0.35 | 3.79±0.49 | 4.89±0.67 | 3.38±0.43 | 3.61±0.51 | 4.31±0.49 |
| uni-a+k | 3.48±0.41 | 3.77±0.47 | 4.66±0.83 | 3.45±0.30 | 3.63±0.44 | 4.48±0.65 |
| bi-ank | 3.47±0.38 | 3.81±0.56 | 4.86±0.76 | | | |
| bi-knee | 3.73±0.36 | 4.06±0.52 | 4.71±0.67 | | | |
| bi-a+k | 3.73±0.51 | 4.08±0.64 | 4.98±0.74 | | | |

**Table 5.4**. Group joint reaction force loading rates (mean ± std; N BWs$^{-1}$)

| Condition | Restricted Limb | | | Unrestricted Limb | | |
|---|---|---|---|---|---|---|
| | Ankle | Knee | Hip | Ankle | Knee | Hip |
| control | 47.57±15.25 | 71.65±17.40 | 92.78±29.34 | 38.06±11.60 | 67.12±33.15 | 83.39±65.03 |
| braced | 44.19±18.00 | 77.77±32.62 | 107.75±79.62 | 33.58±6.07 | 61.37±22.22 | 64.17±26.00 |
| uni-ank | 43.17±20.52 | 65.46±28.23 | 83.39±49.09 | 31.51±10.37 | 51.88±18.32 | 55.14±20.79 |
| uni-knee | 38.66±12.73 | 57.20±18.42 | 66.24±21.56 | 38.45±10.18 | 57.90±21.22 | 55.25±22.17 |
| uni-a+k | 40.61±12.59 | 55.64±12.19 | 59.83±16.26 | 32.15±8.40 | 52.03±16.92 | 55.54±21.09 |
| bi-ank | 45.07±15.78 | 78.06±29.19 | 108.74±75.92 | | | |
| bi-knee | 38.21±8.35 | 55.84±12.77 | 61.78±4.21 | | | |
| bi-a+k | 48.15±13.12 | 64.88±13.79 | 75.48±17.74 | | | |

**Muscle Joint Contact Force Contributions.** On the ipsilateral limb of the unilaterally restricted and braced conditions we found summed ankle forces were significantly affected by the unilateral joint level restriction ($p_{reml}^{uni}$<0.01). Ipsilateral ankle joint muscle force decreased significantly in the *uni-a+k* (0.31 ± 0.09 N BW$^{-1}$, $p_{ph}$<0.01) condition when compared to the *braced* (0.43± 0.10 N BW$^{-1}$) condition. In the *uni-a+k* (0.33 ± 0.08 N BW$^{-1}$) condition the ankle joint muscle force decreased significantly when compared to the *uni-ank* (0.40± 0.13 N BW$^{-1}$, p=0.03) condition. Summed knee forces were significantly affected by the unilateral joint level restriction ($p_{reml}^{uni}$<0.01). At the knee, ipsilateral knee joint muscle force contribution decreased

significantly in the *uni-ank* (0.43±0.11 N BW$^{-1}$, $p_{ph}$ =0.02) and *uni-a+k* (0.38± 0.11 N BW$^{-1}$, $p_{ph}$<0.01) conditions when compared to the *braced* (0.48±0.11 N BW$^{-1}$) condition**.** When the ankle and knee were simultaneously restricted (0.39± 0.09 N BW$^{-1}$) we the knee joint muscle force contribution decreased significantly compared to the *uni-ank* ($p_{ph}$=0.02) condition. Summed hip forces were significantly affected by the unilateral joint level restriction ($p_{reml}^{uni}$<0.01). At the hip we saw a significant decrease in hip joint muscle force contribution in the *uni-knee* (0.61± 0.15 N BW$^{-1}$) condition when compared to the *braced* (0.78± 0.16 N BW$^{-1}$, $p_{ph}$<0.01) condition. Again, we saw the hip joint muscle force contribution decreased in the *uni-a+k* (0.59±0.13 N BW$^{-1}$) condition when compared to the *uni-ank* (0.69± 0.18 N BW$^{-1}$, $p_{ph}$=0.05) condition. On the <u>contralateral</u> limb of the unilaterally restricted and braced conditions, summed ankle ($p_{reml}^{uni}$=0.03) and knee ($p_{reml}^{uni}$=0.01) muscle force contribution was significantly affected by unilateral joint restriction. At the ankle post hoc paired t-tests did not yield any significant comparisons. However, at the knee we found a significant decrease in contralateral knee joint muscle contribution in the *uni-ank* (0.44 ± 0.14 N BW$^{-1}$) condition when compared to the *braced* (0.48 ±0.10 N BW$^{-1}$, $p_{ph}$=0.03) condition. Contralateral hip joint muscle contribution was not significantly affected by unilateral joint restriction. When we compared <u>unilaterally vs bilaterally</u> restricted conditions, we found symmetry of restriction did not significantly affect ankle, knee, or hip joint muscle force contributions. However, the location of restriction (ankle, knee, ankle+knee) did significantly affect the ankle ($p_{reml}^{bi}$=0.01), knee ($p_{reml}^{bi}$=0.01), and hip ($p_{reml}^{bi}$=0.04) joint muscle force contribution. In addition, we found the interaction between restriction symmetry and location of restriction significantly affected the ankle ($p_{reml}^{bi}$<0.01), knee ($p_{reml}^{bi}$= 0.02), and hip ($p_{reml}^{bi}$=0.03) joint muscle force contribution.

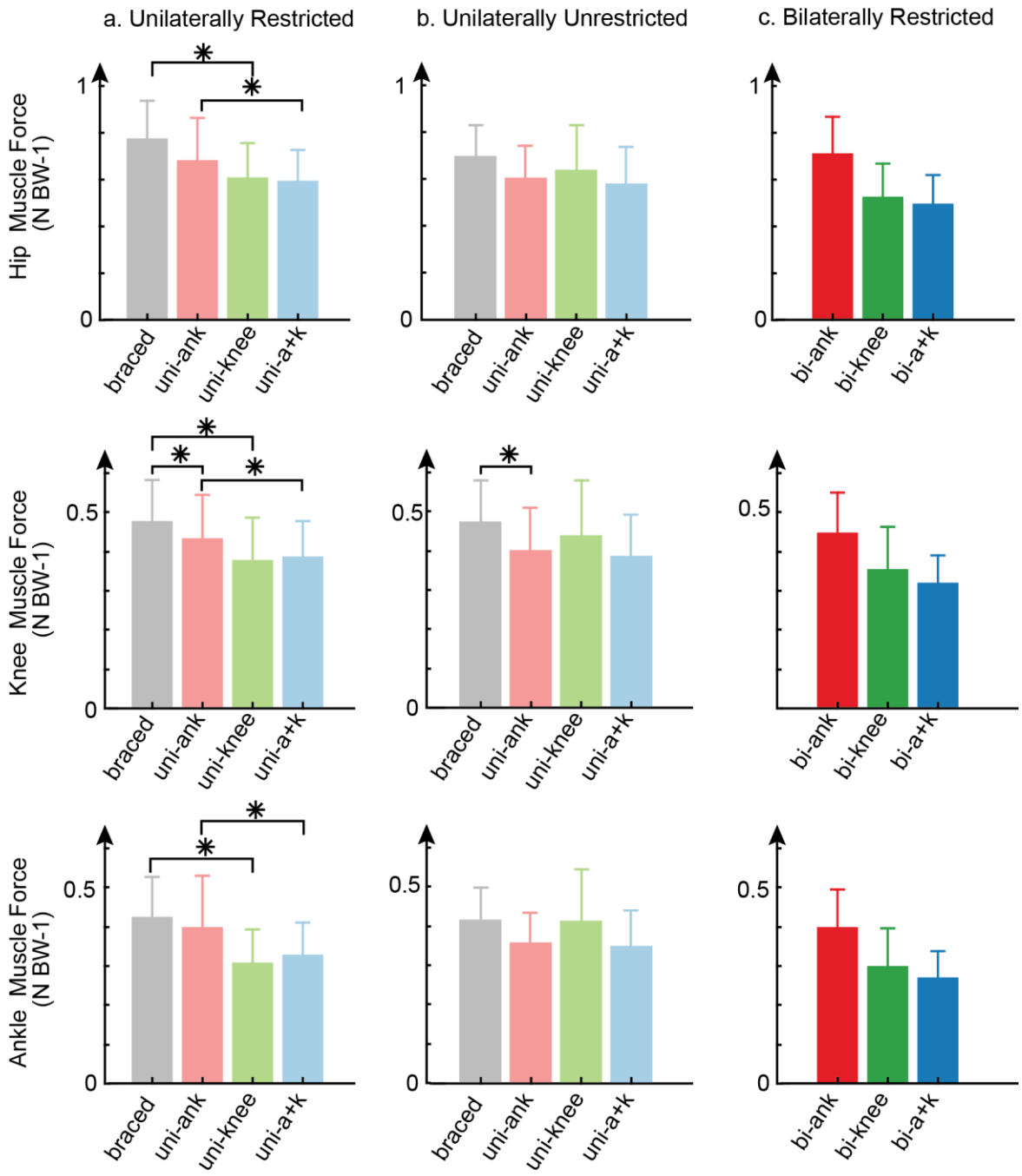


**Figure 5.4.** Group joint muscle forces.

Subject average ± standard deviation for the hip, knee, and ankle, summed joint muscle forces are plotted for the (**a**) restricted limb in the *braced* and *unilaterally* restricted conditions, (**b**) unrestricted limbs in the *braced* and *unilaterally* restricted conditions, and for the (**c**) *bilaterally* restricted conditions.

## Discussion

We employed EMG-driven musculoskeletal modeling simulations of unimpaired participants walking with joint-specific restrictions to investigate the impacts of altered joint range of motion and induced asymmetry on JRFs. Previous researchers have used dynamic analyses and musculoskeletal modeling to investigate the relationships between altered gait kinematics and limb/joint loading (Grabowski and D'Andrea, 2013; Marrocco et al., 2016; Shao et al., 2009) or between JRFs and cartilage degeneration (Morgenroth et al., 2014; Wellsandt et al., 2015), respectively. This research builds upon previous work by using a joint specific bracing approach to manipulate gait kinematics and more directly characterize the impact of changes in kinematics on JRFs. Our approach elicited ipsilateral increases in limb loading quantified by peak GRF and GRF loading rate. However, we saw no corresponding changes in JRFs because reduced muscle forces around the joint offset increases in external limb loading. Our results indicate changes in muscle force contribution to JRF can counteract changes in limb loading and caution against the use of GRFs a proxy for JRFS.

Our approach increased ipsilateral limb loading, as measured via peak GRF and GRF loading rates, as expected. The observed increases in peak GRF and GRF loading rate with knee restriction provides evidence that limiting knee joint motion during weight acceptance may reduce the limb's ability to yield to impulse load; this ability may be further limited with simultaneous restriction, given the increased GRF loading rate observed with simultaneous ankle and knee restriction when compared to ankle restriction alone. On the contralateral limb, we found insufficient evidence that reductions in restricted limb propulsion lead to increased contralateral limb GRF peak and loading rate. Specifically, while GRF loading rate did increase with simultaneous ankle and knee restriction in comparison to ankle restriction alone, neither ankle nor

knee restriction resulted in larger GRF loading rates in comparison to the braced condition. Further, the peak contralateral GRF *decreased* with knee restriction in comparison to the braced condition; while this joint bracing approach engenders propulsive asymmetry (McCain et al., 2021), changes in peak GRF or GRF loading rate are speed dependent (Grabowski and D'Andrea, 2013), and it is possible that increases in collision with ankle bracing were not large enough to be detected at this limited walking speed. Alternatively, participants may have opted to compensate for propulsive deficits after loading response. We expected restoring propulsive symmetry with bilateral restrictions would eliminate asymmetric step-to-step transitions associated with increased collision. Instead, peak GRF and GRF loading rate were significantly increased in the symmetrically restricted conditions compared to the asymmetrically restricted conditions. As we did not observe an increase in contralateral limb loading due to propulsive deficits, it is possible the increase in limb loading resulting from the increased stiffness with bilateral restriction is more influential than reducing effects of propulsive asymmetry.

Increased peaks and loading rates observed in vertical ground reaction forces were not indicative of increased JRFs. Although we hypothesized that reduced joint range of motion would increase ipsilateral peak JRF and JRF loading rate at the ankle, knee, and hip, only the peak knee JRF was significantly affected by joint restriction. Furthermore, we found that the peak knee JRF *decreased* with ankle restriction when compared to the *braced* condition, which was notably the opposite of our hypothesis. With respect to the contralateral limb, since we did not see increases in contralateral peak GRF or GRF loading rates, we reject h1b; contralateral ankle, knee, and hip JRFs were not significantly affected by joint restriction. Lastly, although we found that a symmetric restriction of joint range of motion led to increased GRF peak and rate values compared

to the unilaterally unrestricted limb, there were no significant changes between asymmetric and symmetric JRFs peak or loading rate values.

When knee range of motion was restricted, ipsilateral reductions in muscle force at the ankle, knee, and hip may explain why JRFs are relatively unchanged despite increased GRFs loading rate relative to the braced condition. Specifically, while GRF loading rate increased with knee restriction compared to the *braced* condition, ankle, knee, and hip joint muscle forces decreased, appearing to offset the net JRF values. Similarly, although GRF loading rate increased with simultaneous ankle and knee restriction compared to ankle restriction alone, ankle, knee, and hip joint muscle contributions decreased such that we saw no appreciable change in the JRFs. It is possible that with added knee restriction participants relied on the bracing for joint stability, lessening the requirements of surrounding muscles. It is also possible that restriction of knee motion increased skeletal alignment, or the resistance provided by the skeleton to the acceleration due to gravity, allowing for reduced muscle contributions (Anderson and Pandy, 2003; Liu et al., 2008).

Our results indicate the impacts of altered kinematics, GRFs, and muscle contributions to JRF are such that changes in joint moments or GRF-based metrics cannot adequately account for changes in JRFs in this study. This notion is supported by previous investigations that found knee JRF was unaffected by altered body armor loads (Lenton et al., 2018). Further, in persons with knee osteoarthritis, investigators found no change in knee joint loading profile during weight acceptance, despite changes in joint stiffness quantified by changes in joint range of motion in response to joint moment (Gustafson et al., 2019). Lastly, despite obvious changes in joint kinematics, the knee JRF determined for persons with mild crouch gait was found not to be different from unimpaired gait (Steele et al., 2012).

This investigation includes several limitations. Participants were on average significantly younger when compared to many patient populations, and it is possible this could affect the results. We note that the values predicted here for joint loading are within the range of values calculated or measured for the ankle (Prinold et al., 2016), knee (Gustafson et al., 2019; Lenton et al., 2018), and hip (Harris et al., 2017) in clinical walking. We restricted ankle motion using a polylactic acid ankle stay during ankle restricted conditions and removed the stay for all other conditions; it is possible the added mass could have affected results, although the ankle stay weighed less than 3 ounces. Knee bracing was worn bilaterally for all restricted conditions (either locked or unlocked) and thus the added mass of bracing should not affect the comparisons made here. The gait speed chosen for this work is significantly lower than the speed at which our participants would usually walk, and joint contact forces are known to be sensitive to walking speed (Lenton et al., 2018). While it is possible that walking with joint restriction at increased speeds may have more substantially affected JRFs, our walking speed was selected to allow for participants to be capable of completing bilaterally restricted conditions. Future work should investigate the impact of joint restrictions on joint contact forces across a range of speeds. As prior research has demonstrated that the asymptomatic arthritic knee has increased JRF after thirty minutes of walking due primarily to increased muscle forces (Gustafson et al., 2019), it is possible a longer walking period for each condition would better elucidate changes in contralateral limb loading. We did not measure and therefore could not incorporate the moment applied by bracing to restrict joint motion. However, we note ankle and knee kinematics during loading response are qualitatively similar across conditions, including the control condition, and therefore external moments in this period were likely significantly less impactful than GRFs. Joint restriction by bracing likely affected

muscle activity; however, we attempted to mitigate this limitation by incorporating EMG timing restrictions to inform our simulation of experimental muscle activity.

Our approach was able to limit joint motion asymmetrically and symmetrically and elicit changes in limb loading. We demonstrated that restrictions in knee motion elicited an ipsilateral increase in limb loading, and that simultaneous restriction of ankle and knee motion increased limb loading in comparison to restriction of the ankle or knee in isolation. Although we anticipated symmetric restriction would eliminate increases in limb loading resulting from asymmetric propulsion, instead we found symmetric restriction increased GRF peak and loading rate when compared to the contralateral limb of unilaterally restricted conditions. Interestingly, we did not see changes in JRFs that corresponded to a similar change in limb loading. Instead, we found reductions in muscle forces during loading response with joint restriction offset changes in limb loading resulting in similar JRFs across conditions. Our work demonstrates limited joint range of motion and resultant alterations in limb loading need not indicate alterations in joint contact force due to muscle-level changes and cautions against the use of external forces or joint moments as a proxy for JRFs. Future work is warranted to investigate how reduced joint motion and joint asymmetry relate to JRFs at increased speeds and over prolonged walking.

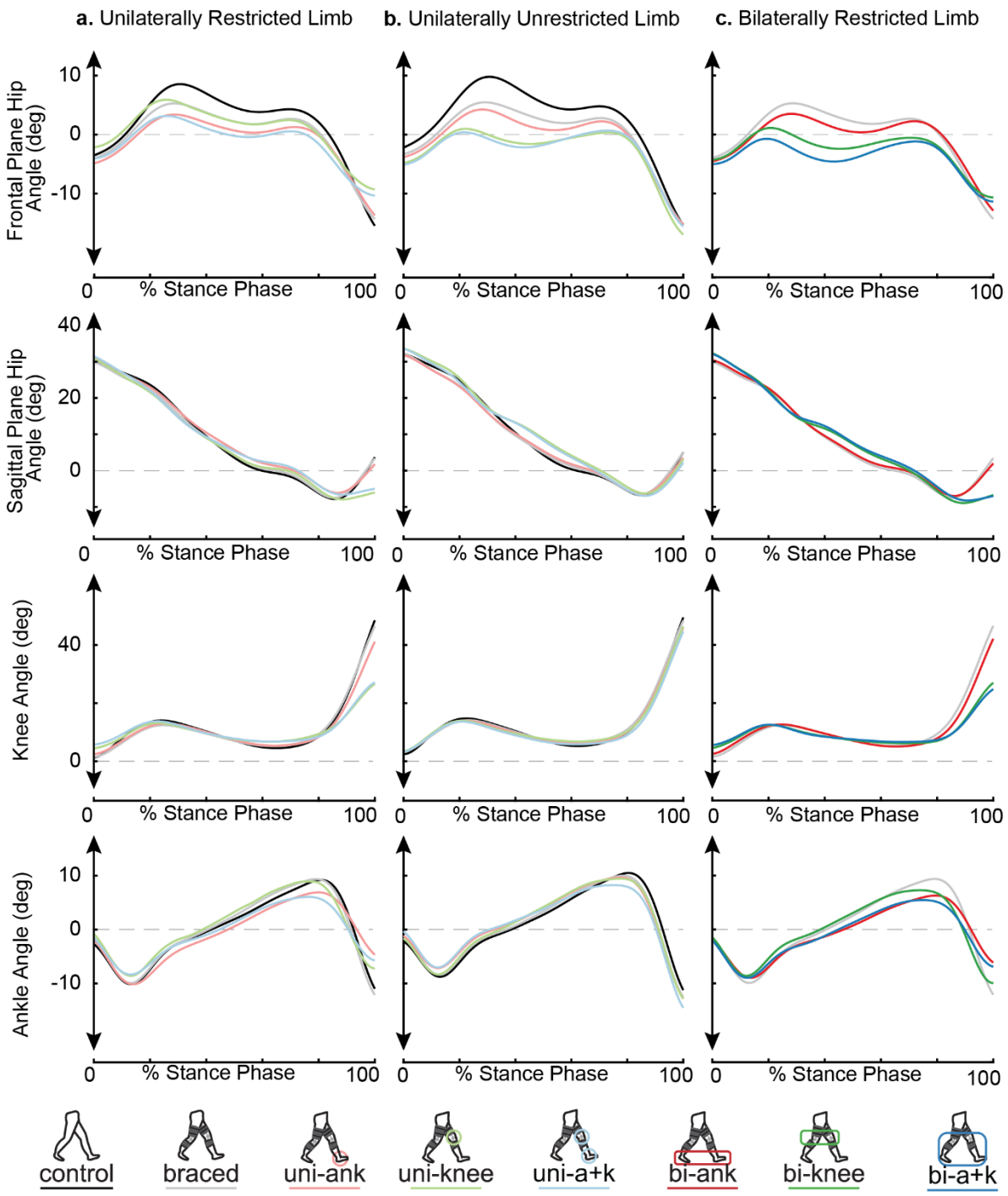


**Figure S5.1**. Subject average joint angles.

Frontal plane hip angle, sagittal plane hip angle, knee angle, and ankle angle are normalized for the (**a**) restricted limb in the *braced* and *unilaterally* restricted conditions, (**b**) unrestricted limbs in the *braced* and *unilaterally* restricted conditions, and for the (**c**) *bilaterally* restricted conditions.

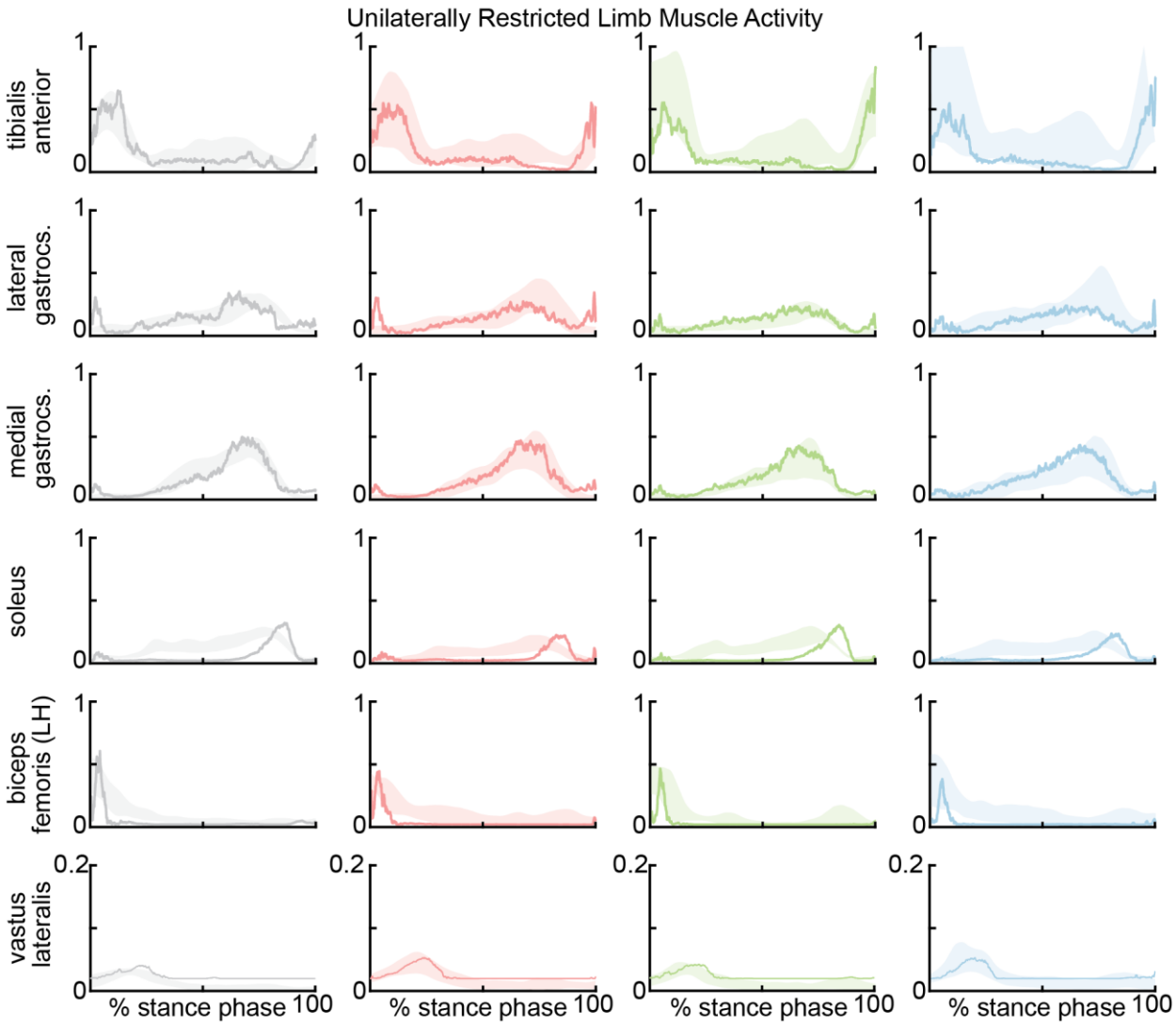


**Figure S5.2** Unilaterally restricted limb measured vs simulated muscle activity.

Muscle activity for (**a**) *braced* condition, restricted limb for the **(b)** *uni-ank*,**(c)** *uni-knee*,*and* **(d)** *uni-a+k* conditions. Activations from computed muscle control are plotted with measured EMG in rows one throuh six for the tibialis anterior, lateral gastrocnemius, medial gastrocneumus, soleus, biceps femoris long head and vastus lateralisWe normalized the peak of experimental EMG signals to the peak simulated activity for the muscle durign the stance phase simulation then calculated the standard deviaiton of the signal used to create a shaded region of emg signal ± std.

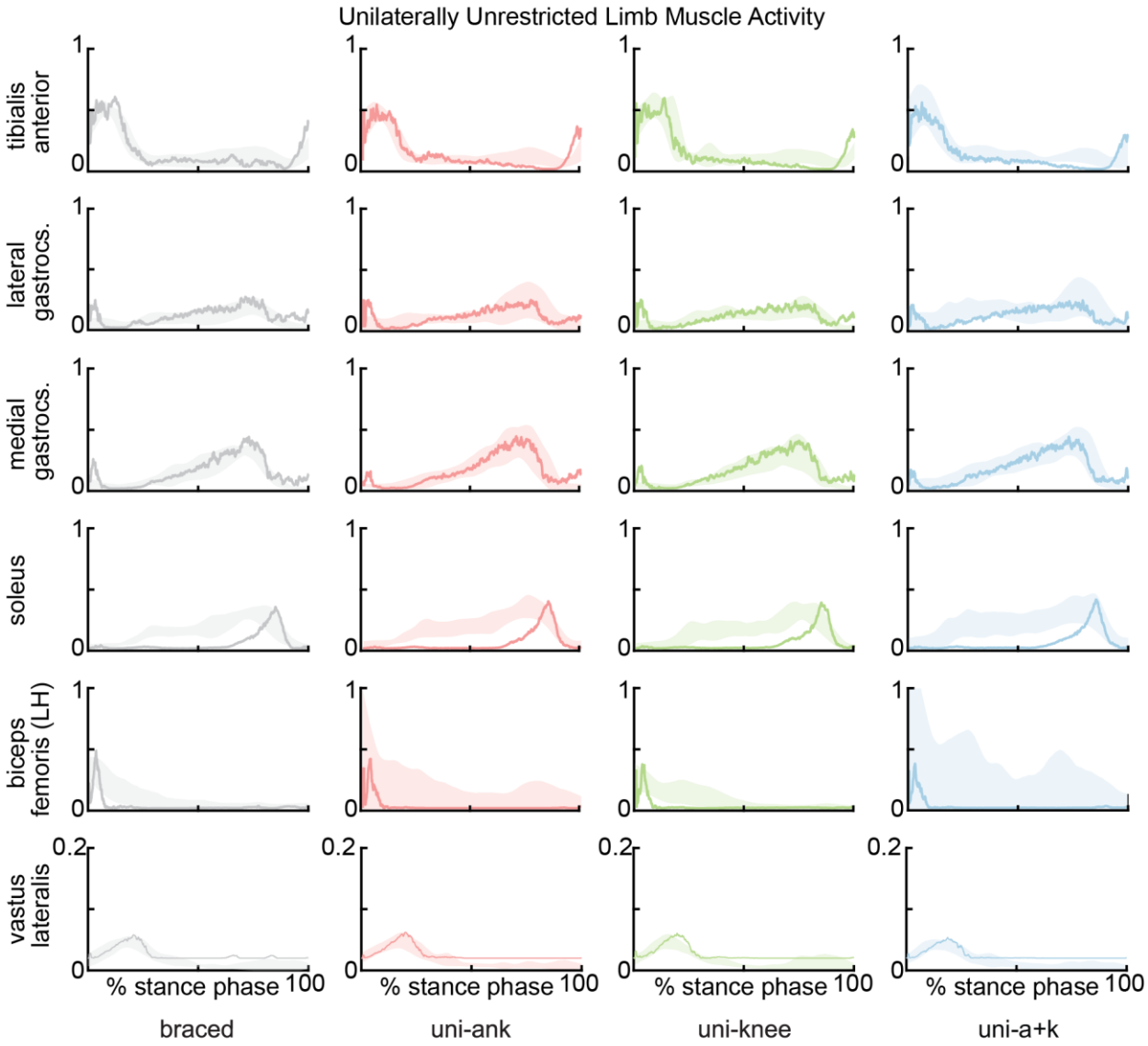


**Figure S5.3**. Unilaterally unrestricted limb measured vs simulated muscle activity.

Muscle activity for (**a**) *braced* condition, unrestricted limb for the **(b)** *uni-ank*,**(c)** *uni-knee,and* **(d)** *uni-a+k* conditions. Activations from computed muscle control are plotted with measured EMG in rows one throuh six for the tibialis anterior, lateral gastrocnemius, medial gastrocneumus, soleus, biceps femoris long head and vastus lateralisWe normalized the peak of experimental EMG signals to the peak simulated activity for the muscle durign the stance phase simulation then calculated the standard deviaiton of the signal used to create a shaded region of emg signal ± std.

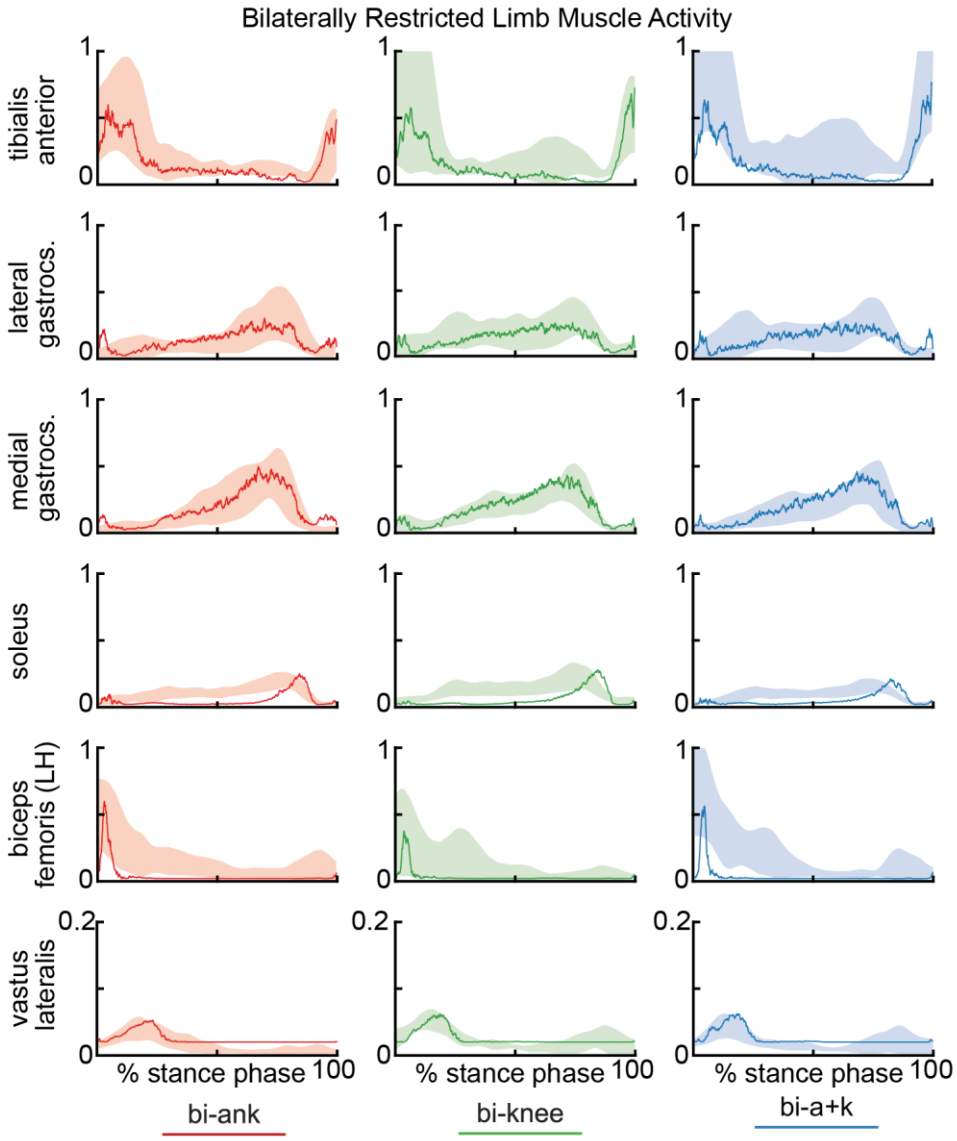


**Figure S5.4** Bilaterally Restricted measured vs simulated muscle activity.

Muscle activity for (**a)** b*i-ank*,**(c)** *bi-knee*,*and* **(d)** *bi-a+k* conditions. Activations from computed muscle control are plotted with measured EMG in rows one throuh six for the tibialis anterior, lateral gastrocnemius, medial gastrocneumus, soleus, biceps femoris long head and vastus lateralisWe normalized the peak of experimental EMG signals to the peak simulated activity for the muscle durign the stance phase simulation then calculated the standard deviaiton of the signal used to create a shaded region of emg signal ± std.

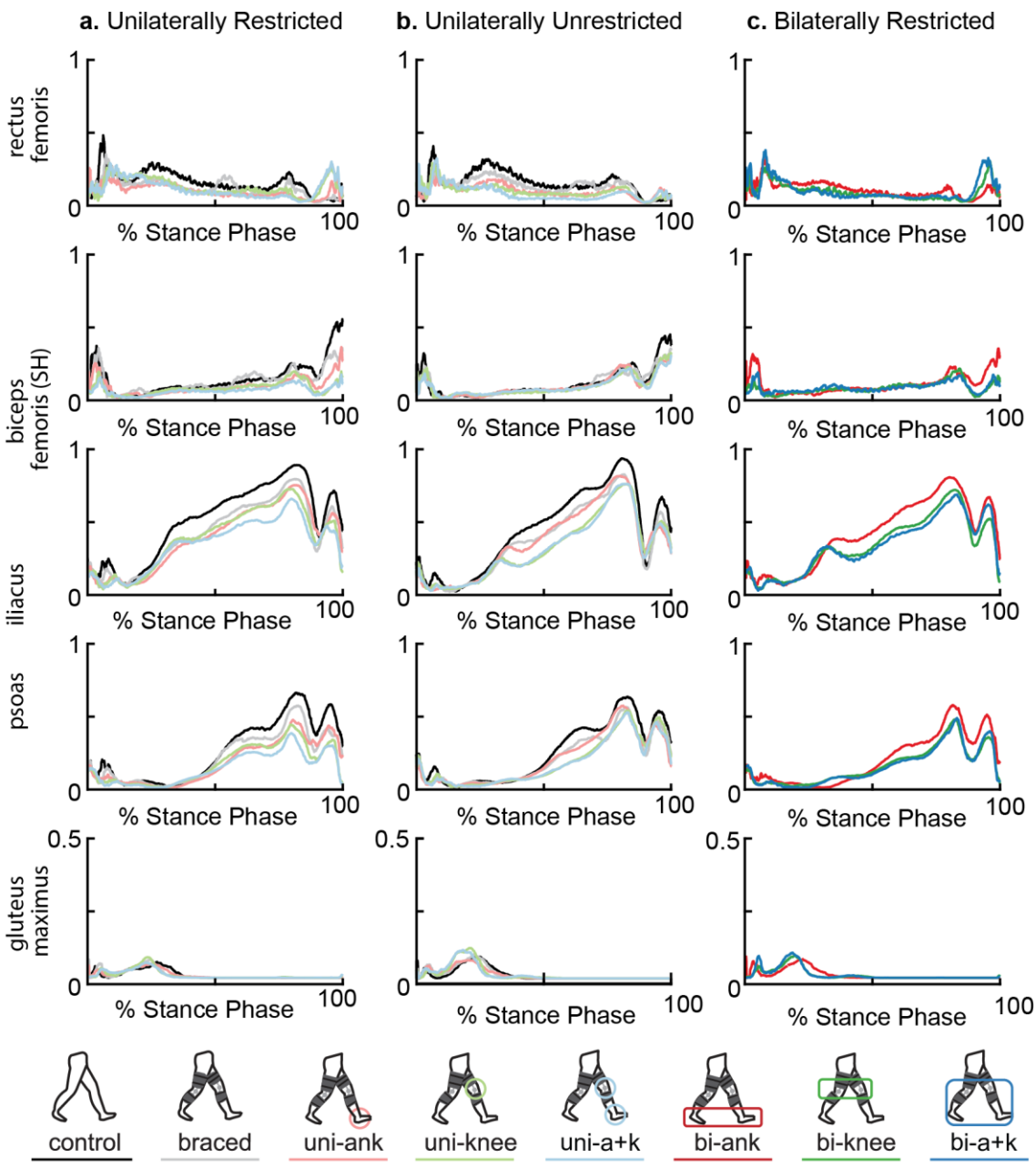


**Figure S5.5** Unconstrained simulated muscle activity.

Muscle Activity for the rectus femoris, biceps femoris short head, psoas, and iliacus muscles on the a) restricted limb in the *braced* and *unilaterally* restricted conditions, (**b**) unrestricted limbs in the *braced* and *unilaterally* restricted conditions, and for the (**c**) *bilaterally* restricted conditions.

# CHAPTER 6: Conclusions

## Contributions

This dissertation represents novel research that will inform and improve design of assistive devices and rehabilitation strategies and targets for walking rehabilitation in clinical populations, leading to several important contributions. First, in Chapter 2 this work characterized the impact of a novel speed-adaptive myoelectric exoskeleton applying assistance to the paretic ankle of persons post-stroke (McCain et al., 2019). While previous research has included analyses of other exoskeletons applying assistance to persons post-stroke as well as unimpaired persons (Awad et al., 2017b; Caputo and Collins, 2014; Collins et al., 2015; Forrester et al., 2016; Koller et al., 2015; Takahashi et al., 2015b), to our knowledge this is the first research including an exoskeleton capable of scaling assistance according to walking speed and muscle activity. We specifically elucidated the relationships among ankle assistance, walking speed, and walking performance parameters. Included in this work were recommendations for incorporating biofeedback or verbal cues to strengthen a person's ability to optimally incorporate applied assistance for maximum potential benefits. In addition, the results of this work emphasized that understanding how joint-level interventions impact limb and whole-body walking function would better inform future device design.

Second, based on the findings in Chapter 2, I developed and implemented a research design to provide critical insight into the possible tradeoffs of intervening at a specific lower limb joint to improve clinical walking performance. Previous work using joint range of motion restrictions either at the ankle (Wutzke et al., 2012) or knee (Lewek et al., 2012) independently; our work built upon previous restrictions by applying unilateral joint restrictions at the ankle, knee, then ankle and knee simultaneously to elucidate the relative impacts of ankle versus knee restriction on

mechanical compensations and energetic penalties of gait (McCain et al., 2021). This work provides novel evaluation of how mechanical restrictions resulting from injury or disease-induced asymmetric impairments may impact walking performance outcomes. Importantly, this approach provides new insight into the separate influences of joint restriction and asymmetry, which were coupled and could not be distinguished in earlier work.

Third, our investigation into the relative metabolic impact of restricting joint at the ankle and knee revealed joint restrictions. Restricting the ankle increased energy cost, and that simultaneous restriction of the ankle and knee was more expensive than restriction of the knee in isolation. This result provides new insight to support the potential of ankle-centric interventions to reduce the energy cost of clinical gait and hopefully lead to improvements in mobility and quality of life.

Fourth, research presented in Chapter 4 of this dissertation demonstrates the number of restricted joints is more metabolically impactful than walking asymmetry. Previous investigations have applied joint restrictions unilaterally (Lewek et al., 2018; Wutzke et al., 2012), but our work included bilateral ankle and knee restrictions that successfully engendered symmetric and asymmetric gait. This work demonstrates asymmetry in and of itself does not drive increases in metabolic cost. Increased in energy requirements instead correlated with the number of restricted degrees of freedom. Our results are compared to previous investigations into the metabolic impact of asymmetry in clinical populations as well as in unimpaired controls. Recommendations were made on the design of rehabilitative strategies to increase the functionality of impaired joints, or degrees of freedom to improve asymmetric and expensive gait walking performance.

Lastly, the research presented in Chapter 5 demonstrates [placeholder for main takeaway still under debate] changes in skeletal alignment prevent increases in ground reaction force loading

from propagating to comparable changes in joint reaction forces. This investigation evaluated the impact of joint restriction and induced asymmetry on joint loading is evaluated through computational musculoskeletal simulations. Previous work has described the use of musculoskeletal modeling to determine joint hip and knee joint reaction forces in clinical populations; however, our final contributions used EMG-informed simulations to investigate the consequences of mechanical joint restrictions and the resulting walking asymmetry on the joint loads seen at all lower limb joints. With joint restrictions we saw increases in ipsilateral grf loading rates but found muscle activity was reduced such that joint reaction forces were relatively unchanged.

## Applications

The work presented in this dissertation has many potential applications. First, we demonstrated joint-level benefits of exoskeleton assistance did not translate to reduced energy cost because the trailing leg was more vertical when using the exoskeleton; this meant suboptimal limb configuration limited conversion of joint-level exoskeleton benefits to forward propulsion and energetic benefits of applied assistance. This result can be used to encourage the inclusion of limb kinematic measures such as trailing limb angle into future assistive device design.

To isolate the impacts of reduced ankle and knee function, we developed a joint restriction protocol, and found ankle and knee joint range of motion restrictions can elicit clinical gait characteristics, including reduced ankle pushoff and increased circumduction of the foot. Future work could apply our joint restriction method to investigate consequences of altered mechanics resulting from injury or disease induced impairments during running, or in sit to stand transitions. In addition, we found that restriction of ankle range of motion was more metabolically expensive than restriction of joint range of motion. This result supports the potential of ankle-centric

rehabilitation to increase walking speed and reduce metabolic demand in the relevant clinical populations.

To isolate the metabolic impact of asymmetric, badly coordinated step to step transitions, we applied joint restrictions unilaterally and bilaterally. We found symmetric restriction was more metabolically expensive than asymmetric restriction, and that the metabolic cost was correlated with the number of restricted joints. These results reinforce recent research indicating asymmetric walking can require less energy than symmetric walking (Browne et al., 2021; Sánchez et al., 2020), and indicate that there may be an increased potential to reduce energy requirements when interventions specifically target improvement in impaired limb function, rather than specific symmetry metrics. This is because targeting symmetry metrics does not prevent subjects from limiting unimpaired limb function to achieve the desired symmetry; further, these results emphasize that asymmetry is only an effective rehabilitative goal if the unimpaired limb performance is representative of pre-injury or illness ability and if increasing the impaired limb function is the method of achieving symmetry.

Lastly, we employed computational musculoskeletal modeling simulations driven with EMG constraints to investigate how joint restriction and induced asymmetry impacted joint-reaction force at all lower limb joints. This kind of musculoskeletal simulation could be expounded upon to directly represent torque provided by an assistive device to elucidate the impact of assistance on joint loading. Our results indicated measured ground reaction forces were congruent with our expectation that limiting knee function would increase limb loading rate during the loading response period. However, we did not observe similar trends in joint reaction force loading. Instead, we found muscle contributions to joint reaction forces decreased and offset the increased limb loading such that joint reacidifies were relatively unchanged conditions. These

results highlight the importance of including muscle forces in joint reaction forces, and caution against the use of limb loading as a proxy for joint loading.

## Future work

### Rehabilitation for Clinical Populations

I found unilateral joint restriction imposed on unimpaired participants could engender relevant clinical walking characteristics including decreased propulsion, increased circumduction, and increased hip hiking. While this work focused exclusively on improving unperturbed walking, similar joint bracing techniques could be applicable understand a myriad of other important clinical considerations. Specifically, researcher could investigate whether changes in circumduction or propulsion affected balance or response to a perturbative force applied to the center of mass.

In addition, this research challenges the exclusive use of measures of symmetry as a rehabilitative goal because symmetry can be achieved by limiting the unimpaired limb rather than strengthening impaired limb function. Further, it was suggested that an optimal asymmetry may exist where the impaired limb function is improved as much as possible. Future work is needed to confirm the metabolic impact of using biofeedback to encourage (1) improvements in impaired limb function with (2) improvements in asymmetry.

### Assistive devices

Our research indicates ankle-centric rehabilitative techniques have potential for reducing energy cost and emphasizes restoring impaired limb or joint function is more metabolically impactful than achieving symmetry. In addition, we demonstrated that translating joint level assistance to whole-body benefits requires assistive device design that considers the interactions among the joint, limb, and center of mass kinematics and kinetics. Taken in conjunction these results support the promise of an ankle-based assistive devices focused on improving impaired

joint function rather than symmetry per se, and with the capacity to account for changes in user coordination by incorporating feedback or altering assistance parameters.

Previous research has demonstrated the efficacy of using feedback to improve clinical gait performance. Specifically, verbal cues can increase overground walking speed in persons-post stroke (Aiello et al., 2005; Dobkin et al., 2010), and visual feedback of impaired limb muscle activity has been used to increase impaired joint power generation (Aiello et al., 2005). Future work could extend this by providing a visual indicator of trailing limb angle while subjects walk with ankle exoskeleton assistance to ensure joint assistance translates to whole body benefits.

The timing and magnitude of exoskeleton assistance is known to impact metabolic costs in healthy controls (Caputo and Collins, 2014), suggesting that walking performance clinical populations may also be sensitive to these parameters. An exoskeleton that explicitly varies timing of assistance to manipulate coordination and magnitude of assistance to impact walking mechanics could help determine the assistance parameters that maximize energy benefits for an individual. Alternatively, researchers could consider providing assistance across multiple joints (Agrawal et al., 2007; Banala et al., 2009; Krishnan et al., 2012), and even incorporate feedback to encourage uses to take advantage of assistance.

We used musculoskeletal modeling simulations with EMG constraints to determine the impact of asymmetry on joint reaction forces. Future work could employ this technique to determine the impact of assistive devices on joint reaction forces by including the assistive torque directly in the simulation. This investigation could help elucidate how changes in assistance timing affect muscle-level changes in coordination and would inform assistive device design by identifying factors of assistance that negatively impact joint loads.

## REFERENCES


Adamczyk, P.G., Kuo, A.D., 2015. Mechanisms of Gait Asymmetry Due to Push-Off Deficiency in Unilateral Amputees. IEEE Trans Neural Syst Rehabil Eng 23, 776-785.

Agrawal, S.K., Banala, S.K., Fattah, A., Sangwan, V., Krishnamoorthy, V., Scholz, J.P., Hsu, W.L., 2007. Assessment of motion of a swing leg and gait rehabilitation with a gravity balancing exoskeleton. IEEE Trans Neural Syst Rehabil Eng 15, 410-420.

Aiello, E., Gates, D.H., Patritti, B.L., Cairns, K.D., Meister, M., Clancy, E.A., Bonato, P., 2005. Visual EMG Biofeedback to Improve Ankle Function in Hemiparetic Gait. Conf Proc IEEE Eng Med Biol Soc 7, 7703-7706.

Akbas, T., Neptune, R.R., Sulzer, J., 2019a. Neuromusculoskeletal Simulation Reveals Abnormal Rectus Femoris-Gluteus Medius Coupling in Post-stroke Gait. Front Neurol 10, 301.

Akbas, T., Prajapati, S., Ziemnicki, D., Tamma, P., Gross, S., Sulzer, J., 2019b. Hip circumduction is not a compensation for reduced knee flexion angle during gait. Journal of biomechanics 87, 150-156.

Akbas, T., Sulzer, J., Year Musculoskeletal simulation framework for impairment-based exoskeletal assistance post-stroke. In 2019 IEEE 16th International Conference on Rehabilitation Robotics (ICORR).

Allen, J.L., Kautz, S.A., Neptune, R.R., 2011. Step length asymmetry is representative of compensatory mechanisms used in post-stroke hemiparetic walking. Gait & Posture 33, 538-543.

Allen, J.L., Kautz, S.A., Neptune, R.R., 2014. Forward propulsion asymmetry is indicative of changes in plantarflexor coordination during walking in individuals with post-stroke hemiparesis. Clin Biomech (Bristol, Avon) 29, 780-786.

Amtmann, D., Morgan, S.J., Kim, J., Hafner, B.J., 2015. Health-related profiles of people with lower limb loss. Archives of physical medicine and rehabilitation 96, 1474-1483.

Anderson, F.C., Goldberg, S.R., Pandy, M.G., Delp, S.L., 2004. Contributions of muscle forces and toe-off kinematics to peak knee flexion during the swing phase of normal gait: an induced position analysis. Journal of biomechanics 37, 731-737.

Anderson, F.C., Pandy, M.G., 2003. Individual muscle contributions to support in normal walking. Gait & Posture 17, 159-169.

Andriacchi, T.P., Mündermann, A., 2006. The role of ambulatory mechanics in the initiation and progression of knee osteoarthritis. Curr Opin Rheumatol 18, 514-518.

Attias, M., Bonnefoy-Mazure, A., De Coulon, G., Cheze, L., Armand, S., 2016. Feasibility and reliability of using an exoskeleton to emulate muscle contractures during walking. Gait Posture 50, 239-245.

Awad, L.N., Bae, J., O'Donnell, K., De Rossi, S.M.M., Hendron, K., Sloot, L.H., Kudzia, P., Allen, S., Holt, K.G., Ellis, T.D., Walsh, C.J., 2017a. A soft robotic exosuit improves walking in patients after stroke. Sci Transl Med 9.

Awad, L.N., Bae, J., O'Donnell, K., De Rossi, S.M.M., Hendron, K., Sloot, L.H., Kudzia, P., Allen, S., Holt, K.G., Ellis, T.D., Walsh, C.J., 2017b. A soft robotic exosuit improves walking in patients after stroke. Science Translational Medicine 9.

Awad, L.N., Binder-Macleod, S.A., Pohlig, R.T., Reisman, D.S., 2015a. Paretic Propulsion and Trailing Limb Angle Are Key Determinants of Long-Distance Walking Function After Stroke. Neurorehabilitation and Neural Repair 29, 499-508.

Awad, L.N., Palmer, J.A., Pohlig, R.T., Binder-Macleod, S.A., Reisman, D.S., 2014a. Walking Speed and Step Length Asymmetry Modify the Energy Cost of Walking After Stroke. Neurorehabilitation and Neural Repair 29, 416-423.

Awad, L.N., Palmer, J.A., Pohlig, R.T., Binder-Macleod, S.A., Reisman, D.S., 2015b. Walking speed and step length asymmetry modify the energy cost of walking after stroke. Neurorehabil Neural Repair 29, 416-423.

Awad, L.N., Reisman, D.S., Kesar, T.M., Binder-Macleod, S.A., 2014b. Targeting paretic propulsion to improve poststroke walking function: a preliminary study. Archives of physical medicine and rehabilitation 95, 840-848.

Awad, L.N., Reisman, D.S., Pohlig, R.T., Binder-Macleod, S.A., 2016. Identifying candidates for targeted gait rehabilitation after stroke: better prediction through biomechanics-informed characterization. J Neuroeng Rehabil 13, 84.

Banala, S.K., Kim, S.H., Agrawal, S.K., Scholz, J.P., 2009. Robot assisted gait training with active leg exoskeleton (ALEX). IEEE Trans Neural Syst Rehabil Eng 17, 2-8.

Beck, O.N., Grabowski, A.M., Ortega, J.D., 2018. Neither total muscle activation nor co-activation explains the youthful walking economy of older runners. Gait & Posture 65, 163-168.

Betschart, M., McFayden, B.J., Nadeau, S., 2020. Lower limb joint moments on the fast belt contribute to a reduction of step length asymmetry over ground after split-belt treadmill training in stroke: A pilot study. Physiother Theory Pract 36, 989-999.

Boffeli, T.J., Collier, R.C., 2014. Minimally invasive soft tissue release of foot and ankle contracture secondary to stroke. J Foot Ankle Surg 53, 369-375.

Bohannon, R.W., 2007. Muscle strength and muscle training after stroke. J Rehabil Med 39, 14-20.

Brach, J.S., VanSwearingen, J.M., Newman, A.B., Kriska, A.M., 2002. Identifying Early Decline of Physical Function in Community-Dwelling Older Women: Performance-Based and Self-Report Measures. Physical Therapy 82, 320-328.

Brockway, J.M., 1987. Derivation of formulae used to calculate energy expenditure in man. Hum Nutr Clin Nutr 41, 463-471.

Brouwer, B., Parvataneni, K., Olney, S.J., 2009. A comparison of gait biomechanics and metabolic requirements of overground and treadmill walking in people with stroke. Clinical Biomechanics 24, 729-734.

Browne, M.G., Smock, C.S., Roemmich, R.T., 2021. The human preference for symmetric walking often disappears when one leg is constrained. J Physiol 599, 1243-1260.

Bytyqi, D., Shabani, B., Lustig, S., Cheze, L., Gjurgjeala, N.K., Neyret, P., 2014. Gait knee kinematic alterations in medial osteoarthritis: three dimensional assessment. International orthopaedics 38, 1191-1198.

Campanini, I., Merlo, A., Damiano, B., 2013. A method to differentiate the causes of stiff-knee gait in stroke patients. Gait & Posture 38, 165-169.

Caputo, J.M., Collins, S.H., 2014. A universal ankle-foot prosthesis emulator for human locomotion experiments. Journal of biomechanical engineering 136, 035002.

Carrier, D.R., Anders, C., Schilling, N., 2011. The musculoskeletal system of humans is not tuned to maximize the economy of locomotion. Proceedings of the National Academy of Sciences 108, 18631-18636.

Chaudhari, A.M., Briant, P.L., Bevill, S.L., Koo, S., Andriacchi, T.P., 2008. Knee kinematics, cartilage morphology, and osteoarthritis after ACL injury. Med Sci Sports Exerc 40, 215-222.

Chen, G., Patten, C., Kothari, D.H., Zajac, F.E., 2005a. Gait deviations associated with post-stroke hemiparesis: improvement during treadmill walking using weight support, speed, support stiffness, and handrail hold. Gait & Posture 22, 57-62.

Chen, G., Patten, C., Kothari, D.H., Zajac, F.E., 2005b. Gait differences between individuals with post-stroke hemiparesis and non-disabled controls at matched speeds. Gait & Posture 22, 51-56.

Chen, G., Patten, C., Kothari, D.H., Zajac, F.E., 2005c. Gait differences between individuals with post-stroke hemiparesis and non-disabled controls at matched speeds. Gait Posture 22, 51-56.

Clark, D.J., Ting, L.H., Zajac, F.E., Neptune, R.R., Kautz, S.A., 2010. Merging of healthy motor modules predicts reduced locomotor performance and muscle coordination complexity post-stroke. Journal of neurophysiology 103, 844-857.

Collins, S.H., Adamczyk, P.G., Kuo, A.D., 2009. Dynamic arm swinging in human walking. Proceedings. Biological sciences 276, 3679-3688.

Collins, S.H., Wiggin, M.B., Sawicki, G.S., 2015. Reducing the energy cost of human walking using an unpowered exoskeleton. Nature 522, 212-215.

Combs, S.A., Van Puymbroeck, M., Altenburger, P.A., Miller, K.K., Dierks, T.A., Schmid, A.A., 2013. Is walking faster or walking farther more important to persons with chronic stroke? Disabil Rehabil 35, 860-867.

Creaby, M.W., Bennell, K.L., Hunt, M.A., 2012. Gait Differs Between Unilateral and Bilateral Knee Osteoarthritis. Archives of physical medicine and rehabilitation 93, 822-827.

Dean, J.C., Bowden, M.G., Kelly, A.L., Kautz, S.A., 2020. Altered post-stroke propulsion is related to paretic swing phase kinematics. Clin Biomech (Bristol, Avon) 72, 24-30.

Delp, S.L., Anderson, F.C., Arnold, A.S., Loan, P., Habib, A., John, C.T., Guendelman, E., Thelen, D.G., 2007. OpenSim: open-source software to create and analyze dynamic simulations of movement. IEEE transactions on bio-medical engineering 54, 1940-1950.

Detrembleur, C., Dierick, F., Stoquart, G., Chantraine, F., Lejeune, T., 2003. Energy cost, mechanical work, and efficiency of hemiparetic walking. Gait Posture 18, 47-55.

Dobkin, B.H., Plummer-D'Amato, P., Elashoff, R., Lee, J., 2010. International randomized clinical trial, stroke inpatient rehabilitation with reinforcement of walking speed (SIRROWS), improves outcomes. Neurorehabil Neural Repair 24, 235-242.

Donelan, J.M., Kram, R., 2001. Mechanical and metabolic determinants of the preferred step width in human walking. Proc R Soc Lond Ser B Biol Sci 268.1480.

Donelan, J.M., Kram, R., Kuo, A.D., 2002. Simultaneous positive and negative external mechanical work in human walking. Journal of biomechanics 35, 117-124.

Ellis, R.G., Howard, K.C., Kram, R., 2013. The metabolic and mechanical costs of step time asymmetry in walking. Proceedings. Biological sciences / The Royal Society 280, 20122784.

Eng, J.J., Winter, D.A., 1995. Kinetic analysis of the lower limbs during walking: what information can be gained from a three-dimensional model? Journal of biomechanics 28, 753-758.

Farris, D.J., Hampton, A., Lewek, M.D., Sawicki, G.S., 2015. Revisiting the mechanics and energetics of walking in individuals with chronic hemiparesis following stroke: from individual limbs to lower limb joints. Journal of NeuroEngineering and Rehabilitation 12, 24.

Farris, D.J., Sawicki, G.S., 2012. The mechanics and energetics of human walking and running: a joint level perspective. J R Soc Interface 9, 110-118.

Fey, N.P., Silverman, A.K., Neptune, R.R., 2010. The influence of increasing steady-state walking speed on muscle activity in below-knee amputees. J Electromyogr Kinesiol 20, 155-161.

Finley, J.M., Bastian, A.J., 2017. Associations Between Foot Placement Asymmetries and Metabolic Cost of Transport in Hemiparetic Gait. Neurorehabilitation and Neural Repair 31, 168-177.

Forrester, L.W., Roy, A., Hafer-Macko, C., Krebs, H.I., Macko, R.F., 2016. Task-specific ankle robotics gait training after stroke: a randomized pilot study. Journal of NeuroEngineering and Rehabilitation 13, 51.

Forrester, L.W., Roy, A., Krebs, H.I., Macko, R.F., 2010. Ankle Training With a Robotic Device Improves Hemiparetic Gait After a Stroke. Neurorehabilitation and Neural Repair 25, 369-377.

Frazzitta, G., Pezzoli, G., Bertotti, G., Maestri, R., 2013. Asymmetry and freezing of gait in parkinsonian patients. J Neurol 260, 71-76.

Fregly, B.J., Besier, T.F., Lloyd, D.G., Delp, S.L., Banks, S.A., Pandy, M.G., D'Lima, D.D., 2012. Grand challenge competition to predict in vivo knee loads. Journal of orthopaedic research : official publication of the Orthopaedic Research Society 30, 503-513.

Fritz, S., Lusardi, M., 2009. White paper:"walking speed: the sixth vital sign". Journal of geriatric physical therapy 32, 2-5.

Galle, S., Malcolm, P., Collins, S.H., De Clercq, D., 2017. Reducing the metabolic cost of walking with an ankle exoskeleton: interaction between actuation timing and power. J Neuroeng Rehabil 14, 35.

Gao, F., Zhang, L.Q., 2008. Altered contractile properties of the gastrocnemius muscle poststroke. Journal of applied physiology 105, 1802-1808.

Geerse, D.J., Roerdink, M., Marinus, J., van Hilten, J.J., 2019. Walking adaptability for targeted fall-risk assessments. Gait & Posture 70, 203-210.

Gerus, P., Sartori, M., Besier, T.F., Fregly, B.J., Delp, S.L., Banks, S.A., Pandy, M.G., D'Lima, D.D., Lloyd, D.G., 2013. Subject-specific knee joint geometry improves predictions of medial tibiofemoral contact forces. Journal of biomechanics 46, 2778-2786.

Grabowski, A.M., D'Andrea, S., 2013. Effects of a powered ankle-foot prosthesis on kinetic loading of the unaffected leg during level-ground walking. J Neuroeng Rehabil 10, 49.

Graham, J.E., Fisher, S.R., Bergés, I.-M., Kuo, Y.-F., Ostir, G.V., 2010. Walking Speed Threshold for Classifying Walking Independence in Hospitalized Older Adults. Physical Therapy 90, 1591-1597.

Gustafson, J.A., Anderton, W., Sowa, G.A., Piva, S.R., Farrokhi, S., 2019. Dynamic knee joint stiffness and contralateral knee joint loading during prolonged walking in patients with unilateral knee osteoarthritis. Gait Posture 68, 44-49.

Hak, L., Houdijk, H., van der Wurff, P., Prins, M.R., Mert, A., Beek, P.J., van Dieën, J.H., 2013. Stepping strategies used by post-stroke individuals to maintain margins of stability during walking. Clin Biomech (Bristol, Avon) 28, 1041-1048.

Hampton, A., Farris, D.J., Sawicki, G.S., Year Mechanics and energetics of post-stroke walking: Towards a muscle-level understanding. In 35th Annual Meeting of American Society of Biomechanics. Long Beach, CA.

Harris, M.D., MacWilliams, B.A., Foreman, K.B., Peters, C.L., Weiss, J.A., Anderson, A.E., 2017. Higher medially-directed joint reaction forces are a characteristic of dysplastic hips: A comparative study using subject-specific musculoskeletal models. Journal of biomechanics 54, 80-87.

Hendershot, B.D., Wolf, E.J., 2014. Three-dimensional joint reaction forces and moments at the low back during over-ground walking in persons with unilateral lower-extremity amputation. Clin Biomech (Bristol, Avon) 29, 235-242.

Houdijk, H., Pollmann, E., Groenewold, M., Wiggerts, H., Polomski, W., 2009. The energy cost for the step-to-step transition in amputee walking. Gait Posture 30, 35-40.

Hsiao, H., Gray, V.L., Creath, R.A., Binder-Macleod, S.A., Rogers, M.W., 2017. Control of lateral weight transfer is associated with walking speed in individuals post-stroke. Journal of biomechanics 60, 72-78.

Hsiao, H., Knarr, B.A., Higginson, J.S., Binder-Macleod, S.A., 2015. Mechanisms to increase propulsive force for individuals poststroke. J Neuroeng Rehabil 12, 40.

Huang, T.P., Shorter, K.A., Adamczyk, P.G., Kuo, A.D., 2015. Mechanical and energetic consequences of reduced ankle plantarflexion in human walking. The Journal of experimental biology.

Imani Nejad, Z., Khalili, K., Hosseini Nasab, S.H., Schütz, P., Damm, P., Trepczynski, A., Taylor, W.R., Smith, C.R., 2020. The Capacity of Generic Musculoskeletal Simulations to Predict Knee Joint Loading Using the CAMS-Knee Datasets. co-c

Ann Biomed Eng 48, 1430-1440.

Isakov, E., Burger, H., Krajnik, J., Gregoric, M., Marincek, C., 1997. Double-limb support and step-length asymmetry in below-knee amputees. Scandinavian journal of rehabilitation medicine 29, 75-79.

Isakov, E., Keren, O., Benjuya, N., 2000. Trans-tibial amputee gait: time-distance parameters and EMG activity. Prosthetics and orthotics international 24, 216-220.

Jonkers, I., Delp, S., Patten, C., 2008. Capacity to increase walking speed is limited by impaired hip and ankle power generation in lower functioning persons post-stroke. Gait Posture.

Kerrigan, D.C., Karvosky, M.E., Riley, P.O., 2001. Spastic paretic stiff-legged gait: joint kinetics. American journal of physical medicine & rehabilitation / Association of Academic Physiatrists 80, 244-249.

Kesar, T.M., Perumal, R., Jancosko, A., Reisman, D.S., Rudolph, K.S., Higginson, J.S., Binder-Macleod, S.A., 2010. Novel patterns of functional electrical stimulation have an immediate effect on dorsiflexor muscle function during gait for people poststroke. Phys Ther 90, 55-66.

Kesar, T.M., Reisman, D.S., Perumal, R., Jancosko, A.M., Higginson, J.S., Rudolph, K.S., Binder-Macleod, S.A., 2011. Combined effects of fast treadmill walking and functional electrical stimulation on post-stroke gait. Gait Posture 33, 309-313.

Kim, M., Cho, K., Lee, W., 2014. Community walking training program improves walking function and social participation in chronic stroke patients. The Tohoku journal of experimental medicine 234, 281-286.

Kim, W.-S., Kim, M.J., 2017. Individual joint contribution to body weight support in the affected lower limb during walking in post-stroke hemiplegia. Topics in Stroke Rehabilitation 24, 170-176.

Koller, J.R., Jacobs, D.A., Ferris, D.P., Remy, C.D., 2015. Learning to walk with an adaptive gain proportional myoelectric controller for a robotic ankle exoskeleton. Journal of NeuroEngineering and Rehabilitation 12, 97.

Krishnan, C., Ranganathan, R., Kantak, S.S., Dhaher, Y.Y., Rymer, W.Z., 2012. Active robotic training improves locomotor function in a stroke survivor. J Neuroeng Rehabil 9, 57.

Lamontagne, A., Malouin, F., Richards, C.L., Dumas, F., 2002. Mechanisms of disturbed motor control in ankle weakness during gait after stroke. Gait Posture 15, 244-255.

Lenton, G.K., Bishop, P.J., Saxby, D.J., Doyle, T.L.A., Pizzolato, C., Billing, D., Lloyd, D.G., 2018. Tibiofemoral joint contact forces increase with load magnitude and walking speed but remain almost unchanged with different types of carried load. PLoS One 13, e0206859.

Leung, J., Smith, R., Harvey, L.A., Moseley, A.M., Chapparo, J., 2014. The impact of simulated ankle plantarflexion contracture on the knee joint during stance phase of gait: a within-subject study. Clin Biomech (Bristol, Avon) 29, 423-428.

Lewek, M.D., Braun, C.H., Wutzke, C., Giuliani, C., 2018. The role of movement errors in modifying spatiotemporal gait asymmetry post stroke: a randomized controlled trial. Clin Rehabil 32, 161-172.

Lewek, M.D., Osborn, A.J., Wutzke, C.J., 2012. The Influence of Mechanically and Physiologically Imposed Stiff-Knee Gait Patterns on the Energy Cost of Walking. Archives of physical medicine and rehabilitation 93, 123-128.

Lewek, M.D., Poole, R., Johnson, J., Halawa, O., Huang, X., 2010. Arm swing magnitude and asymmetry during gait in the early stages of Parkinson's disease. Gait & posture 31, 256-260.

Lewek, M.D., Sawicki, G.S., 2019. Trailing limb angle is a surrogate for propulsive limb forces during walking post-stroke. Clin Biomech (Bristol, Avon) 67, 115-118.

Little, V.L., McGuirk, T.E., Patten, C., 2014. Impaired limb shortening following stroke: what's in a name? PLoS One 9, e110140.

Little, V.L., McGuirk, T.E., Perry, L.A., Patten, C., 2018. Pelvic excursion during walking post-stroke: A novel classification system. Gait & Posture 62, 395-404.

Little, V.L., Perry, L.A., Mercado, M.W.V., Kautz, S.A., Patten, C., 2020. Gait asymmetry pattern following stroke determines acute response to locomotor task. Gait & Posture 77, 300-307.

Liu, M.Q., Anderson, F.C., Schwartz, M.H., Delp, S.L., 2008. Muscle contributions to support and progression over a range of walking speeds. Journal of biomechanics 41, 3243-3252.

Loureiro, A., Constantinou, M., Diamond, L.E., Beck, B., Barrett, R., 2018. Individuals with mild-to-moderate hip osteoarthritis have lower limb muscle strength and volume deficits. BMC musculoskeletal disorders 19, 1-9.

Lugade, V., Wu, A., Jewett, B., Collis, D., Chou, L.-S., 2010. Gait asymmetry following an anterior and anterolateral approach to total hip arthroplasty. Clinical Biomechanics 25, 675-680.

Mahon, C.E., Darter, B.J., Dearth, C.L., Hendershot, B.D., 2019. The Relationship Between Gait Symmetry and Metabolic Demand in Individuals With Unilateral Transfemoral Amputation: A Preliminary Study. Mil Med 184, e281-e287.

Mahon, C.E., Farris, D.J., Sawicki, G.S., Lewek, M.D., 2015. Individual limb mechanical analysis of gait following stroke. Journal of biomechanics 48, 984-989.

Malcolm, P., Derave, W., Galle, S., De Clercq, D., 2013. A simple exoskeleton that assists plantarflexion can reduce the metabolic cost of human walking. PloS One 8.

Maly, M.R., 2008. Abnormal and cumulative loading in knee osteoarthritis. Current opinion in rheumatology 20, 547-552.

Manal, K., Buchanan, T.S., 2013. An Electromyogram-Driven Musculoskeletal Model of the Knee to Predict in Vivo Joint Contact Forces During Normal and Novel Gait Patterns. Journal of biomechanical engineering 135, 021014.

Margaria, R., 1976. Biomechanics and energetics of muscular exercise. Clarendon Press, Oxford [England].

Marra, M.A., Vanheule, V., Fluit, R., Koopman, B.H.F.J.M., Rasmussen, J., Verdonschot, N., Andersen, M.S., 2015. A Subject-Specific Musculoskeletal Modeling Framework to Predict In Vivo Mechanics of Total Knee Arthroplasty. Journal of biomechanical engineering 137.

Marrocco, S., Crosby, L.D., Jones, I.C., Moyer, R.F., Birmingham, T.B., Patterson, K.K., 2016. Knee loading patterns of the non-paretic and paretic legs during post-stroke gait. Gait Posture 49, 297-302.

Mattes, S.J., Martin, P.E., Royer, T.D., 2000. Walking symmetry and energy cost in persons with unilateral transtibial amputations: matching prosthetic and intact limb inertial properties. Archives of physical medicine and rehabilitation 81, 561-568.

McCain, E.M., Dick, T.J.M., Giest, T.N., Nuckols, R.W., Lewek, M.D., Saul, K.R., Sawicki, G.S., 2019. Mechanics and energetics of post-stroke walking aided by a powered ankle exoskeleton with speed-adaptive myoelectric control. Journal of NeuroEngineering and Rehabilitation 16, 57.

McCain, E.M., Libera, T.L., Berno, M.E., Sawicki, G.S., Saul, K.R., Lewek, M.D., 2021. Isolating the energetic and mechanical consequences of imposed reductions in ankle and knee flexion during gait. Journal of NeuroEngineering and Rehabilitation 18, 1-13.

McFarland, D.C., McCain, E.M., Poppo, M.N., Saul, K.R., 2019. Spatial Dependency of Glenohumeral Joint Stability During Dynamic Unimanual and Bimanual Pushing and Pulling. Journal of biomechanical engineering 141.

McGowan, C.P., Neptune, R.R., Kram, R., 2008. Independent effects of weight and mass on plantar flexor activity during walking: implications for their contributions to body support and forward propulsion. Journal of applied physiology 105, 486-494.

Michael, K.M., Allen, J.K., Macko, R.F., 2005. Reduced Ambulatory Activity After Stroke: The Role of Balance, Gait, and Cardiovascular Fitness. Archives of physical medicine and rehabilitation 86, 1552-1556.

Middleton, A., Fritz, S.L., Lusardi, M., 2015. Walking speed: the functional vital sign. Journal of aging and physical activity 23, 314-322.

Mills, K., Hettinga, B.A., Pohl, M.B., Ferber, R., 2013. Between-Limb Kinematic Asymmetry During Gait in Unilateral and Bilateral Mild to Moderate Knee Osteoarthritis. Archives of physical medicine and rehabilitation 94, 2241-2247.

Montero-Odasso, M., Schapira, M., Soriano, E.R., Varela, M., Kaplan, R., Camera, L.A., Mayorga, L.M., 2005. Gait velocity as a single predictor of adverse events in healthy seniors aged 75 years and older. J Gerontol A Biol Sci Med Sci 60, 1304-1309.

Morgenroth, D.C., Medverd, J.R., Seyedali, M., Czerniecki, J.M., 2014. The relationship between knee joint loading rate during walking and degenerative changes on magnetic resonance imaging. Clinical biomechanics 29, 664-670.

Mulroy, S.J., Eberly, V.J., Gronely, J.K., Weiss, W., Newsam, C.J., 2010. Effect of AFO design on walking after stroke: impact of ankle plantar flexion contracture. Prosthetics and orthotics international 34, 277-292.

Nadeau, S., Gravel, D., Arsenault, A.B., Bourbonnais, D., 1999. Plantarflexor weakness as a limiting factor of gait speed in stroke subjects and the compensating role of hip flexors. Clinical Biomechanics 14, 125-135.

Nguyen, T.M., Jackson, R.W., Aucie, Y., de Kam, D., Collins, S.H., Torres-Oviedo, G., 2020. Self-selected step length asymmetry is not explained by energy cost minimization in individuals with chronic stroke. Journal of neuroengineering and rehabilitation 17, 119-119.

Nolan, L., Lees, A., 2000. The functional demands on the intact limb during walking for active trans-femoral and trans-tibial amputees. Prosthetics and orthotics international 24, 117-125.

Nolan, L., Wit, A., Dudzinski, K., Lees, A., Lake, M., Wychowanski, M., 2003. Adjustments in gait symmetry with walking speed in trans-femoral and trans-tibial amputees. Gait Posture 17, 142-151.

Nuckols, R.W., Collins, S.H., Sawicki, G.S., 2015. An emulator system to characterize optimal elastic ankle exoskeleton stiffness during human walking and running, Dynamic Walking Conference, Columbus Ohio.

Olney, S.J., Griffin, M.P., Monga, T.N., McBride, I.D., 1991. Work and power in gait of stroke patients. Archives of physical medicine and rehabilitation 72, 309-314.

Ong, C.F., Geijtenbeek, T., Hicks, J.L., Delp, S.L., 2019. Predicting gait adaptations due to ankle plantarflexor muscle weakness and contracture using physics-based musculoskeletal simulations. PLoS Comput Biol 15, e1006993.

Padmanabhan, P., Rao, K.S., Gulhar, S., Cherry-Allen, K.M., Leech, K.A., Roemmich, R.T., 2020. Persons post-stroke improve step length symmetry by walking asymmetrically. J Neuroeng Rehabil 17, 105.

Patten, C., Lexell, J., Brown, H.E., 2004. Weakness and strength training in persons with poststroke hemiplegia: rationale, method, and efficacy. J Rehabil Res Dev 41, 293-312.

Patterson, K.K., Gage, W.H., Brooks, D., Black, S.E., McIlroy, W.E., 2010. Changes in Gait Symmetry and Velocity After Stroke: A Cross-Sectional Study From Weeks to Years After Stroke. Neurorehabilitation and Neural Repair 24, 783-790.

Perry, J., Garrett, M., Gronley, J.K., Mulroy, S.J., 1995. Classification of walking handicap in the stroke population. Stroke 26, 982-989.

Peterson, C.L., Cheng, J., Kautz, S.A., Neptune, R.R., 2010a. Leg extension is an important predictor of paretic leg propulsion in hemiparetic walking. Gait Posture 32, 451-456.

Peterson, C.L., Hall, A.L., Kautz, S.A., Neptune, R.R., 2010b. Pre-swing deficits in forward propulsion, swing initiation and power generation by individual muscles during hemiparetic walking. Journal of biomechanics 43, 2348-2355.

Piazza, S.J., Delp, S.L., 1996. The influence of muscles on knee flexion during the swing phase of gait. Journal of biomechanics 29, 723-733.

Pollock, A., St George, B., Fenton, M., Firkins, L., 2014. Top 10 Research Priorities Relating to Life after Stroke – Consensus from Stroke Survivors, Caregivers, and Health Professionals. International Journal of Stroke 9, 313-320.

Prinold, J.A., Mazzà, C., Di Marco, R., Hannah, I., Malattia, C., Magni-Manzoni, S., Petrarca, M., Ronchetti, A.B., De Horatio, L.T., van Dijkhuizen, E.P., 2016. A patient-specific foot model for the estimate of ankle joint forces in patients with juvenile idiopathic arthritis. Annals of biomedical engineering 44, 247-257.

Quesada, R.E., Caputo, J.M., Collins, S.H., 2016. Increasing ankle push-off work with a powered prosthesis does not necessarily reduce metabolic rate for transtibial amputees. Journal of biomechanics 49, 3452-3459.

Raja, B., Neptune, R.R., Kautz, S.A., 2012. Coordination of the non-paretic leg during hemiparetic gait: expected and novel compensatory patterns. Clinical biomechanics (Bristol, Avon) 27, 1023-1030.

Rajagopal, A., Dembia, C.L., DeMers, M.S., Delp, D.D., Hicks, J.L., Delp, S.L., 2016. Full-Body Musculoskeletal Model for Muscle-Driven Simulation of Human Gait. IEEE transactions on bio-medical engineering 63, 2068-2079.

Rambaud, A.J.M., Semay, B., Samozino, P., Morin, J.B., Testa, R., Philippot, R., Rossi, J., Edouard, P., 2017. Criteria for Return to Sport after Anterior Cruciate Ligament reconstruction with lower reinjury risk (CR'STAL study): protocol for a prospective observational study in France. BMJ Open 7, e015087.

Reiber, G.E., McFarland, L.V., Hubbard, S., Maynard, C., Blough, D.K., Gambel, J.M., Smith, D.G., 2010. Servicemembers and veterans with major traumatic limb loss from Vietnam war and OIF/OEF conflicts: survey methods, participants, and summary findings. J Rehabil Res Dev 47, 275-297.

Reisman, D.S., Kesar, T.M., Perumal, R., Roos, M.A., Rudolph, K.S., Higginson, J., Helm, E., Binder-Macleod, S., 2013a. Time course of functional and biomechanical improvements during a gait training intervention in persons with chronic stroke. Journal of neurologic physical therapy : JNPT 37, 159-165.

Reisman, D.S., McLean, H., Keller, J., Danks, K.A., Bastian, A.J., 2013b. Repeated Split-Belt Treadmill Training Improves Poststroke Step Length Asymmetry. Neurorehabil Neural Repair.

Roemmich, R.T., Leech, K.A., Gonzalez, A.J., Bastian, A.J., 2019. Trading Symmetry for Energy Cost During Walking in Healthy Adults and Persons Poststroke. Neurorehabil Neural Repair 33, 602-613.

Ryan, H.P., Husted, C., Lewek, M.D., 2020. Improving Spatiotemporal Gait Asymmetry Has Limited Functional Benefit for Individuals Poststroke. J Neurol Phys Ther 44, 197-204.

Sadeghi, H., Allard, P., Duhaime, P.M., 2001. Muscle power compensatory mechanisms in below-knee amputee gait. American journal of physical medicine & rehabilitation / Association of Academic Physiatrists 80, 25-32.

Sánchez, N., Finley, J.M., 2018. Individual Differences in Locomotor Function Predict the Capacity to Reduce Asymmetry and Modify the Energetic Cost of Walking Poststroke. Neurorehabil Neural Repair 32, 701-713.

Sánchez, N., Simha, S.N., Donelan, J.M., Finley, J.M., 2019. Taking advantage of external mechanical work to reduce metabolic cost: the mechanics and energetics of split-belt treadmill walking. J Physiol 597, 4053-4068.

Sánchez, N., Simha, S.N., Donelan, J.M., Finley, J.M., 2020. Using asymmetry to your advantage: learning to acquire and accept external assistance during prolonged split-belt walking. bioRxiv, 2020.2004.2004.025619.

Sawicki, G.S., Ferris, D.P., 2008. Mechanics and energetics of level walking with powered ankle exoskeletons. The Journal of experimental biology 211.

Sawicki, G.S., Lewis, C.L., Ferris, D.P., 2009. It pays to have a spring in your step. Exercise and sport sciences reviews 37, 130-138.

Schmalz, T., Blumentritt, S., Jarasch, R., 2002. Energy expenditure and biomechanical characteristics of lower limb amputee gait: the influence of prosthetic alignment and different prosthetic components. Gait Posture 16, 255-263.

Shafrin, J., Sullivan, J., Goldman, D.P., Gill, T.M., 2017. The association between observed mobility and quality of life in the near elderly. PloS one 12, e0182920-e0182920.

Shakoor, N., Hurwitz, D.E., Block, J.A., Shott, S., Case, J.P., 2003. Asymmetric knee loading in advanced unilateral hip osteoarthritis. Arthritis & Rheumatism 48, 1556-1561.

Shao, Q., Bassett, D.N., Manal, K., Buchanan, T.S., 2009. An EMG-driven model to estimate muscle forces and joint moments in stroke patients. Computers in biology and medicine 39, 1083-1088.

Shih, Y.O., Teng, H.L., Powers, C.M., 2019. Lower Extremity Stiffness Predicts Ground Reaction Force Loading Rate in Heel Strike Runners. Med Sci Sports Exerc 51, 1692-1697.

Silverman, A.K., Fey, N.P., Portillo, A., Walden, J.G., Bosker, G., Neptune, R.R., 2008. Compensatory mechanisms in below-knee amputee gait in response to increasing steady-state walking speeds. Gait Posture 28, 602-609.

Silverman, A.K., Neptune, R.R., 2012. Muscle and prosthesis contributions to amputee walking mechanics: a modeling study. Journal of biomechanics 45, 2271-2278.

Son, J., Rymer, W.Z., 2020. Effects of Changes in Ankle Joint Angle on the Relation Between Plantarflexion Torque and EMG Magnitude in Major Plantar Flexors of Male Chronic Stroke Survivors. Front Neurol 11, 224.

Son, J., Rymer, W.Z., Lee, S.S.M., 2020. Limited fascicle shortening and fascicle rotation may be associated with impaired voluntary force-generating capacity in pennate muscles of chronic stroke survivors. Clinical Biomechanics 75, 105007.

Soo, C.H., Donelan, J.M., 2010. Mechanics and energetics of step-to-step transitions isolated from human walking. The Journal of experimental biology 213, 4265-4271.

Soo, C.H., Donelan, J.M., 2012. Coordination of push-off and collision determine the mechanical work of step-to-step transitions when isolated from human walking. Gait Posture 35, 292-297.

Stanhope, V.A., Knarr, B.A., Reisman, D.S., Higginson, J.S., 2014. Frontal plane compensatory strategies associated with self-selected walking speed in individuals post-stroke. Clinical Biomechanics 29, 518-522.

Steele, K.M., DeMers, M.S., Schwartz, M.H., Delp, S.L., 2012. Compressive tibiofemoral force during crouch gait. Gait & Posture 35, 556-560.

Stenum, J., Choi, J.T., 2016. Neuromuscular effort predicts walk-run transition speed in normal and adapted human gaits. The Journal of experimental biology 219, 2809-2813.

Stenum, J., Choi, J.T., 2020. Step time asymmetry but not step length asymmetry is adapted to optimize energy cost of split-belt treadmill walking. J Physiol 598, 4063-4078.

Stoquart, G., Detrembleur, C., Lejeune, T.M., 2012a. The reasons why stroke patients expend so much energy to walk slowly. Gait Posture 36, 409-413.

Stoquart, G., Detrembleur, C., Lejeune, T.M., 2012b. The reasons why stroke patients expend so much energy to walk slowly. Gait & Posture 36, 409-413.

Studenski, S., Perera, S., Wallace, D., Chandler, J.M., Duncan, P.W., Rooney, E., Fox, M., Guralnik, J.M., 2003. Physical performance measures in the clinical setting. J Am Geriatr Soc 51, 314-322.

Takahashi, K.Z., Horne, J.R., Stanhope, S.J., 2015a. Comparison of mechanical energy profiles of passive and active below-knee prostheses: a case study. Prosthetics and orthotics international 39, 150-156.

Takahashi, K.Z., Lewek, M.D., Sawicki, G.S., 2015b. A neuromechanics-based powered ankle exoskeleton to assist walking post-stroke: a feasibility study. J Neuroeng Rehabil 12, 23.

Takahashi, K.Z., Lewek, M.D.a., Sawicki, G.S., 2015c. A neuromechanics-based powered ankle exoskeleton to assist walking post-stroke: a feasibility study. J Neuroeng Rehabil 12, 23.

Tateuchi, H., Koyama, Y., Akiyama, H., Goto, K., So, K., Kuroda, Y., Ichihashi, N., 2017. Daily cumulative hip moment is associated with radiographic progression of secondary hip osteoarthritis. Osteoarthritis and Cartilage 25, 1291-1298.

Thelen, D.G., Anderson, F.C., 2006. Using computed muscle control to generate forward dynamic simulations of human walking from experimental data. Journal of biomechanics 39, 1107-1115.

Tyrell, C.M., Roos, M.A., Rudolph, K.S., Reisman, D.S., 2011. Influence of Systematic Increases in Treadmill Walking Speed on Gait Kinematics After Stroke. Physical Therapy 91, 392-403.

Vanderpool, M.T., Collins, S.H., Kuo, A.D., 2008. Ankle fixation need not increase the energetic cost of human walking. Gait Posture 28, 427-433.

Waters, R.L., Mulroy, S., 1999. The energy expenditure of normal and pathologic gait. Gait Posture 9, 207-231.

Wellsandt, E., Failla, M.J., Snyder-Mackler, L., 2017. Limb symmetry indexes can overestimate knee function after anterior cruciate ligament injury. journal of orthopaedic & sports physical therapy 47, 334-338.

Wellsandt, E., Gardinier, E.S., Manal, K., Axe, M.J., Buchanan, T.S., Snyder-Mackler, L., 2015. Decreased Knee Joint Loading Associated With Early Knee Osteoarthritis After Anterior Cruciate Ligament Injury. The American Journal of Sports Medicine 44, 143-151.

Wiggin, M.B., Collins, S.H., Sawicki, G.S., Year An exoskeleton using controlled energy storage and release to aid ankle propulsion. In IEEE International Conference on Rehabilitation Robotics (ICORR). Zurich, Switzerland.

Winter, D.A., Sienko, S.E., 1988. Biomechanics of below-knee amputee gait. Journal of biomechanics 21, 361-367.

Wonsetler, E.C., Bowden, M.G., 2017. A systematic review of mechanisms of gait speed change post-stroke. Part 1: spatiotemporal parameters and asymmetry ratios. Top Stroke Rehabil 24, 435-446.

Wutzke, C.J., Sawicki, G.S., Lewek, M.D., 2012. The influence of a unilateral fixed ankle on metabolic and mechanical demands during walking in unimpaired young adults. Journal of biomechanics 45, 2405-2410.

Xergia, S.A., Pappas, E., Zampeli, F., Georgiou, S., Georgoulis, A.D., 2013. Asymmetries in Functional Hop Tests, Lower Extremity Kinematics, and Isokinetic Strength Persist 6 to 9 Months Following Anterior Cruciate Ligament Reconstruction. Journal of Orthopaedic & Sports Physical Therapy 43, 154-162.

Zelik, K.E., Huang, T.W., Adamczyk, P.G., Kuo, A.D., 2014. The role of series ankle elasticity in bipedal walking. Journal of theoretical biology 346, 75-85.

Zmitrewicz, R.J., Neptune, R.R., Sasaki, K., 2007. Mechanical energetic contributions from individual muscles and elastic prosthetic feet during symmetric unilateral transtibial amputee walking: a theoretical study. Journal of biomechanics 40, 1824-1831.

Zmitrewicz, R.J., Neptune, R.R., Walden, J.G., Rogers, W.E., Bosker, G.W., 2006. The effect of foot and ankle prosthetic components on braking and propulsive impulses during transtibial amputee gait. Archives of physical medicine and rehabilitation 87, 1334-1339.

# APPENDICES

## Appendix A. Data for Chapter 2

The Datasets used and/or analyzed in Chapter 2 are available at: https://sites.gatech.edu/hpl/archival-data-from-publications/ . Downloads include a .mat file and a .xls file with subject data. Specifically, .mat files contain a structure of individual time series data (.IND), mean time series data (.MN), and metabolic data(.MET). The .xlsx file contains summary data and additional details on variable names and condition label.

## Appendix B. Data for Chapter 3

The Datasets used and/or analyzed in Chapter 3 are available at: https://sites.gatech.edu/hpl/archival-data-from-publications/ . Downloads include a .mat file and a .xls file with subject data. Specifically, The .mat file contains several data structures. Data is normalized over a gait cycle for each participant and trial (ALL). Subject specific means (SSM) and subject average means (SAM) are also provided. Additional information is available in the readme file include within the data repository.

## Appendix C. Data for Chapter 4

The Datasets used and/or analyzed in Chapter 4 are available at: https://sites.gatech.edu/hpl/archival-data-from-publications/ . Downloads include a .mat file and a .xls file with subject data. The .mat file includes several data structures including data normalized over a gait cycle for each participant. Additional information is available in the readme file included within the data repository.

## Appendix D. Data for Chapter 5

### Limb Loading

| Unlocked limb ground reaction force first peak (N/BW) | | | | | | | | |
|---|---|---|---|---|---|---|---|---|
| **subjects** | **control** | **braced** | **uni-ank** | **uni-knee** | **uni-a+k** | **bi-ank** | **bi-knee** | **bi-a+k** |
| **1** | 10.69 | 10.64 | 10.85 | 10.18 | 10.39 | 10.87 | 10.61 | 10.72 |
| **2** | 11.53 | 11.23 | 11.46 | 10.80 | 11.14 | 11.58 | 11.74 | 11.53 |
| **3** | 10.88 | 10.83 | 11.15 | 10.09 | 11.19 | 11.59 | 10.60 | 10.72 |
| **4** | 11.63 | 11.81 | 10.99 | 11.30 | 11.42 | 11.20 | 11.61 | 12.03 |
| **5** | 11.01 | 10.64 | 10.40 | 10.59 | 10.64 | 10.57 | 10.47 | 11.01 |
| **6** | 10.70 | 10.35 | 10.22 | 10.51 | 10.37 | 10.04 | 10.97 | 10.74 |
| **7** | 10.89 | 10.98 | 11.42 | 10.52 | 11.21 | 11.50 | 11.36 | 12.11 |
| **8** | 10.75 | 10.39 | 10.65 | 9.86 | 10.73 | 10.32 | 10.47 | 11.19 |

| Locked limb ground reaction force first peak (N/BW) | | | | | | | | |
|---|---|---|---|---|---|---|---|---|
| **subjects** | **control** | **braced** | **uni-ank** | **uni-knee** | **uni-a+k** | **bi-ank** | **bi-knee** | **bi-a+k** |
| **1** | 10.47 | 10.40 | 10.84 | 10.77 | 10.88 | 10.75 | 10.19 | 10.71 |
| **2** | 11.51 | 11.39 | 11.37 | 11.54 | 11.74 | 11.90 | 11.43 | 12.13 |
| **3** | 10.82 | 10.84 | 10.88 | 10.79 | 11.49 | 11.20 | 10.26 | 10.56 |
| **4** | 11.95 | 11.81 | 11.75 | 11.96 | 11.88 | 11.68 | 11.60 | 11.55 |
| **5** | 10.17 | 10.22 | 10.39 | 10.42 | 10.67 | 10.83 | 10.32 | 10.52 |
| **6** | 10.43 | 10.58 | 11.04 | 11.30 | 10.65 | 10.95 | 12.13 | 12.54 |
| **7** | 10.67 | 10.69 | 10.63 | 10.96 | 10.96 | 11.55 | 11.85 | 11.92 |
| **8** | 10.59 | 10.61 | 10.27 | 11.56 | 10.63 | 10.76 | 11.50 | 13.45 |

| Unlocked limb ground reaction force loading rate (N/BWs) | | | | | | | | |
|---|---|---|---|---|---|---|---|---|
| **subjects** | **control** | **braced** | **uni-ank** | **uni-knee** | **uni-a+k** | **bi-ank** | **bi-knee** | **bi-a+k** |
| **1** | 123.18 | 142.94 | 165.00 | 128.61 | 157.89 | 153.80 | 130.43 | 166.93 |
| **2** | 104.18 | 109.54 | 107.55 | 126.71 | 129.93 | 119.05 | 231.16 | 226.70 |
| **3** | 112.56 | 105.09 | 123.90 | 129.08 | 153.62 | 134.91 | 186.10 | 203.79 |
| **4** | 100.05 | 107.41 | 134.66 | 111.09 | 123.34 | 118.10 | 165.61 | 249.92 |
| **5** | 103.67 | 106.96 | 101.47 | 106.10 | 116.78 | 155.13 | 155.46 | 188.08 |
| **6** | 125.60 | 110.85 | 142.46 | 139.53 | 131.50 | 137.31 | 187.45 | 208.38 |
| **7** | 114.91 | 164.39 | 181.62 | 135.50 | 183.53 | 226.18 | 229.86 | 312.33 |
| **8** | 89.98 | 133.28 | 121.10 | 139.14 | 175.71 | 125.16 | 198.73 | 245.11 |

| Locked limb ground reaction force loading rate (N/BWs) | | | | | | | | |
|---|---|---|---|---|---|---|---|---|
| **subjects** | **control** | **braced** | **uni-ank** | **uni-knee** | **uni-a+k** | **bi-ank** | **bi-knee** | **bi-a+k** |
| **1** | 110.07 | 127.17 | 149.22 | 174.43 | 238.80 | 139.49 | 172.62 | 231.09 |
| **2** | 93.32 | 106.80 | 117.66 | 203.21 | 201.35 | 109.66 | 231.70 | 282.07 |
| **3** | 100.30 | 112.75 | 104.95 | 151.18 | 200.56 | 103.05 | 168.01 | 184.43 |
| **4** | 118.54 | 99.68 | 130.67 | 130.25 | 174.08 | 114.18 | 141.73 | 260.23 |
| **5** | 98.26 | 116.52 | 130.43 | 153.51 | 184.94 | 191.07 | 175.81 | 191.82 |
| **6** | 133.86 | 130.65 | 159.08 | 169.96 | 177.70 | 159.97 | 185.40 | 245.84 |
| **7** | 104.60 | 141.21 | 126.94 | 201.75 | 229.82 | 215.49 | 256.68 | 331.16 |
| **8** | 109.02 | 145.80 | 106.76 | 186.08 | 169.77 | 140.40 | 224.26 | 259.22 |

**Joint Reaction Forces**

| Unlocked limb ankle joint reaction force first peak (N/BW) | | | | | | | | |
|---|---|---|---|---|---|---|---|---|
| **subjects** | **control** | **braced** | **uni-ank** | **uni-knee** | **uni-a+k** | **bi-ank** | **bi-knee** | **bi-a+k** |
| **1** | 3.38 | 3.24 | 3.23 | 3.21 | 3.42 | 3.44 | 3.73 | 3.61 |
| **2** | 3.30 | 3.07 | 2.90 | 3.63 | 2.98 | 3.47 | 3.30 | 3.18 |
| **3** | 2.92 | 2.75 | 2.77 | 3.10 | 3.46 | 2.91 | 3.23 | 3.29 |
| **4** | 2.96 | 3.48 | 3.02 | 3.23 | 3.31 | 3.05 | 3.68 | 3.09 |
| **5** | 3.05 | 3.43 | 3.09 | 3.63 | 3.43 | 3.02 | 3.38 | 3.19 |
| **6** | 3.13 | 3.25 | 3.35 | 3.55 | 3.59 | 3.52 | 3.95 | 3.81 |
| **7** | 3.85 | 3.54 | 4.10 | 4.06 | 4.05 | 4.61 | 3.74 | 5.13 |
| **8** | 2.45 | 2.65 | 3.09 | 2.63 | 3.34 | 2.60 | 3.02 | 3.48 |

| Locked limb ankle joint reaction force first peak (N/BW) | | | | | | | | |
|---|---|---|---|---|---|---|---|---|
| **subjects** | **control** | **braced** | **uni-ank** | **uni-knee** | **uni-a+k** | **bi-ank** | **bi-knee** | **bi-a+k** |
| **1** | 3.34 | 3.37 | 3.26 | 3.41 | 3.42 | 3.53 | 3.97 | 3.83 |
| **2** | 3.40 | 3.33 | 3.32 | 2.98 | 2.99 | 3.70 | 3.26 | 3.28 |
| **3** | 3.53 | 2.97 | 3.33 | 2.93 | 3.72 | 3.32 | 3.44 | 3.48 |
| **4** | 3.77 | 3.56 | 3.07 | 3.59 | 3.62 | 3.32 | 3.90 | 3.48 |
| **5** | 2.97 | 3.25 | 2.68 | 2.98 | 2.91 | 2.95 | 3.32 | 3.11 |
| **6** | 3.66 | 3.89 | 4.09 | 3.89 | 3.79 | 4.01 | 4.19 | 4.14 |
| **7** | 4.11 | 3.82 | 4.33 | 3.56 | 4.13 | 3.85 | 4.07 | 4.68 |
| **8** | 2.84 | 2.89 | 2.81 | 3.17 | 3.27 | 3.04 | 3.73 | 3.81 |

| Unlocked limb knee joint reaction force first peak (N/BW) | | | | | | | | |
|---|---|---|---|---|---|---|---|---|
| **subjects** | **control** | **braced** | **uni-ank** | **uni-knee** | **uni-a+k** | **bi-ank** | **bi-knee** | **bi-a+k** |
| **1** | 3.74 | 3.53 | 3.51 | 3.50 | 3.36 | 3.42 | 3.87 | 3.51 |
| **2** | 4.68 | 4.36 | 4.24 | 4.63 | 4.01 | 4.55 | 4.90 | 4.52 |
| **3** | 3.53 | 3.61 | 3.14 | 3.64 | 3.79 | 3.44 | 3.28 | 3.33 |
| **4** | 3.88 | 3.52 | 3.74 | 3.76 | 3.69 | 3.52 | 3.83 | 4.53 |
| **5** | 3.25 | 3.28 | 2.91 | 3.41 | 3.20 | 3.26 | 3.41 | 3.22 |
| **6** | 3.25 | 3.21 | 3.34 | 3.22 | 3.14 | 3.23 | 3.62 | 3.56 |
| **7** | 4.42 | 3.90 | 4.41 | 3.84 | 4.41 | 5.04 | 4.26 | 5.96 |
| **8** | 3.05 | 2.91 | 3.07 | 2.90 | 3.44 | 2.81 | 3.02 | 3.15 |

| Locked limb knee joint reaction force first peak (N/BW) | | | | | | | | |
|---|---|---|---|---|---|---|---|---|
| **subjects** | **control** | **braced** | **uni-ank** | **uni-knee** | **uni-a+k** | **bi-ank** | **bi-knee** | **bi-a+k** |
| **1** | 3.77 | 3.92 | 3.51 | 3.72 | 3.71 | 3.59 | 4.27 | 3.88 |
| **2** | 4.28 | 3.96 | 4.19 | 4.39 | 4.13 | 4.26 | 4.39 | 4.27 |
| **3** | 4.47 | 3.90 | 3.49 | 3.70 | 3.97 | 3.95 | 3.69 | 3.52 |
| **4** | 4.22 | 3.97 | 3.60 | 3.99 | 3.82 | | 4.42 | 4.34 |
| **5** | 3.08 | 3.28 | 2.74 | 2.99 | 3.02 | 3.20 | 3.37 | 3.31 |
| **6** | 3.92 | 4.11 | 3.93 | 4.02 | 3.70 | 3.97 | 4.11 | 4.20 |
| **7** | 4.62 | 4.47 | 4.22 | 4.30 | 4.51 | 4.75 | 4.82 | 5.37 |
| **8** | 3.00 | 3.09 | 2.83 | 3.18 | 3.26 | 3.02 | 3.40 | 3.76 |

| Unlocked limb hip joint reaction force first peak (N/BW) | | | | | | | | |
|---|---|---|---|---|---|---|---|---|
| **subjects** | **control** | **braced** | **uni-ank** | **uni-knee** | **uni-a+k** | **bi-ank** | **bi-knee** | **bi-a+k** |
| **1** | 5.13 | 5.60 | 4.88 | 4.46 | 4.59 | 4.58 | 4.64 | 4.25 |
| **2** | 6.45 | 5.67 | 5.36 | 4.86 | 4.59 | 5.77 | 4.62 | 4.50 |
| **3** | 4.56 | 4.53 | 4.19 | 4.57 | 4.95 | 4.51 | 5.11 | 5.00 |
| **4** | 4.71 | 3.98 | 4.22 | 4.46 | 4.53 | 4.03 | 4.53 | 4.92 |
| **5** | 4.07 | 3.66 | 3.50 | 3.80 | 4.17 | 4.02 | 3.84 | 4.29 |
| **6** | 4.75 | 3.76 | 4.02 | 3.59 | 3.64 | 3.54 | 3.68 | 4.08 |
| **7** | 5.96 | 4.97 | 5.28 | 4.85 | 5.62 | 5.68 | 5.49 | 6.45 |
| **8** | 4.29 | 3.82 | 3.60 | 3.92 | 3.71 | 3.76 | 4.04 | 4.21 |

| Locked limb hip joint reaction force first peak (N/BW) | | | | | | | | |
|---|---|---|---|---|---|---|---|---|
| **subjects** | **control** | **braced** | **uni-ank** | **uni-knee** | **uni-a+k** | **bi-ank** | **bi-knee** | **bi-a+k** |
| **1** | 5.79 | 6.60 | 5.54 | 5.24 | 5.31 | 5.39 | 5.39 | 4.96 |
| **2** | 5.71 | 5.13 | 4.97 | 5.43 | 4.99 | 5.19 | 4.66 | 5.26 |
| **3** | 5.89 | 5.70 | 4.30 | 5.37 | 4.61 | 4.59 | 4.81 | 4.33 |
| **4** | 6.11 | 4.69 | 4.72 | 4.90 | 5.00 | 5.11 | 5.02 | 5.58 |
| **5** | 4.41 | 4.11 | 4.12 | 4.01 | 4.45 | 4.39 | 3.99 | 4.25 |
| **6** | 5.69 | 5.36 | 5.08 | 4.87 | 4.51 | 5.26 | 4.02 | 5.24 |
| **7** | 6.27 | 5.43 | 5.26 | 5.55 | 5.54 | 5.65 | 5.77 | 6.19 |
| **8** | 3.77 | 3.65 | 2.86 | 3.77 | 2.84 | 3.27 | 4.03 | 4.04 |

| Unlocked limb ankle joint reaction force loading rate (N/BWs) | | | | | | | | |
|---|---|---|---|---|---|---|---|---|
| **subjects** | **control** | **braced** | **uni-ank** | **uni-knee** | **uni-a+k** | **bi-ank** | **bi-knee** | **bi-a+k** |
| **1** | 46.25 | 46.99 | 38.05 | 43.89 | 36.10 | 46.14 | 57.65 | 49.37 |
| **2** | 39.01 | 30.15 | 24.54 | 51.16 | 22.34 | 57.02 | 36.17 | 30.56 |
| **3** | 33.33 | 37.55 | 27.38 | 40.65 | 43.37 | 31.64 | 28.18 | 30.42 |
| **4** | 28.30 | 29.65 | 34.33 | 42.50 | 35.46 | 30.77 | 35.04 | 31.73 |
| **5** | 31.58 | 28.41 | 19.74 | 23.30 | 19.89 | 29.53 | 31.12 | 32.58 |
| **6** | 35.03 | 31.64 | 33.19 | 30.13 | 28.12 | 35.02 | 23.44 | 32.53 |
| **7** | 62.74 | 32.11 | 52.00 | 48.29 | 40.92 | 75.06 | 28.08 | 71.81 |
| **8** | 28.26 | 32.14 | 22.82 | 27.63 | 30.97 | 26.30 | 25.63 | 31.10 |

| Locked limb ankle joint reaction force loading rate (N/BWs) | | | | | | | | |
|---|---|---|---|---|---|---|---|---|
| **subjects** | **control** | **braced** | **uni-ank** | **uni-knee** | **uni-a+k** | **bi-ank** | **bi-knee** | **bi-a+k** |
| **1** | 45.26 | 40.71 | 51.09 | 35.14 | 57.61 | 41.23 | 41.88 | 53.54 |
| **2** | 48.19 | 46.81 | 51.62 | 29.53 | 29.95 | 60.76 | 35.55 | 35.49 |
| **3** | 26.46 | 24.75 | 27.40 | 29.24 | 37.69 | 31.32 | 28.61 | 33.51 |
| **4** | 59.51 | 36.01 | 35.28 | 44.63 | 41.76 | 43.79 | 50.43 | 41.51 |
| **5** | 39.55 | 25.92 | 22.28 | 30.17 | 26.39 | 39.61 | 32.35 | 45.54 |
| **6** | 57.54 | 77.37 | 76.42 | 67.52 | 55.41 | 75.67 | 33.20 | 60.62 |
| **7** | 72.42 | 62.72 | 62.43 | 36.01 | 49.51 | 40.56 | 50.20 | 71.99 |
| **8** | 31.65 | 39.18 | 18.88 | 37.01 | 26.55 | 27.64 | 33.47 | 42.96 |

| Unlocked limb knee joint reaction force loading rate (N/BWs) | | | | | | | | |
|---|---|---|---|---|---|---|---|---|
| subjects | control | braced | uni-ank | uni-knee | uni-a+k | bi-ank | bi-knee | bi-a+k |
| 1 | 141.01 | 112.47 | 88.08 | 100.32 | 80.22 | 82.49 | 43.91 | 48.50 |
| 2 | 59.81 | 41.39 | 40.39 | 66.68 | 39.13 | 65.92 | 55.57 | 43.32 |
| 3 | 82.61 | 66.47 | 51.94 | 67.93 | 74.73 | 74.15 | 41.70 | 49.49 |
| 4 | 50.69 | 61.88 | 60.35 | 57.75 | 57.87 | 52.91 | 53.66 | 55.10 |
| 5 | 42.02 | 55.03 | 37.96 | 30.02 | 38.63 | 51.06 | 67.70 | 50.81 |
| 6 | 39.39 | 45.06 | 50.91 | 42.47 | 42.54 | 41.17 | 53.19 | 61.53 |
| 7 | 70.45 | 57.01 | 58.06 | 48.11 | 42.69 | 89.92 | 41.20 | 93.14 |
| 8 | 50.98 | 51.68 | 27.34 | 49.89 | 40.39 | 42.53 | 42.89 | 47.33 |

| **Locked limb knee joint reaction force loading rate (N/BWs)** | | | | | | | | |
|---|---|---|---|---|---|---|---|---|
| **subjects** | **control** | **braced** | **uni-ank** | **uni-knee** | **uni-a+k** | **bi-ank** | **bi-knee** | **bi-a+k** |
| **1** | 88.71 | 143.85 | 113.21 | 45.31 | 70.80 | 135.46 | 46.10 | 67.89 |
| **2** | 74.54 | 69.95 | 79.22 | 56.59 | 53.57 | 76.05 | 50.21 | 48.60 |
| **3** | 47.77 | 55.84 | 58.67 | 39.99 | 55.59 | 93.58 | 36.54 | 49.67 |
| **4** | 76.00 | 72.81 | 55.65 | 69.11 | 57.56 | 62.93 | 73.43 | 65.21 |
| **5** | 49.04 | 37.48 | 32.21 | 48.21 | 39.43 | 52.92 | 61.93 | 57.70 |
| **6** | 88.82 | 100.60 | 91.23 | 97.49 | 71.81 | 95.33 | 65.88 | 84.32 |
| **7** | 88.50 | 82.50 | 62.53 | 49.89 | 57.34 | 61.71 | 66.18 | 84.44 |
| **8** | 59.80 | 59.14 | 30.97 | 51.00 | 39.03 | 46.48 | 46.41 | 61.18 |

| **Unlocked limb hip joint reaction force loading rate (N/BWs)** | | | | | | | | |
|---|---|---|---|---|---|---|---|---|
| **subjects** | **control** | **braced** | **uni-ank** | **uni-knee** | **uni-a+k** | **bi-ank** | **bi-knee** | **bi-a+k** |
| **1** | 229.92 | 122.87 | 96.49 | 101.00 | 82.99 | 97.21 | 45.29 | 32.85 |
| **2** | 54.16 | 44.96 | 43.34 | 55.66 | 39.76 | 59.18 | 63.96 | 47.47 |
| **3** | 127.13 | 74.90 | 65.24 | 72.52 | 90.39 | 104.10 | 43.66 | 54.93 |
| **4** | 55.31 | 62.07 | 61.09 | 52.26 | 56.46 | 53.10 | 60.18 | 73.36 |
| **5** | 56.09 | 61.72 | 38.09 | 32.40 | 49.85 | 74.43 | 69.22 | 60.88 |
| **6** | 40.77 | 46.46 | 55.71 | 45.56 | 44.56 | 36.37 | 55.05 | 54.78 |
| **7** | 55.46 | 56.72 | 53.25 | 37.12 | 35.55 | 86.02 | 39.11 | 87.44 |
| **8** | 48.26 | 43.63 | 27.87 | 45.44 | 36.79 | 46.78 | 50.12 | 60.17 |

| Locked limb hip joint reaction force loading rate (N/BWs) | | | | | | | | |
|---|---|---|---|---|---|---|---|---|
| **subjects** | **control** | **braced** | **uni-ank** | **uni-knee** | **uni-a+k** | **bi-ank** | **bi-knee** | **bi-a+k** |
| **1** | 122.72 | 296.71 | 188.83 | 42.40 | 82.54 | 285.25 | 65.57 | 73.26 |
| **2** | 67.08 | 64.01 | 61.70 | 58.98 | 52.87 | 65.34 | 59.11 | 55.91 |
| **3** | 65.51 | 85.09 | 74.18 | 57.78 | 58.67 | 124.13 | 54.07 | 49.22 |
| **4** | 125.42 | 73.75 | 71.10 | 82.33 | 61.86 | 90.63 | 61.36 | 93.33 |
| **5** | 57.76 | 56.72 | 48.73 | 60.26 | 41.83 | 70.30 | 65.46 | 65.67 |
| **6** | 120.06 | 130.80 | 117.75 | 112.36 | 78.79 | 117.87 | 61.79 | 91.66 |
| **7** | 110.39 | 85.06 | 71.68 | 57.07 | 65.90 | 64.12 | 66.88 | 96.48 |
| **8** | 73.30 | 69.88 | 33.14 | 58.78 | 36.15 | 52.29 | 59.97 | 78.32 |

## Muscle Force Contributions

| Unlocked limb ankle muscle force contribution (N/BW) | | | | | | | | |
|---|---|---|---|---|---|---|---|---|
| **subjects** | **control** | **braced** | **uni-ank** | **uni-knee** | **uni-a+k** | **bi-ank** | **bi-knee** | **bi-a+k** |
| **1** | 3.38 | 3.24 | 3.23 | 3.21 | 3.42 | 3.44 | 3.73 | 3.61 |
| **2** | 3.30 | 3.07 | 2.90 | 3.63 | 2.98 | 3.47 | 3.30 | 3.18 |
| **3** | 2.92 | 2.75 | 2.77 | 3.10 | 3.46 | 2.91 | 3.23 | 3.29 |
| **4** | 2.96 | 3.48 | 3.02 | 3.23 | 3.31 | 3.05 | 3.68 | 3.09 |
| **5** | 3.05 | 3.43 | 3.09 | 3.63 | 3.43 | 3.02 | 3.38 | 3.19 |
| **6** | 3.13 | 3.25 | 3.35 | 3.55 | 3.59 | 3.52 | 3.95 | 3.81 |
| **7** | 3.85 | 3.54 | 4.10 | 4.06 | 4.05 | 4.61 | 3.74 | 5.13 |
| **8** | 2.45 | 2.65 | 3.09 | 2.63 | 3.34 | 2.60 | 3.02 | 3.48 |

| Locked limb ankle muscle force contribution (N/BW) | | | | | | | | |
|---|---|---|---|---|---|---|---|---|
| **subjects** | **control** | **braced** | **uni-ank** | **uni-knee** | **uni-a+k** | **bi-ank** | **bi-knee** | **bi-a+k** |
| **1** | 3.34 | 3.37 | 3.26 | 3.41 | 3.42 | 3.53 | 3.97 | 3.83 |
| **2** | 3.40 | 3.33 | 3.32 | 2.98 | 2.99 | 3.70 | 3.26 | 3.28 |
| **3** | 3.53 | 2.97 | 3.33 | 2.93 | 3.72 | 3.32 | 3.44 | 3.48 |
| **4** | 3.77 | 3.56 | 3.07 | 3.59 | 3.62 | 3.32 | 3.90 | 3.48 |
| **5** | 2.97 | 3.25 | 2.68 | 2.98 | 2.91 | 2.95 | 3.32 | 3.11 |
| **6** | 3.66 | 3.89 | 4.09 | 3.89 | 3.79 | 4.01 | 4.19 | 4.14 |
| **7** | 4.11 | 3.82 | 4.33 | 3.56 | 4.13 | 3.85 | 4.07 | 4.68 |
| **8** | 2.84 | 2.89 | 2.81 | 3.17 | 3.27 | 3.04 | 3.73 | 3.81 |

| Unlocked limb knee muscle force contribution (N/BW) | | | | | | | | |
|---|---|---|---|---|---|---|---|---|
| **subjects** | **control** | **braced** | **uni-ank** | **uni-knee** | **uni-a+k** | **bi-ank** | **bi-knee** | **bi-a+k** |
| **1** | 3.74 | 3.53 | 3.51 | 3.50 | 3.36 | 3.42 | 3.87 | 3.51 |
| **2** | 4.68 | 4.36 | 4.24 | 4.63 | 4.01 | 4.55 | 4.90 | 4.52 |
| **3** | 3.53 | 3.61 | 3.14 | 3.64 | 3.79 | 3.44 | 3.28 | 3.33 |
| **4** | 3.88 | 3.52 | 3.74 | 3.76 | 3.69 | 3.52 | 3.83 | 4.53 |
| **5** | 3.25 | 3.28 | 2.91 | 3.41 | 3.20 | 3.26 | 3.41 | 3.22 |
| **6** | 3.25 | 3.21 | 3.34 | 3.22 | 3.14 | 3.23 | 3.62 | 3.56 |
| **7** | 4.42 | 3.90 | 4.41 | 3.84 | 4.41 | 5.04 | 4.26 | 5.96 |
| **8** | 3.05 | 2.91 | 3.07 | 2.90 | 3.44 | 2.81 | 3.02 | 3.15 |

| Locked limb knee muscle force contribution (N/BW) | | | | | | | | |
|---|---|---|---|---|---|---|---|---|
| **subjects** | **control** | **braced** | **uni-ank** | **uni-knee** | **uni-a+k** | **bi-ank** | **bi-knee** | **bi-a+k** |
| **1** | 3.77 | 3.92 | 3.51 | 3.72 | 3.71 | 3.59 | 4.27 | 3.88 |
| **2** | 4.28 | 3.96 | 4.19 | 4.39 | 4.13 | 4.26 | 4.39 | 4.27 |
| **3** | 4.47 | 3.90 | 3.49 | 3.70 | 3.97 | 3.95 | 3.69 | 3.52 |
| **4** | 4.22 | 3.97 | 3.60 | 3.99 | 3.82 | 3.72 | 4.42 | 4.34 |
| **5** | 3.08 | 3.28 | 2.74 | 2.99 | 3.02 | 3.20 | 3.37 | 3.31 |
| **6** | 3.92 | 4.11 | 3.93 | 4.02 | 3.70 | 3.97 | 4.11 | 4.20 |
| **7** | 4.62 | 4.47 | 4.22 | 4.30 | 4.51 | 4.75 | 4.82 | 5.37 |
| **8** | 3.00 | 3.09 | 2.83 | 3.18 | 3.26 | 3.02 | 3.40 | 3.76 |

| Unlocked limb hip muscle force contribution (N/BW) | | | | | | | | |
|---|---|---|---|---|---|---|---|---|
| **subjects** | **control** | **braced** | **uni-ank** | **uni-knee** | **uni-a+k** | **bi-ank** | **bi-knee** | **bi-a+k** |
| **1** | 5.13 | 5.60 | 4.88 | 4.46 | 4.59 | 4.58 | 4.64 | 4.25 |
| **2** | 6.45 | 5.67 | 5.36 | 4.86 | 4.59 | 5.77 | 4.62 | 4.50 |
| **3** | 4.56 | 4.53 | 4.19 | 4.57 | 4.95 | 4.51 | 5.11 | 5.00 |
| **4** | 4.71 | 3.98 | 4.22 | 4.46 | 4.53 | 4.03 | 4.53 | 4.92 |
| **5** | 4.07 | 3.66 | 3.50 | 3.80 | 4.17 | 4.02 | 3.84 | 4.29 |
| **6** | 4.75 | 3.76 | 4.02 | 3.59 | 3.64 | 3.54 | 3.68 | 4.08 |
| **7** | 5.96 | 4.97 | 5.28 | 4.85 | 5.62 | 5.68 | 5.49 | 6.45 |
| **8** | 4.29 | 3.82 | 3.60 | 3.92 | 3.71 | 3.76 | 4.04 | 4.21 |

| Locked limb hip muscle force contribution (N/BW) | | | | | | | | |
|---|---|---|---|---|---|---|---|---|
| **subjects** | **control** | **braced** | **uni-ank** | **uni-knee** | **uni-a+k** | **bi-ank** | **bi-knee** | **bi-a+k** |
| **1** | 5.79 | 6.60 | 5.54 | 5.24 | 5.31 | 5.39 | 5.39 | 4.96 |
| **2** | 5.71 | 5.13 | 4.97 | 5.43 | 4.99 | 5.19 | 4.66 | 5.26 |
| **3** | 5.89 | 5.70 | 4.30 | 5.37 | 4.61 | 4.59 | 4.81 | 4.33 |
| **4** | 6.11 | 4.69 | 4.72 | 4.90 | 5.00 | 5.11 | 5.02 | 5.58 |
| **5** | 4.41 | 4.11 | 4.12 | 4.01 | 4.45 | 4.39 | 3.99 | 4.25 |
| **6** | 5.69 | 5.36 | 5.08 | 4.87 | 4.51 | 5.26 | 4.02 | 5.24 |
| **7** | 6.27 | 5.43 | 5.26 | 5.55 | 5.54 | 5.65 | 5.77 | 6.19 |
| **8** | 3.77 | 3.65 | 2.86 | 3.77 | 2.84 | 3.27 | 4.03 | 4.04 |